Viscoelastic Models for Ligaments and Tendons

Ratchada Sopakayang

Dissertation submitted to the Faculty of the

Virginia Polytechnic Institute and State University

in partial fulfillment of the requirements for the degree of

Doctor of Philosophy

in

Engineering Mechanics

Raffaella De Vita, Chair

David A. Dillard

Scott W. Case

Mark S. Cramer

Rafael V. Davalos

December 08, 2010

Blacksburg, Virginia

Keywords: Nonlinear Viscoelastic Models, Preconditioning, A Cross-linked Collagen Fiber,

Ligaments, Tendons

Viscoelastic Models of Ligaments and Tendons

Ratchada Sopakayang

(ABSTRACT)

Collagenous tissues such as ligaments and tendons are viscoelastic materials. They exhibit a slow continuous increase in strain over time, or creep, when subjected to a constant stress and a slow continuous decrease in stress over time, or stress relaxation, when subjected to a constant strain. Moreover, the loading and unloading stress-strain curves are different when the tissues are subjected to cyclic loading, showing hysteresis and softening phenomena. The micro-structural origin of the viscoelasticity of these tissues is still unknown and the subject of debate among experts in biomechanics. Therefore, formulating viscoelastic models by accounting for the mechanical contributions of the structural components of these tissues can help in understanding the genesis of viscoelasticity.

A nonlinear viscoelastic modeling framework has been developed to describe the elastic and viscoelastic properties of ligaments and tendons by considering their main structural components, the collagen fibers and proteoglycan-rich matrix. The mathematical models derived within this framework can illustrate the tensile behavior, stress relaxation and creep by assuming that the collagen fibers are elastic and the surrounding proteoglycan-rich matrix is viscoelastic. The collagen fibers are represented by linear elastic springs that are engaged to support load at different values of the tissue's strain according to a Weibull distribution function. The mechanical contribution of the matrix is introduced via a Maxwell-type viscoelastic element arranged in parallel with the collagen fibers. According to the proposed mathematical framework, both the collagen fibers and the proteoglycan-rich matrix are responsible for resisting tensile loads. However, the collagen fibers play a significant role in creep while the proteoglycan-rich matrix has a dominant role in stress relaxation. The model

parameters that define the stress relaxation and strain stiffening phenomena are estimated by using published experimental on rabbit medial collateral ligaments and are then used to predict creep.

The above modeling framework has been also extended to capture the influence of preconditioning on the mechanical properties of ligaments and tendons. The stress softening and decrease in hysteresis that are observed during successive loading cycles in preconditioning are assumed to be determined by a decrease in the elastic properties of the collagen fibers and proteoglycan-rich matrix. Preliminary data collected on stress relaxation and preconditioning on rat medial collateral ligaments by collaborators are used to evaluate the model parameters and analyze its predictions.

The elastic and viscoelastic properties of single collagen fibers are studied by formulating a nonlinear viscoelastic framework by accounting for their main components: microfibrils, cross-links and proteoglycan-rich matrix. The model illustrates tensile behavior and stress relaxation of a single collagen fiber by assuming that the microfibrils and the cross-links are elastic and the surrounding proteoglycan-rich matrix is viscoelastic. The mechanical contribution of the microfibrils is included via a linear elastic spring while the cross-links are represented by linear elastic springs that progressively fail at different values of the tissue's strain according to an exponential distribution function. The matrix is defined by linear dashpots arranged in parallel with each single spring that represents an individual cross-link. The viscous properties of the matrix associated with the unbroken and broken cross-links are assumed to have different values. In the model formulation, the microfibrils and the cross-

links are assumed to determine the elastic response of the fibers while the proteoglycan-rich matrix determines the stress relaxation. Microfibrils, cross-links and the proteoglycan-rich matrix are responsible for resisting the loading force during tensile behavior. Experimental data collected by performing incremental stress relaxation tests by other investigators on reconstituted rat tail tendons are used to estimate the parameters in the model and evaluate its performance.

This work is based upon work supported by Thai Government under Science and Technology Scholarship and partially supported by the National Science Foundation under Grant No. 0932024.

Acknowledgments

I would like to give special thanks to my advisor, Dr. Raffaella De Vita, for her guidance and encouragement over these years. I also would like to thank the committee members, Dr. Case, Dr. Cramer, Dr. Davalos and Dr. Dillard, for their comments and advices. Finally, I would like to thank Mr. Albert Kwansa from the Musculoskeletal Tissue Regeneration Laboratory and Mr. Jeffrey Morelli from the Mechanics of Soft Biological Systems Laboratory at Virginia Tech for providing the experimental data used for developing and validating the models presented in this dissertation, and of course, my lab mates, my parents, my brother and my friends who have always been there for me.

Contents

List of Figures

List of Tables

Chapter 1

Introduction

1.1 Motivation

Ligaments and tendons are essential components of the musculoskeletal system: ligaments connect bones to bones and tendons connect muscles to bones. Their main functions are transferring forces between the tissues that they connect and stabilizing the movement of joints. Injuries to ligaments and tendons have reached epidemic proportion in the United States due to the increasing number of people participating in sport. Recent studies have estimated, for example, that 80,000 ACL tears occur every year in United States. These injuries constitute a significant economic burden to the society resulting in almost a billion dollars in medical expenses [32].

The prevention and treatment of injuries require a complete characterization of the mechan-

ical properties of ligaments and tendons. Tensile tests, creep and stress relaxation experiments have been performed over the past fifty years to determine the mechanical response of these tissues during normal physical activities and during physical activities leading to injuries. However, there are still crucial knowledge gaps in the current understanding of the mechanical role of the tissues' components. Studies aimed at linking the composition and mechanics of these tissues are essential, for example, for the advancement of tissue engineering. Many scaffold materials used for the replacement of injured ligaments and tendons are indeed designed to mimic their internal architecture.

The over-arching theme of this dissertation is developing new mathematical models that can accurately describe the elastic and viscoelastic properties of ligaments and tendons including collagen fibers by considering the composition and organization of the tissues. In this chapter, the structure and composition of ligaments and tendons are presented together with previous experimental and theoretical studies, which are relevant to the different viscoelastic models presented in chapters 2, 3 and 4.

1.2 Hierarchical Structure of Ligaments and Tendons

The main component of ligaments and tendons is collagen. Collagen, which is the most abundant protein in our body, is deemed responsible for resisting forces in many tissues. There are about 28 different types of collagen [25]. In the human body, the most common types of collagen (80-90 percent) are collagen type I, II and III. Type I collagen is usually

found in ligaments, tendons, skin, bone, cornea, lung and the vasculature while type II collagen is found in cartilage, developing cornea and vitreous humor. Type III collagen can be found in the walls of arteries, embryonic skin, lung, blood vessels and other hollow organs [38].

Structure of Collagen Molecules

Collagen type I is composed of three polypeptide chains (α-chains) twisted together in a right-handed triple helical structure. This triple helix forms the collagen molecule, also called tropocollagen, and has been shown to be about 300 nm in length and 1.5 nm in diameter [25]. Each polypeptide chain consists of the repeating of Gly-X-Y connection where Gly is a glycine residue and X and Y are usually a proline or hydroxyproline residue. However, the type, the number and the ratio of these amino acids (X and Y) is different depending on the type of collagen [25]. The bonds that stabilize the triple-helical collagen molecule are hydrogen bonds between the N-H of the glycine residues of one chain and C=O of the proline residues of another chain.

Structure of Collagen Microfibrils

A microfibril is made of collagen molecules staggered along its axial direction. The collagen molecules are stabilized by the proteoglycan-rich matrix and the covalent cross-links. However, the mechanisms of interaction of the matrix and cross-links with the collagen molecules are still unknown [10, 36]. A microfibril is composed of 5 strands of collagen molecules wound

in a spiral configuration.

Cross-links within and between Microfibrils

The age-related changes in mechanical properties of ligaments and tendons are due to the cross-links between the collagen molecules within the tissues. The structure and location of cross-links during maturation of ligaments and tendons are still under investigation. However, it has been reported that the development of cross-links could be driven by enzymic and non-enzymic mechanisms. For enzymic mechanism, the cross-link in collagen molecules is developed from the single telopeptide lysine or hydroxylysine residue by a precisely controlled enzymic method to form immature cross-links. The immature cross-links will develop to become mature cross-links, which are stiffer than immature cross-links, during maturation. Most of the immature cross-links connect the collagen molecules within the same microfibrils while most of mature cross-links connect the collagen molecules of different microfibrils. For non-enzymic mechanism, the intermolecular cross-link is developed from the reaction of lysine residues and glucose called glycation. The glycation cross-links occur during aging and cause dysfunction of the tissue. Glycation cross-links are intermolecular cross-links and found in individual microfibrils and between microfibrils [1]. Figure 1.1 shows the location of the cross-links.

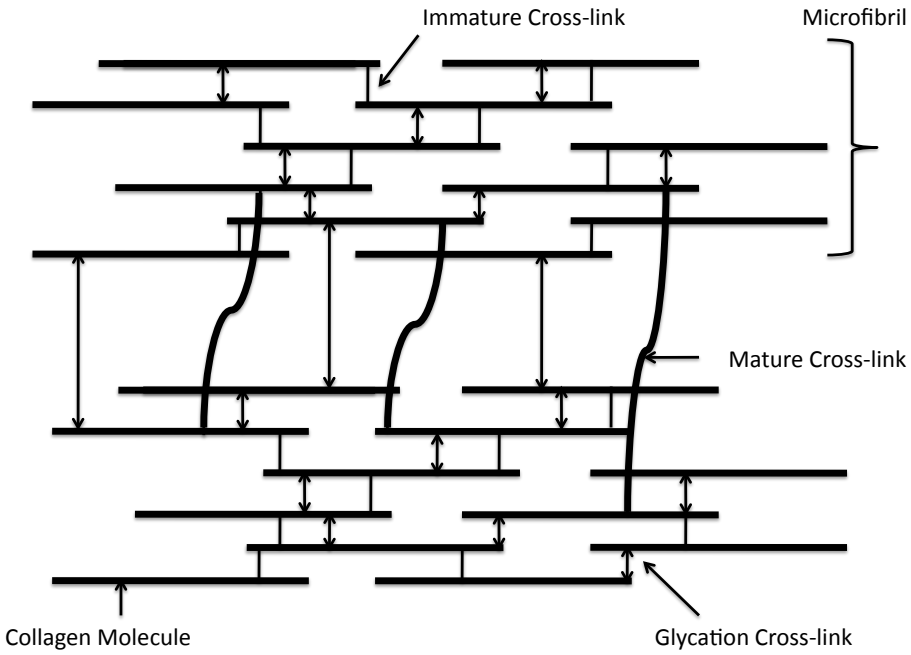

Figure 1.1: Location of cross-links [1].

Collagen Fibril, Fiber, Fascicle, Ligament and Tendon Structure

A collagen fibril is made up from a large number of microfibrils, which are embedded in a ground substance [54]. Collagen fibrils are assembled into a collagen fiber and bounded together by the ground substance [54]. Collagen fibers are assembled into a subfascicle, subfascicles into a fascicle and fascicles into ligaments or tendons [39].

Ground Substance

The ground substance in ligaments and tendons is mainly composed of proteoglycans, glycosaminoglycans (GAGs) and water. Proteoglycans and GAGs constitute approximately 1 percent of the total dry weight of tendons and ligaments, while water comprises 60-80 percent of the total wet weight of these tissues. The proteoglycans consist of a core polypeptide chain attaching one or more GAG side chains. The GAGs are mainly composed of hyaluronic acid, chondroitin sulphate and dermatan sulphate. Some constituents of the GAGs, chondroitin and dermatan sulphates, are covalently linked to some polypeptide chains to create a large number of hydroxyl groups which attract water through hydrogen bonds [12].

1.3 Literature Review

1.3.1 Review of Experimental Studies

Tensile, Creep and Stress Relaxation Properties

Results from tensile tests at a constant strain rate have shown that the stress-strain curves in collagenous tissues is nonlinear and can be divided into three regions as shown in Figure 1.2. In the first region (O-A), called toe region, the elastic modulus is observed to gradually increase with strain. In the second region (A-B), called linear region, the elastic modulus is constant and the stress-strain curve is linear. In the third region (B-C), called failure

region, the elastic modulus gradually decreases with strain until the tissues reaches failure [26]. Some of the values of the elastic modulus of the linear region for different types of ligaments and tendons are listed in Table 1.1.

Table 1.1: Elastic moduli of different types of ligaments and tendons.

Ligament and tendon type	Elastic modulus (MPa)
Human MCL [55]	332.2 ± 58.3
Human PL [60]	811.7 ± 154.1
Human QT [60]	462.8 ± 68.5
Rabbit MCL [77]	740 ± 90
Rabbit ACL [76]	516 ± 64

It has been observed that the collagen fibrils are crimped when the ligaments and tendons are at rest. For example, Yahia and Drouin examined the fibrillar crimp in canine anterior cruciate ligaments and patellar tendons by using light and scanning electron microscopy. They found that a helical waveform occured in both tissues while a planar waveform was observed only in the center of fascicle of the anterior cruciate ligaments [79]. When the tissues are stretched, the amplitude of the waviness of the fibrils is found to decrease. For example, Franchi and et al. found by using polarized light microscopy that when rat Achilles tendons were slightly stretched, the fibrillar crimp gradually decreases [24]. The uncrimping of the fibrils is considered to be the main cause of the nonlinear stress-strain relationship of the toe region.

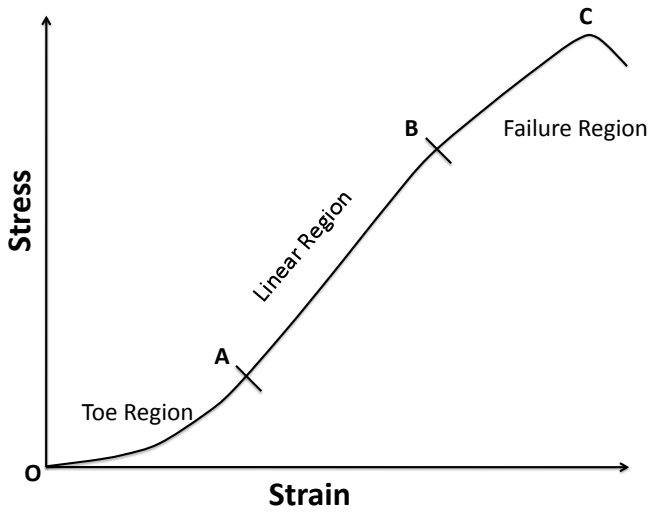

Figure 1.2: Typical tensile stress-strain curve of ligaments and tendons.

Several experimental studies have shown that matrix surrounding fibers significantly influenced the mechanical behavior of ligaments and tendons [47, 48, 81, 61]. For example, Screen et al. performed tensile tests of normal rat tail tendon fascicles and rat tail tendon fascicles in which the dermatan sulphate and chondroitin sulphate glycosaminoglycans were removed by using a chondroitinase treatment. They found that the ultimate load of normal rat tail tendon fascicles was much higher than the ultimate load of rat tail tendon fascicles with digested proteoglycans. Therefore, they concluded that the proteoglycan-rich matrix has a significant effect on the tensile properties of the tissues [61].

Viscoelastic properties of ligaments and tendons have been widely studied by performing static creep and stress relaxation experiments. During static creep experiments, the stress is

maintained constant and the strain is observed to increase over time until it becomes almost constant. It was demonstrated by static creep experiments that time needed for the strain to achieve a steady value for different stress levels and different types of ligaments and tendons were different. For example, Thornton et al. showed that for female rabbits MCLs at 14 MPa-stress level and 0.05-initial strain, the strain increases by about 16 percent within 20 minutes [70]. Some creep experiments have been conducted for 100-240 seconds without obtaining a steady value of the strain [50, 35, 7]. Hingorani et al. demonstrated that the interval of time needed to achieve a steady value of the strain at higher stress levels is smaller at lower stress levels [35]. Thornton et al. noticed by using polarized light microscopy that, during static creep tests, the progressive recruitment of collagen fibers was responsible for the increase in strain over time [71].

During static stress relaxation tests, the strain is maintained constant and the stress is observed to decrease over time until it finally reaches a steady value. Relaxation experiments at different strain levels of different types of ligaments and tendons have different relaxation times. For example, Thornton et al. showed that for female rabbit MCLs at a 0.05-strain level and 14 MPa-initial stress, the stress decreases by about 34.8 percent within 20 minutes [70]. Some studies indicates that the stress does not reach a steady value during relaxation experiments even after 100-240 seconds [50, 35, 7]. Some investigators proved that the relaxation time at higher strain levels was smaller than the relaxation time at smaller strain levels [27, 35, 41]. Gupta et al. revealed by using confocal microscopy that during relaxation tests adjacent collagen fibers were sliding relative to each other within the inter-fiber ground

substance. Thus, they suggested that the inter-fiber ground substance plays a significant role in stress relaxation [33].

The relation between creep and stress relaxation has been investigated by performing creep and relaxation experiments at the corresponding stress and strain levels, respectively. Provenzano et al. performed creep and relaxation tests of rat MCLs while Hingorani et al. performed creep and relaxation tests of rabbit MCLs. They concluded that stress relaxation proceeds faster than creep for the corresponding strain and stress levels [50, 35].

Effect of Cross-links on Mechanical Properties

The locations and types of cross-links in ligaments and tendons are still not known [57]. However, it is well known that microfibrils are stabilized by covalent cross-links [58, 13]. The density of the cross-links increases with aging [9]. Couppe et al. collected stress-strain data of in vivo tests of patellar tendons of young men (27 $\pm$ 2 years old) and old men (67 $\pm$ 3 years old) and determined that the stiffness of patellar tendons in old men was greater than the stiffness of patellar tendons in young men [9].

The increase in cross-links affects the mechanical properties by producing an increase in the stiffness of ligaments and tendons [54, 34]. The effect of cross-links on the tensile behavior of ligaments and tendons has been studied by testing specimens from animals with different ages [9] or by treating the specimens with chemicals that digest or increase the cross-links [34, 54].

Recently, Puxkandl et al. and Hansen et al. 's studies showed that the increase in cross-links changes the mechanical properties by producing an increase in stiffness [54, 34]. Puxkandl et al. studied the effect of cross-links in tendons by performing tensile tests of normal rat tail tendons and chemically treated rat tail tendons in which the cross-links were digested. They found that the ultimate load of normal rat tail tendons was much higher than the ultimate load of chemically treated rat tail tendons, but the ultimate deformations for these two groups of tendons were not significantly different. Thus, they concluded that the lack of cross-links reduced the ultimate fracture load without a large decrease in extension [54]. Hansen et al. performed tensile tests on single fibrils and fascicles of normal rat tail tendons and chemically treated rat tail tendons with increased cross-links. They found that the elastic modulus of chemically treated rat tail tendons at the fibril level considerably increased while it only slightly increased at the fascicle level. Thus, they concluded that the stiffness of the whole tissue mainly depended on the cross-links in collagen fibrils [34].

Preconditioning Experiments

Preconditioning is an experimental procedure in which cyclic loading is applied to soft biological specimens before recording the results of mechanical testing until the stress-strain curves from successive cycles remain unchanged. Hysteresis in successive cycles also decreases during preconditioning due to the changes occurring in the internal structure of the tissues [26]. As many other biological tissues, ligaments and tendons are usually preconditioned before performing tensile, relaxation, creep and hysteresis tests. Preconditioning can

be performed by controlling the load or the displacement. In load controlled experiments, the maximum load of each cycle is kept constant while, in displacement controlled experiments, the maximum displacement of each cycle is maintained constant.

Preconditioning significantly influences the mechanical properties of ligaments and tendons. For example, Schatzmann et al. performed tensile tests of human quadricep tendons and patellar ligaments before and after preconditioning. They found that the ultimate failure load and the stiffness in the linear region of these tissues were lower after preconditioning [60]. Graf et al. performed relaxation experiments of primate patellar tendons before and after preconditioning and showed that the relaxation times were lower after preconditioning [31].

The mechanism of softening during preconditioning is still unclear. Yahia and Drouin suggested that the interfibrillar matrix containing water and other material such as proteoglycans and hyaluronic acid might be associated with the observed hysteresis during the preconditioning process. They compared the energy absorption (area in a hysteresis loop) of the first and the last hysteresis loops during preconditioning of normal canine anterior cruciate ligaments (ACLs) and treated canine ACLs in which the hyaluronic acid was enzymatically digested. They found that the energy absorption of the first hysteresis loop of treated ACLs was much smaller than the energy absorption of the first hysteresis loop of normal ACLs while they were not significantly different at the last loops for both groups [80].

1.3.2 Review of Mathematical Models

Models for Tensile, Relaxation and Creep Responses

Several researchers in biomechanics have not only modeled the gross mechanical behavior of ligaments and tendons but also tried to understand the role of their internal structure in defining their mechanical behavior. Thus, mechanical models have been created by taking into the account the role of the individual components of the tissues. The approach used to model the mechanical behavior of materials by accounting for their structure is called the structural approach. There are several structural models that illustrate the quasi-static tensile behavior but not many of these models are extended to describe creep and stress relaxation phenomena.

Many researchers assumed in their models that the mechanical behavior of ligaments and tendons is dominated by the collagenous fibers and that the collagen fibers are aligned in one direction, the direction of physiological loading [74, 54, 15, 17]. The interaction between the matrix surrounding fibers and the fibers themselves remain unclear and several assumptions have been made [74, 54, 15, 17].

Some researchers claimed that the matrix had an important role in defining the overall mechanical behavior of ligaments and tendons [74, 54]. Thus, they model the mechanics of these tissues by considering both the collagen fibers and the surrounding matrix. In his early work [74], Viidik assumed that the total strain of the tissue was a summation of the total strain of the fibers and the matrix's strain. The matrix was modeled as a parallel arrangement of

a linear spring and dashpot while fibers were modeled as a parallel arrangement of several springs having different lengths and stiffness. The springs with different lengths were introduced to model the different waviness of the collagen fibers. These springs became active at different lengths in carrying the load in order to represent the fiber's recruitment during tissue's stretching. The model could describe the nonlinearity in the toe region of tensile stress-strain curves and was extended to describe the stress relaxation phenomenon. The comparison of the numerical results with experimental data was not carried out in his work [74]. Puxkandl et al. also modeled the tendons by assuming that the total strain of the tissues was a summation of the total strain of the collagen fibrils and matrix's strain. Both the fibrils and the matrix were modeled as Kelvin-Voigt elements. The model fit the tensile experimental data of rat tail tendons well but was not used for creep and stress relaxation responses [54].

Several experts in biomechanics modeled the tensile behavior of ligaments and tendons by neglecting the effect of the matrix and assumed that only the collagenous fiber component was responsible for resisting the force applied to the tissues. Therefore, the total strain of the fibers was assumed to be equal to the total strain of the tissues. De Vita and Slaughter structurally modeled the tensile behavior of ligaments at different strain rates. The ligament was modeled as a parallel arrangement of Kelvin-Voigt elements. Each Kelvin-Voigt element represented a collagen fiber and was assumed to become taut at different stretches. The fiber's recruitment process was described by a Weibull distribution function. The model could fit well the tensile experimental data at different strain rates [15].

Other investigators suggested that collagen fibers were purely elastic and dominated the elastic properties of ligaments and tendons [17]. Decraemer et al. proposed a mechanical model to describe the quasi-elastic stress-strain relation of soft tissues by assuming that all the fibers are aligned in the direction of the loading. The tissues were modeled as numerous linear springs in parallel which would become active at different strains. Each spring represented a fiber and had the same Young's modulus. The strains at which the springs became active were described by using a normal distribution function. The model showed good agreement with the experimental data collected by performing tensile tests on human vein and human tympanic membrane [17].

The above-cited works focused on modeling mainly the tensile behavior of collagenous tissues and were only extended in some cases to include the description of stress relaxation. Thornton et al. showed that ligament creep behavior could be predicted from stress relaxation by incorporating fiber's recruitment in the creep model [69]. The stress relaxation function in the QLV model used in the cited study was determined by fitting the stress relaxation data. The stress relaxation function was then inverted to predict the creep function. The creep function was used to estimate the Young's modulus of a single fiber. The fibers were assumed to support load only when they were straight. The results showed that the model was able to predict creep from stress relaxation experimental data with reasonable accuracy. Thus, they suggested that fibers' recruitment occurred during creep and was important in understanding both the viscoelastic experimental and theoretical findings [69].

Models on the Effects of Cross-links

Because the effect of cross-links on determining the mechanical behavior of ligaments and tendons is not well understood, to date there is no micro-structural model at the fibril level that accounts for them. Few simple viscoelastic models of tendons have been proposed to represent the contribution of fibrils and cross-links between them [54, 33].

Puxkandl et al. modeled tendons as a series of two different Kelvin-Voigt elements. The first Kelvin-Voigt element represented the contribution of collagen fibrils with the cross-links between them. The second Kelvin-Voigt element represented the contribution of the proteoglycan-matrix. The elastic modulus of the spring in the first Kelvin-Voigt element was assumed to depend on the density of the cross-links in the fibrils while the viscosity of the dashpot in the first Kelvin-Voigt element was assumed to be due to friction between molecules in fibrils. The model was not compared to the experimental data at the fibril level but was shown to fit tensile data of normal and cross-link-deficient rat tail tendons well [54].

Gupta et al. proposed a viscoelastic model of tendons as a series of a Kelvin-Voigt element with two different Maxwell elements. The Kelvin-Voigt element represented the collagen fibrils with the cross-links between them. One Maxwell element represented the proteoglycan-matrix between fibrils while the other Maxwell element represented the ground substance between fibers. The model fitted well stress relaxation data at both fibril and fiber levels. The authors suggested that the stress relaxation of tendons could be described by using at least two different Maxwell elements. The tensile behavior with different density of cross-

links was not studied in this work [33].

Preconditioning Models

The role of the structural components in ligaments and tendons during preconditioning procedure is still unclear. Moreover, there is no protocol for preconditioning that is widely used among experimentalists. Few authors have extended their models to describe preconditioning. For example, Sverdlik and Lanir proposed a mathematical model to describe the tensile and stress relaxation behavior of tendons by including preconditioning effects [66]. A single fiber was assumed to be quasi-linear viscoelastic. The quasi-linear viscoelastic model is a phenomenological model proposed by Fung [26] and used to illustrate the viscoelastic behavior of soft tissues. In the quasi-linear viscoelastic model, the stress is defined as a single integral of a relaxation function, which is separable into the product of a function of time and a function of strain. In the work by Sverdlik and Lanir, the fibers were assumed to have different waviness and become straight at different strains defined by a Beta probability distribution function. The fiber's straightening strain was assumed to change over time during preconditioning due to increasing fiber elongation. The results obtained from the model for stress relaxation before and after preconditioning had good agreement with some experimental data. The fitting of the model to tensile data before preconditioning was good but no comparison of the model with tensile data after preconditioning was presented. The work by Sverdlik and Lanir is the first attempt made to model preconditioning [66]. Ciarletta et al. used a pseudo-hyperelastic constitutive model for the tensile behavior of tendons,

which was extended to describe the effect of preconditioning. The authors assumed that the stress softening and energy dissipation associated with preconditioning is determined by the breakage of fibers. The model was shown to have good agreement with the tensile loading and unloading experimental data from tendons [6].

The mathematical models published in the biomechanics literature have some parameters which are related to the structure of ligaments and tendons while some others are not linked to the structural changes that occur in these tissues during preconditioning. A structural model for ligaments and tendons that can predict the number of cycles required for full preconditioning and can describe both stress-controlled and strain-controlled tests could be a valuable tool to establish correct preconditioning protocols.

1.4 Conclusions

The mechanical properties of ligaments and tendons have been studied theoretically and experimentally. Different types of forces or deformations have been experimentally applied to ligaments and tendons. Tensile, creep, stress relaxation and hysteresis experiments are the most commonly performed and physiologically relevant experiments. In theoretical studies, several structural models have been presented to describe the responses of ligaments and tendons to different mechanical stimuli. The main purpose of these studies has been to understand the relation existing between the physiology of ligaments and tendons and their mechanical responses. Indeed, it is well know that the mechanics of ligaments and tendons

is strongly influenced by their complicated structure.

To our knowledge, a general structural framework that can describe the tensile behavior, relaxation, creep and preconditioning in ligaments and tendons is still missing. Therefore, formulating such framework is important since it can lead to a better understanding of the role of the tissue's components in different physiological loading scenarios. Therefore, in this dissertation, a mathematical framework describing tensile, stress relaxation and creep phenomena was formulated and presented in Chapter 2. The same mathematical framework was also extended in Chapter 4 to illustrate the stress softening and hysteresis observed during strain-controlled preconditioning experiments. Finally, viscoelastic models of a single collagen fiber accounting for the influence of the cross-links were formulated and presented in Chapter 3 to describe the results of incremental stress relaxation tests.

Chapter 2

Mathematical Models for Creep, Relaxation and Strain Stiffening in Ligaments and Tendons

2.1 Introduction

Collagenous tissues such as ligaments and tendons are characterized by long-term viscoelastic properties. They exhibit a slow continuous increase in strain over time, or creep, when subjected to a constant stress and a slow continuous decrease in stress over time, or stress relaxation, when subjected to a constant strain. The micro-structural origin of the long-term viscoelasticity of these tissues is still unknown and subject of debate among experts in

biomechanics. Synchrotron X-ray scattering studies coupled with mechanical testing have indicated that the collagen fibers, which constitute the main load bearing components of the tissues, may be intrinsically viscoelastic [54] and that the interface between the collagen fibers and the surrounding proteoglycan-rich matrix may also determine the viscoelasticity of the tissues [53]. In many studies, however, the viscoelasticity of the tissues has been attributed to the proteoglycan-rich matrix that surrounds the collagen fibers [47, 4, 22, 33].

The difference in the experimental findings suggests the need for more studies aimed at understanding the mechanisms that control the long-term viscoelasticity in ligaments and tendons. As suggested early by Fung [26] and experimentally observed by Thornton et al. [69] and Gupta et al. [33], different structural components of the tissues and their organization are responsible for different viscoelastic phenomena: the recruitment of collagen fibers governs creep [69] while sliding between collagen fibrils/fibers due to the presence of the proteoglycan-rich matrix is predominant in relaxation [33]. Together with histo-mechanical experiments, mathematical models that are formulated by accounting for the micro-structure of collagenous tissues can help in elucidating the relative role of different components of these tissues in determining their long-term viscoelasticity.

The most successful viscoelastic models for creep and relaxation in collagenous tissues are the quasi-linear viscoelastic (QLV) models introduced by Fung [26]. Despite their enormous success, the QLV models have been shown to have limitations since they cannot account for creep rate and relaxation rate dependency as exhibited by ligaments at high stress and strain levels, respectively [50] and, most importantly, cannot interrelate creep and relaxation [70,

42]. Nonlinear viscoelastic theories, such as Schapery's theory and the modified superposition method, have been proposed to overcome some of the limitations of the QLV models [52]. Both the QLV models and the newly proposed models are, however, phenomenological models with parameters that lack physical meaning and do not relate to the micro-structural changes that are associated with creep and relaxation.

The long-term viscoelasticity of ligaments and tendons has been described by several structurally-based constitutive models [18, 78, 23, 37, 69, 66, 73, 7, 5, 21]. However, only in the linear viscoelastic model proposed by Thornton et al. [69] creep was predicted from relaxation and this was accomplished by accounting for the recruitment of collagen fibers. By performing histological studies, the authors observed that the collagen fibers were gradually recruited during creep due to the increase in strain over time. Moreover, they found that during relaxation only a discrete group of fibers was recruited at the fixed constant strain. Their model was, however, formulated by assuming a specific geometry for the ligaments and arrangement of the wavy collagen fibers.

A simple constitutive framework for modeling relaxation and creep including the strain stiffening in parallel-fibered collagenous tissues is presented. The collagen fibers are assumed to be oriented along the physiological direction of loading. They gradually lose their waviness and become straight under strain at which point they behave as linear elastic springs. The collagen fibers are arranged in parallel with the surrounding matrix that exhibits a Maxwell-type viscoelastic behavior. The model parameters that define the relaxation and strain stiffening phenomena are estimated by using published experimental data by Hingorani et

al. [35] on rabbit medial collateral ligaments and are then used to predict creep. The influence of each parameter on describing the long-term viscoelastic properties of collagenous tissues is also analyzed.

2.2 Model Formulation

In this study, the overall viscoelastic behavior of ligaments and tendons is assumed to be determined by its major components: the collagen fibers and the intervening proteoglycan-rich matrix. The collagen fibers are assumed to be aligned along the direction of loading. They are wavy when unstrained and straighten gradually as the overall tissue's strain increases. After becoming straight, the collagen fibers behave as linear elastic springs with equal elastic modulus. The proteoglycan-rich matrix is assumed to behave as a Maxwell-type viscoelastic material, which is described by a linear elastic spring and linear viscous dashpot arranged in series. A schematic of the proposed model, which is described in detail hereafter, is shown in Figure 2.1.

2.2.1 Modeling Framework

Ligaments and tendons are modeled as parallel arrangements of linear elastic collagen fibers, each having different waviness and a linear viscoelastic proteoglycan-rich matrix. Then, the total stress of the tissue, $\sigma(t)$, where t denotes the time, is given by

$$\sigma(t) = \sigma_f(t) + \sigma_m(t)\,, \tag{2.1}$$

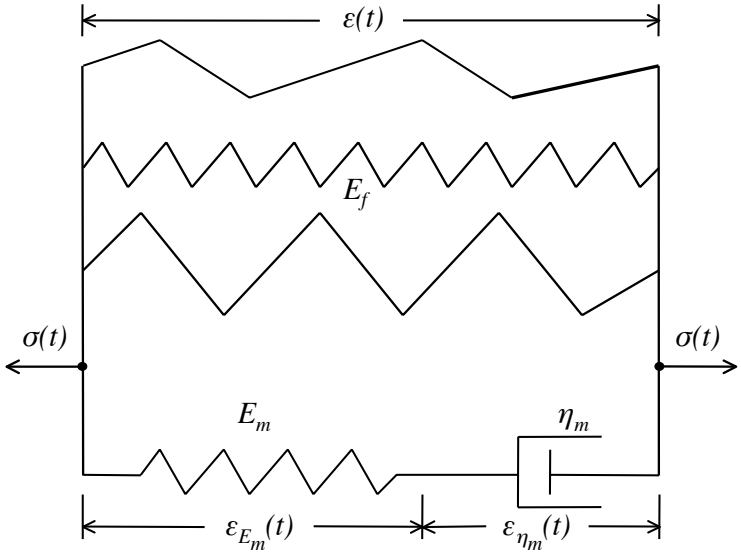

Figure 2.1: Schematic of the viscoelastic model.

where $\sigma_f(t)$ is the stress of the collagen fibers and $\sigma_m(t)$ is the stress of the matrix. Moreover, the strain of the tissue, $\varepsilon(t)$, is

$$\varepsilon(t) = \varepsilon_f(t) = \varepsilon_m(t)\,, \tag{2.2}$$

where $\varepsilon_f(t)$ is the strain of the fibers and $\varepsilon_m(t)$ is the strain of the matrix.

Due to the arrangement in series of the elastic spring and viscous dashpot of the matrix, one has that

$$\sigma_m(t) = \sigma_{E_m}(t) = \sigma_{\eta_m}(t)\,, \tag{2.3}$$

where $\sigma_{E_m}(t)$ and $\sigma_{\eta_m}(t)$ are the elastic and viscous stresses of the matrix, respectively.

Furthermore, the strain of the matrix, $\varepsilon_m(t)$, is

$$\varepsilon_m(t) = \varepsilon_{E_m}(t) + \varepsilon_{\eta_m}(t)\,, \tag{2.4}$$

where $\varepsilon_{E_m}(t)$ and $\varepsilon_{\eta_m}(t)$ are the strain of the spring and the strain of the viscous dashpot for the matrix, respectively.

The elastic stress of the matrix is defined as

$$\sigma_{E_m}(t) = E_m \varepsilon_{E_m}(t) \tag{2.5}$$

where E_m denotes the elastic modulus of the matrix. The viscous stress of the matrix is defined as

$$\sigma_{\eta_m}(t) = \eta_m \varepsilon'_{\eta_m}(t)\,, \tag{2.6}$$

where η_m denotes the viscous modulus of the matrix and a prime denotes differentiation with respect to t.

After noting that $\sigma_m(t) = \sigma_{E_m}(t)$ from Eq. 2.3 and that $\sigma_m(t) = \sigma(t) - \sigma_f(t)$ from Eq. 2.1, Eq. 2.5 can be rewritten as

$$\varepsilon_{E_m}(t) = \frac{\sigma(t) - \sigma_f(t)}{E_m}\,. \tag{2.7}$$

Moreover, since $\varepsilon_{\eta_m}(t) = \varepsilon_m(t) - \varepsilon_{E_m}(t)$ from Eq. 2.4 and $\varepsilon(t) = \varepsilon_m(t)$ from Eq. 2.2, Eq. 2.6 becomes

$$\sigma_{\eta_m}(t) = \eta_m \varepsilon'(t) - \eta_m \varepsilon'_{E_m}(t)\,. \tag{2.8}$$

By recalling that $\sigma_m(t) = \sigma_{\eta_m}(t)$ from Eq. 2.3 and using Eq. 2.8, Eq. 2.1 takes the form

$$\sigma(t) = \sigma_f(t) + \eta_m \varepsilon'(t) - \eta_m \varepsilon'_{E_m}(t)\,. \tag{2.9}$$

Finally, after computing $\varepsilon'_{E_m}(t)$ from Eq. 2.7 and substituting the resulting expression into Eq. 2.9 one obtains the governing equation for the system described in Fig. 2.1

$$\sigma'(t) + \frac{E_m}{\eta_m}\sigma(t) = \sigma'_f(t) + \frac{E_m}{\eta_m}\sigma_f(t) + E_m\varepsilon'(t)\,. \tag{2.10}$$

The ratio $\frac{\eta_m}{E_m}$ is a characteristic time, τ, usually called the *relaxation time*. The above governing equation can be then rewritten as

$$\sigma'(t) + \frac{\sigma(t)}{\tau} = \sigma'_f(t) + \frac{\sigma_f(t)}{\tau} + E_m\varepsilon'(t)\,. \tag{2.11}$$

Once the stress of collagen fibers, $\sigma_f(t)$, is defined, the governing Eq. 2.11 with appropriate initial condition can be used to describe relaxation, creep, and strain stiffening phenomena.

2.2.2 Stress of Collagen Fibers

The stress of the fibrous component of the tissue, $\sigma_f(t)$, is defined by using a structural approach as previously done by other investigators [43, 15, 16]. The collagen fibers are assumed to become straight at different strains, $\varepsilon_s \geq 0$, defined by the following Weibull probability density function

$$p(\varepsilon_s) = \frac{\alpha}{\beta}\left(\frac{\varepsilon_s}{\beta}\right)^{\alpha-1} e^{-\left(\frac{\varepsilon_s}{\beta}\right)^{\alpha}} \quad \text{with} \quad \int_0^{\infty} p(\varepsilon_s)d\varepsilon_s = 1\,, \tag{2.12}$$

where $\alpha > 0$ is the so-called *shape parameter* and $\beta > 0$ is the so-called *scale parameter*. The stress of collagen fibers is given for $\varepsilon \geq \varepsilon_s$ by

$$\sigma_f(t) = \int_0^{\varepsilon(t)} E_f(\varepsilon(t) - \varepsilon_s) p(\varepsilon_s) d\varepsilon_s \,, \tag{2.13}$$

where E_f denotes the elastic modulus of each straight collagen fiber. The above equation can also be written as (see Appendix A)

$$\sigma_f(t) = E_f \left[\varepsilon(t) - \frac{\beta}{\alpha} \gamma \left(\frac{1}{\alpha}, \left(\frac{\varepsilon(t)}{\beta} \right)^{\alpha} \right) \right] , \tag{2.14}$$

where

$$\gamma(x, y) = \int_0^y \xi^{x-1} e^{-\xi} d\xi \tag{2.15}$$

is the so-called *lower incomplete gamma function.*

2.2.3 Stress Relaxation

Relaxation is a continuous decrease in stress that is observed in collagenous tissues when they are subjected to constant strain. First, one must note that for any strain history, $\varepsilon(t)$, the solution to the governing Eq. 2.11 is

$$\sigma(t) = \sigma_f(t) + \frac{\int_0^t E_m \varepsilon'(t) e^{t/\tau} dt + C}{e^{t/\tau}} \,, \tag{2.16}$$

where C is a constant that is determined by the initial condition. In order to describe relaxation by using Eq. 2.16, the strain history of the tissue, $\varepsilon(t)$, is assumed to have the

form

$$\varepsilon(t) = \begin{cases} at & \text{for } 0 \leq t < t_0\,, \\ \varepsilon_0 & \text{for } t \geq t_0\,, \end{cases} \tag{2.17}$$

where a, ε_0 and t_0 are constants and $at_0 = \varepsilon_0$. For $0 \leq t < t_0$, $\varepsilon'(t) = a$ and, hence, Eq. 2.16 takes the form

$$\sigma(t) = \sigma_f(t) + E_m a\tau[1 - e^{-\frac{t}{\tau}}] + Ce^{\frac{-t}{\tau}}\,. \tag{2.18}$$

By imposing the initial condition $\sigma(0) = 0$ and noting that $\varepsilon(0) = 0$, one obtains that $C = 0$ in Eq. 2.18. Therefore, in the interval $0 \leq t < t_0$, the stress of the tissue is

$$\sigma(t) = \sigma_f(t) + E_m a\tau[1 - e^{-\frac{t}{\tau}}]\,. \tag{2.19}$$

For $t > t_0$, $\varepsilon(t) = \varepsilon_0$ and $\varepsilon'(t) = 0$ so that Eq. 2.16 becomes

$$\sigma(t) = \sigma_f(t) + Ce^{\frac{-t}{\tau}}\,. \tag{2.20}$$

By using the initial condition $\sigma(t_0) = \sigma_f(t_0) + E_m a\tau[1 - e^{-\frac{t_0}{\tau}}]$ computed by using Eqs. 2.19-2.20, one obtains that

$$C = E_m a\tau(e^{\frac{t_0}{\tau}} - 1)\,. \tag{2.21}$$

For $t > t_0$, the stress of the tissue can be written as

$$\sigma(t) = \sigma_f(t) + E_m a\tau\left(e^{\frac{t_0 - t}{\tau}} - e^{-\frac{t}{\tau}}\right)\,. \tag{2.22}$$

The above equation describes the relaxation that is exhibited by the tissue when a constant strain ε_0 is applied. In this case, the stress of the collagen fibers, $\sigma_f(t)$, defined by Eq. 2.14

is constant and has the form

$$\sigma_f(t) = E_f \left[\varepsilon_0 - \frac{\beta}{\alpha} \gamma \left(\frac{1}{\alpha}, \left(\frac{\varepsilon_0}{\beta} \right)^{\alpha} \right) \right] . \tag{2.23}$$

2.2.4 Nonlinear Strain Stiffening Behavior

A nonlinear strain stiffening behavior is observed in collagenous tissues subjected to a constantly increasing strain. As already noted, the solution to Eq. 2.11, for any strain history, is

$$\sigma(t) = \sigma_f(t) + \frac{\int_0^t E_m \varepsilon'(t) e^{t/\tau} dt + C}{e^{t/\tau}} . \tag{2.24}$$

In this case, the strain history has the form $\varepsilon(t) = bt$ for $t > 0$ where b is a constant. Moreover, since the initial condition is $\sigma(0) = 0$ and, thus, $\varepsilon(0) = 0$, it follows that $C = 0$ in Eq. 2.24 so that the stress of the tissue is

$$\sigma(t) = \sigma_f(t) + E_m b \tau [1 - e^{-\frac{t}{\tau}}] . \tag{2.25}$$

2.2.5 Creep

Creep is a continuous deformation of the tissue under constant stress. In this case, the governing Eq. 2.11 needs to be solved to compute the strain of the tissue, $\varepsilon(t)$. Firstly, by applying Leibniz's rule for differentiation of an integral to Eq. 2.13 one obtains that

$$\sigma_f'(t) = E_f \varepsilon'(t) \int_0^{\varepsilon} p(\varepsilon_s) d\varepsilon_s . \tag{2.26}$$

It must be noted that for $p(\varepsilon_s)$ defined by Eq. 2.12, $\int_0^{\varepsilon} p(\varepsilon_s)d\varepsilon_s = 1 - e^{-(\frac{\varepsilon}{\beta})^{\alpha}}$, which is the Weibull cumulative density function. Thus, Eq. 2.26 can be written as

$$\sigma_f'(t) = E_f\varepsilon'(t)\left(1 - e^{-\left(\frac{\varepsilon}{\beta}\right)^{\alpha}}\right). \tag{2.27}$$

By using Eq. 2.27, the governing Eq. 2.11 can be rewritten as

$$\varepsilon'(t) = \frac{\sigma'(t) + \frac{\sigma(t)}{\tau} - \frac{\sigma_f}{\tau}}{E_f\left(1 - e^{-\left(\frac{\varepsilon}{\beta}\right)^{\alpha}}\right) + E_m}. \tag{2.28}$$

Equations 2.27-2.28 form a system of ordinary differential equations that can be solved numerically to find $\varepsilon(t)$ and $\sigma_f(t)$ after assigning the initial conditions.

In order to describe creep, the stress history of the tissue, $\sigma(t)$, is assumed to have the form

$$\sigma(t) = \begin{cases} ct & \text{for } 0 \le t < t_0\,, \\ \\ \sigma_0 & \text{for } t \ge t_0\,, \end{cases} \tag{2.29}$$

where c, σ_0, and t_0 are constants and $ct_0 = \sigma_0$.

For $0 \le t < t_0$, $\sigma'(t) = c$ and $\sigma(t) = ct$. Then, Eq. 2.28 becomes

$$\varepsilon'(t) = \frac{c + \frac{ct}{\tau} - \frac{\sigma_f}{\tau}}{E_f\left(1 - e^{-\left(\frac{\varepsilon}{\beta}\right)^{\alpha}}\right) + E_m}, \tag{2.30}$$

which can be solved numerically together with Eq. 2.27 to find the strain of the tissue, $\varepsilon(t)$, by imposing the initial conditions $\varepsilon(0) = 0$ and $\sigma_f(0) = 0$.

For all $t > t_0$, $\sigma(t) = \sigma_0$ and $\sigma'(t) = 0$. Thus, Eqs. 2.28 takes the form

$$\varepsilon'(t) = \frac{\frac{\sigma_0}{\tau} - \frac{\sigma_f}{\tau}}{E_f\left(1 - e^{-\left(\frac{\varepsilon}{\beta}\right)^{\alpha}}\right) + E_m}. \tag{2.31}$$

The above equation and Eq. 2.27 form a system of ordinary differential equations that can be solved numerically to determine the creep response of the tissue under constant stress σ_0. The initial conditions, $\varepsilon(t_0)$ and $\sigma_f(t_0)$, can be obtained form experimental data and by using Eq. 2.13.

2.3 Results

There were 5 parameters $\{E_f, \alpha, \beta, E_m, \tau\}$ that needed to be computed to describe the viscoelastic properties of ligaments and tendons by using the proposed modeling framework. Experimental data on relaxation, creep, and strain stiffening phenomena, published results by Hingorani et al. [35] on rabbit medial collateral ligaments, were used to analyze the capability of the model. To the authors' knowledge, these data together with similar data published by the same group [50] were the only complete set of data published in the biomechanics literature that interrelated creep and relaxation.

In the above-cited study [35], stress relaxation experimental data were collected by subjecting the ligament to a constant strain, $\varepsilon_0 = 0.81\%$, along its physiological loading direction. Creep experimental data were also collected by subjecting the contralateral ligament to a constant stress, $\sigma_0 = 2.98$ MPa, along the physiological loading direction. The constant stress value used during creep was chosen to be the peak stress observed during relaxation at $\varepsilon_0 = 0.81\%$ in order to compare relaxation and creep responses. Moreover, isochronal stress-strain data were derived from relaxation data collected for different values of constant strains at the

same time, $t = 2.4$ s. The relaxation data were then successfully fitted by the equation $\sigma = 2.4488t^{-0.2619}$, the creep data by the equation $\varepsilon = 0.60681t^{0.13927}$, and the stress-strain curve that described the strain-stiffening phenomenon by the equation $\sigma = 4.095\varepsilon^{1.835}$ [35]. These three equations were used in this study to generate the relaxation, strain-stiffening, and creep data that were needed to compute the model parameters and evaluate its prediction.

The two parameters, E_m and τ, which characterized the mechanical response of the proteoglycan-rich matrix, and the constant stress of the collagen fibers, σ_f, were evaluated by curve fitting Eq. 2.22 to the stress relaxation data generated by the equation $\sigma = 2.4488t^{-0.2619}$ and published by Hingorani et al. [35]. It must be noted that $\varepsilon_0 = 0.81\%$ and, therefore, $t_0 = 0.081$ in Eq. 2.22 since the experiments were conducted at a constant strain rate, $\varepsilon'(t) = a = 10\%/\text{s}$. The curve fitting was performed by employing the Levenberg-Marquardt nonlinear least squares algorithm implemented in Matlab (The MathWorks, Inc.) by imposing restrictions that E_m, τ, and σ_f were greater than zero. The results of the curve fitting were shown in Figure 2.2. The parameters were uniquely determined to be $E_m = 130.4$ MPa, $\tau = 14.91$ s, and $\sigma_f = 0.7962$ MPa with $R^2 = 0.9719$.

The three parameters, E_f, α, and β, which defined the response of the collagen fibers, were then computed by curve fitting Eq. 2.25 with Eq. 2.13 to the nonlinear stress-strain data describing strain-stiffening presented by Hingorani et al. [35]. The strain history was $\varepsilon(t) = bt$, where $b = 10\%/\text{s}$, and $E_m = 130.4$ MPa and $\tau = 14.91$ s. The parameters were uniquely estimated to be $E_f = 3536$ MPa, $\alpha = 1.189$, and $\beta = 0.04124$ by using the Levenberg-Marquardt nonlinear least squares algorithm ($R^2 \approx 1$). In Figure 2.3, the

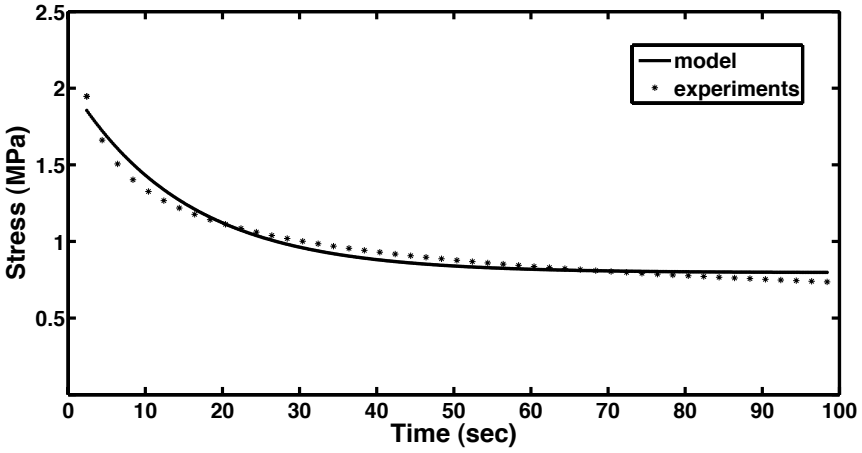

Figure 2.2: Stress relaxation data [35] and model fit with $E_m = 130.4$ MPa, $\tau = 14.91$ s, and $\sigma_f = 0.7962$ MPa ($R^2 = 0.9719$).

stress-strain data generated by the equation $\sigma = 4.095\varepsilon^{1.835}$ and the model fit were reported.

After determining all the model parameters, the creep behavior was *predicted* by numerically solving the system of ordinary differential equations formed by Eqs. 2.27 and 2.31 with $\sigma_0 = 2.98$ MPa as dictated by the experiments. The initial conditions were obtained from the experimental data for $t_0 = 2.4$ s, $\varepsilon(t_0) = 0.69\%$, and $\sigma_f(t_0)$ computed from Eq. 2.14. Figure 2.4 presented the creep data generated by using the equation $\varepsilon = 0.60681t^{0.13927}$ [35] and the model prediction with $E_m = 130.4$ MPa, $\tau = 14.91$ s, $E_f = 3536$ MPa, $\alpha = 1.189$, and $\beta = 0.04124$ as previously computed by fitting relaxation and strain stiffening data ($R^2 = 0.67$).

The effect of the model parameters in illustrating relaxation and creep responses were studied by varying their numerical values. The parameters that were not varied were fixed to

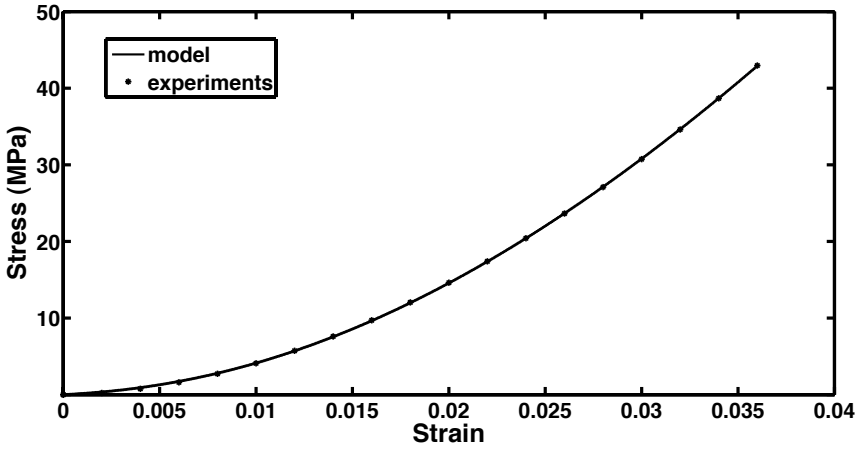

Figure 2.3: Nonlinear elastic stress-strain data describing strain stiffening [35] and model fit with $E_f = 3536$ MPa, $\alpha = 1.189$, and $\beta = 0.04124$ ($R^2 \approx 1$).

the numerical values computed by curve fitting the published relaxation and stress-strain data [35]. Figures 2.5 and 2.7 illustrated the influence of E_m on the relaxation and creep phenomena. One could observe that as E_m increased, the peak stress and the stress over time increased while creep remained almost unchanged. As shown in Figures 2.6 and 2.8, changes in τ influenced relaxation and creep similarly: both creep and relation reached faster a steady state value of strain and stress as τ decreased. In Figure 2.9, the creep response was presented for different values of the fiber's elastic modulus, E_f. It could be noted that as E_f increased, the strain of the tissue decreased over time.

Finally, the effects of the shape and scale parameters of the Weibull distribution that described the recruitment of collagen fibers during creep were analyzed. The creep behavior for different values of the shape parameter α was shown in Figure 2.10 while the correspond-

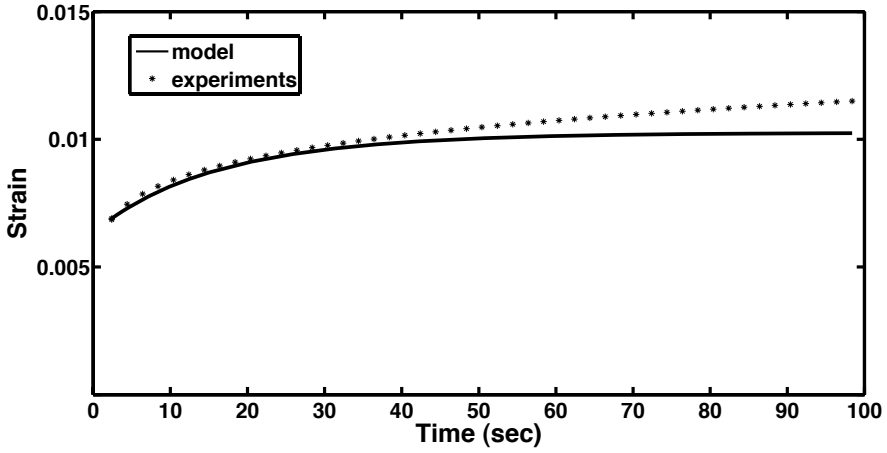

Figure 2.4: Creep data [35] and model prediction for values of the parameters computed by curve fitting relaxation and strain-stiffening data ($R^2 = 0.67$).

ing Weibull probability density function was presented in Figure 2.11. It can be seen from Figure 2.11 that for smaller values of α, more collagen fibers were recruited at lower values of the strain and the strain over time increased less while the tissue reached a steady state faster. Similarly, in Figure 2.12 one could observe that as the scale parameter β increased, the collagen fibers were recruited more uniformly. Therefore, the strain of the tissue over time increased more and reached a greater steady state value as presented in Figure 2.12.

2.4 Discussion and Conclusions

A simple model was presented to describe relaxation, creep, and strain-stiffening phenomena in parallel-fibered collagenous tissues. The model, which is schematically presented in Figure 2.1, was formulated by accounting for the mechanical contributions of the collagen fibers

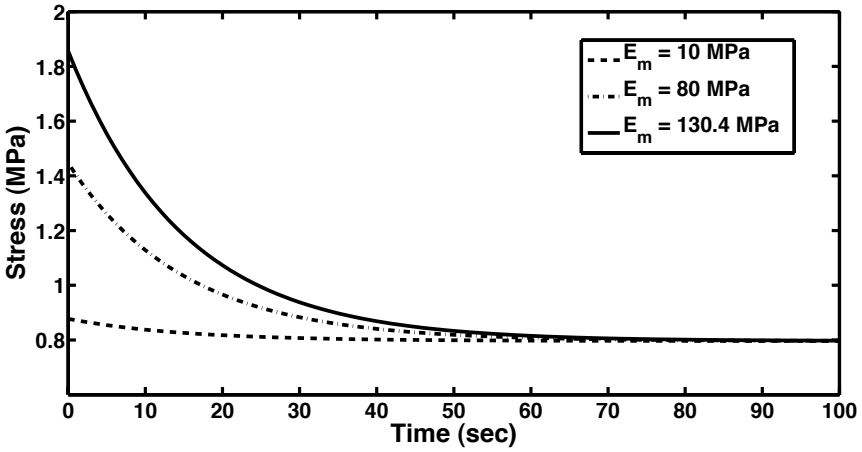

Figure 2.5: Influence of the elastic modulus of the proteoglycan-rich matrix E_m on relaxation.

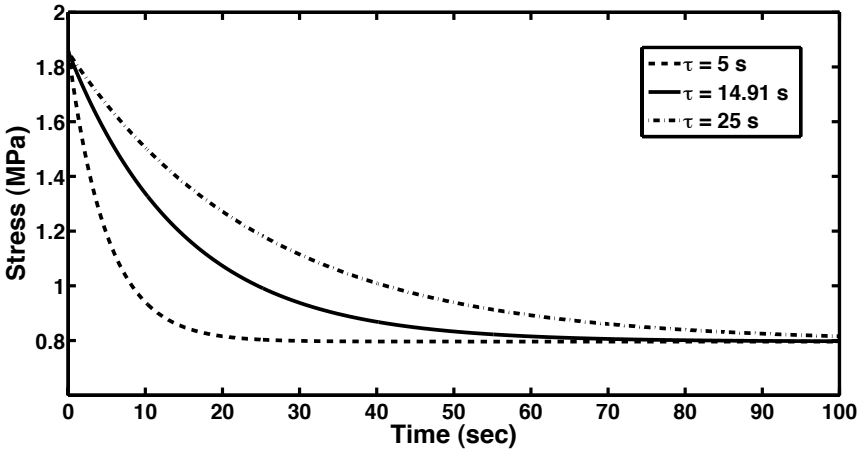

Figure 2.6: Influence of the relaxation time $\tau = \frac{\eta_m}{E_m}$ on relaxation.

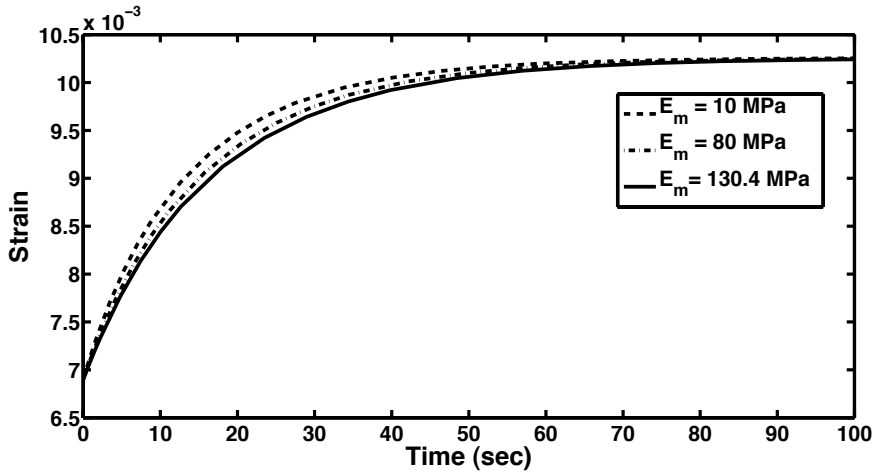

Figure 2.7: Influence of the elastic modulus of the proteoglycan-rich matrix E_m on creep.

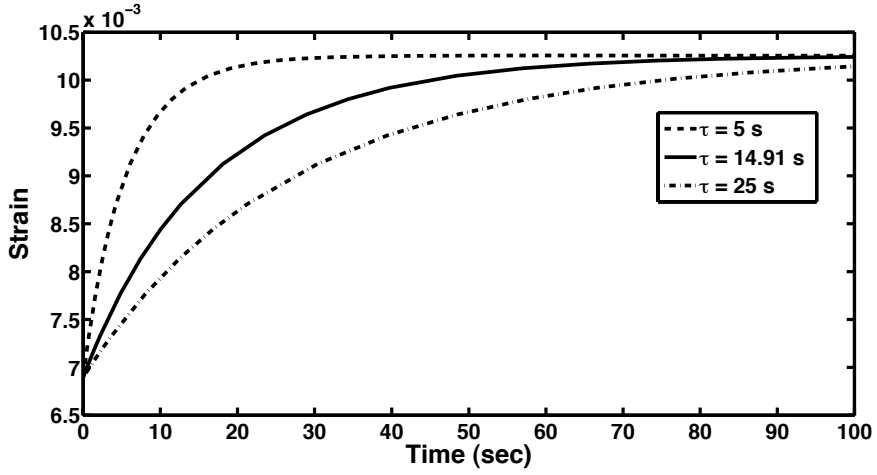

Figure 2.8: Influence of the relaxation time $\tau = \frac{\eta_m}{E_m}$ on creep.

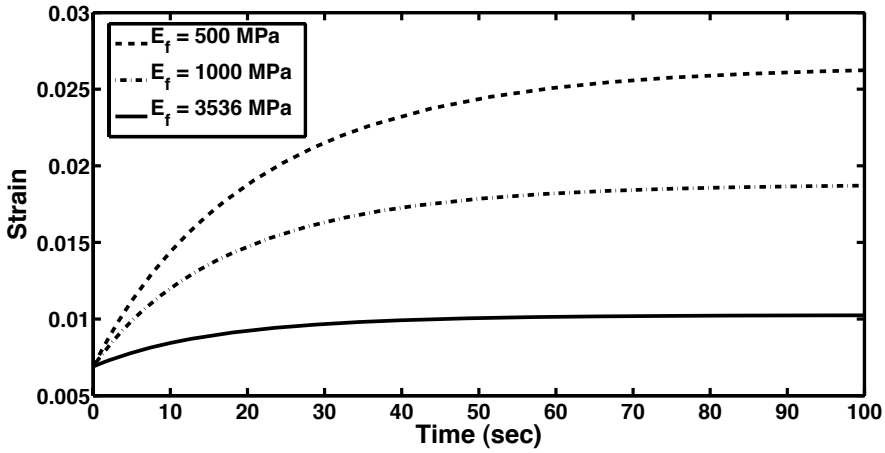

Figure 2.9: Influence of the elastic modulus of the collagen fiber E_f on creep.

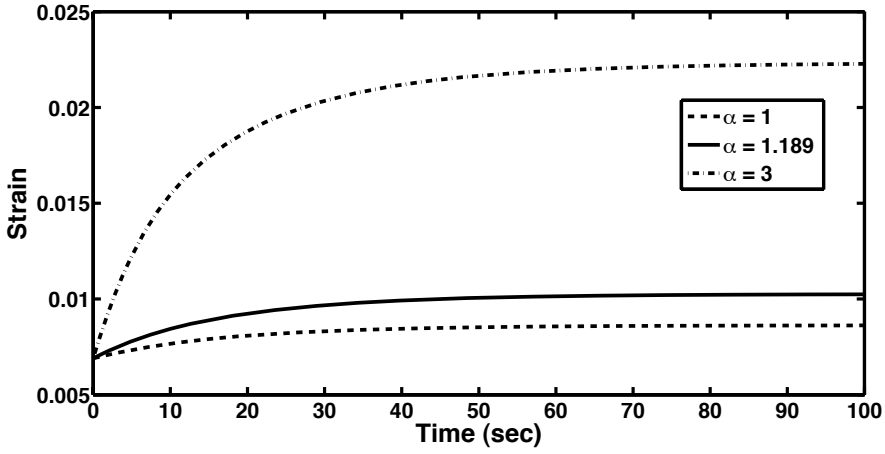

Figure 2.10: Effect of the shape parameter α of the Weibull probability density function on creep.

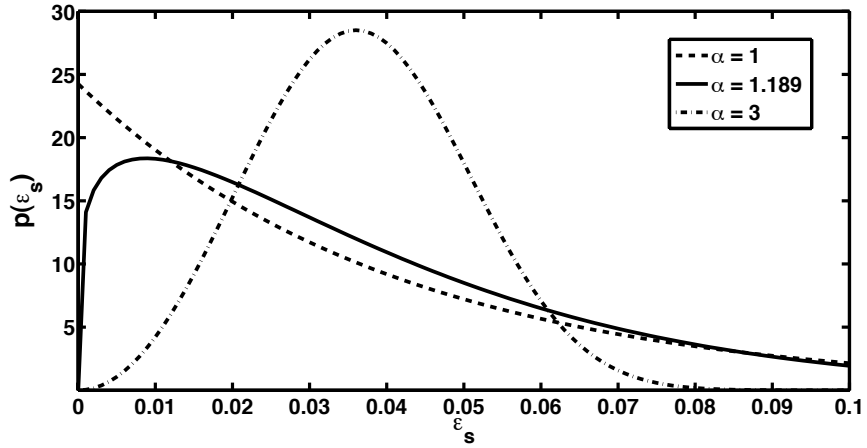

Figure 2.11: Effect of the shape parameter α on the Weibull probability density function.

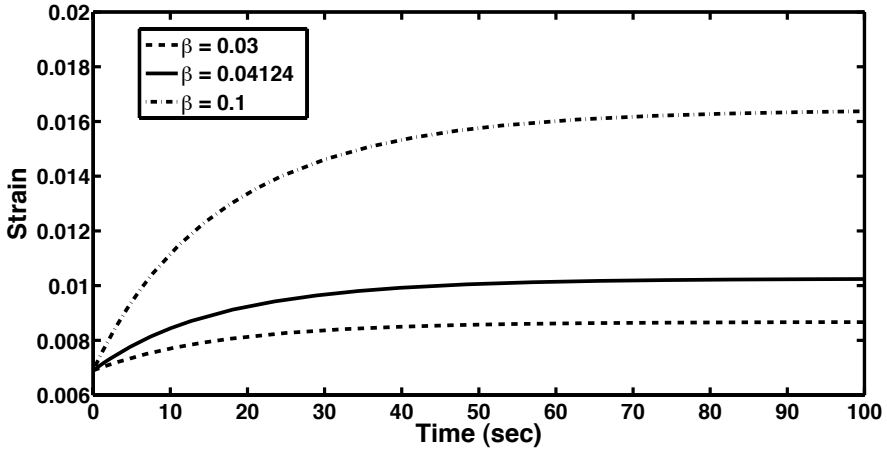

Figure 2.12: Effect of the scale parameter β of the Weibull probability density function on creep.

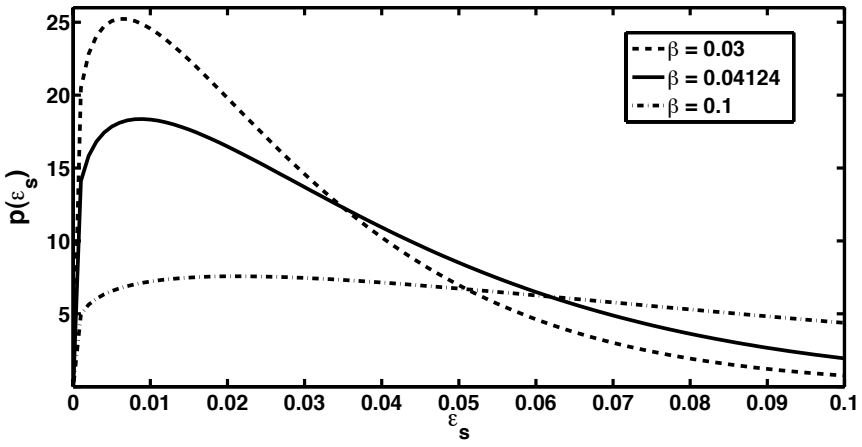

Figure 2.13: Effect of the shape parameter β of the Weibull probability density function on creep.

comprising the tissues and the proteoglycan-rich matrix that surrounds the collagen fibers. In agreement with experimental observations [33] and previous histo-mechanical studies [69], the recruitment of collagen fibers was assumed to be responsible for the creep response of the tissues. The relaxation response was mainly determined by the viscoelasticity of the proteoglycan-rich matrix. Due to the lack of experimental data, the model parameters were estimated by using published data on rabbit medial collateral ligaments by [35]. Although the results obtained were promising, additional experimental data were needed to fully validate the model and its predictions. For this reason, by varying the model parameters within the range of values obtained from curve fitting the experimental data, the model predictions were also presented.

Several structurally-based models have been proposed to describe the long-term viscoelas-

ticity of ligaments and tendons [69, 44, 18]. Unlike the cited models, the proposed model could describe relaxation and creep including the strain-stiffening phenomenon. The simple formulation presented here took into account important structural features of the tissues: the collagen fibers are gradually recruited during creep while the proteoglycan-rich matrix is mainly responsible for relaxation. The nonlinear strain-stiffening behavior typically observed in these tissues was described by assuming that the nonlinearity in the toe region of the stress-strain curve is determined by the gradual recruitment of collagen fibers.

The results of curve fitting the model to the relaxation and strain-stiffening data presented by Hingorani et al. [35] were presented in Figures 2.2 and 2.3 and the prediction of the creep response was presented in Figure 2.4. The elastic modulus and viscous modulus of the proteoglycan-rich matrix were found to be $E_m = 130.4$ MPa, $\eta_m = \tau E_m = 1944$ MPa s. The elastic modulus of the collagen fibers, E_f, was estimated to be 3.5 GPa which is within the range of values reported in the literature [25]. The shape parameter α and scale parameters β defined the strain-based recruitment process of collagen fibers during strain-stiffening and creep phenomena. The values computed by fitting the experimental data collected on rabbit medial collateral ligaments suggested that several fibers were straight and thus contributed to the total stress already at very small strains (see Figure 2.11 or 2.13, continuous line).

While the model displayed good agreement with the experimental data, there were limitations that needed to be discussed. The curve fittings were performed by using the data generated by the equations given by Hingorani et al. [35] and not by using the original published data. Clearly, this introduced some errors in the determination of the numerical values of the

parameters. The model with the parameters computed from fitting relaxation and strain-stiffening data was then used to *predict* the creep phenomenon. The comparison with the experimental data shown in Figure 2.4 indicated that the strain in the tissue reached a steady state much faster in the model prediction than in the experimental study with an error of 11.5% at $t = 100$ s. The value of the relaxation time, τ, was responsible for determining the time interval required to achieve a steady value of the strain as was shown in Figure 2.8.

The effects of the model parameters in illustrating relaxation and creep were shown in Figure 2.5-2.13. The parameters that defined the relaxation response were the elastic modulus of the proteoglycan-rich matrix, E_m, and the relaxation time, $\tau = \frac{\eta_m}{E_m}$. In Figure 2.5 the relaxation response was shown for different numerical values of E_m and in Fig. 2.6 for different numerical values of τ while the values of the remaining parameters were fixed. As E_m increased, the initial stress of the tissue during relaxation also increased, but the time needed to reach a steady stress value remained unaltered (Figure 2.5) and was only affected by changes in τ (Figure 2.6). These parametric studies clearly indicated that the relaxation phenomenon was determined solely by the viscoelasticity of the proteoglycan-rich matrix, in agreement with recent experimental findings[33].

The model parameters E_f, α, β, τ, and E_m were also varied to analyze their influence on creep. In Figures 2.7 and 2.8, the creep response was presented for different numerical values of the elastic modulus of the proteoglycan-rich matrix, E_m, while the other parameters were kept fixed. One could note that when E_m increased, the strain during creep appeared to become steady slightly later in time. The steady value of strain corresponded to the total

strain of the collagen fibers. On the other hand, the model parameter $\tau = \frac{\eta_m}{E_m}$ significantly influenced the creep behavior: as τ increased, the viscous modulus of the proteoglycan-rich matrix also increased and the strain reached a steady value later in time. These results suggested that the behavior of the tissue during creep was affected mainly by the viscosity of the proteoglycan-rich matrix and only slightly by its elasticity.

The elastic modulus of the collagen fiber, E_f, clearly affected the creep response of the tissue. From Figure 2.9, one could note that as the collagen fiber became stiffer, the strain over time decreased during creep and, thus, the overall tissue was more elastic and less viscoelastic as expected. In Figures 2.10-2.11 and Figures 2.12-2.13, the creep responses and the corresponding probability density functions that defined the recruitment of collagen fibers were presented for different values of the shape parameter, α, and the scale parameter, β, respectively, as previously described. As α increased, more collagen fibers became straight earlier, at lower values of the strain of the tissue (Figure 2.11) and, as expected, the strain of the tissue during creep increased (Figure 2.10). By changing the values of β, the probability density function described different modes of recruitment: as β increased the collagen fibers became straight more gradually and, as a consequence, the strain of the tissue over time was greater. These findings emphasized the importance of incorporating the recruitment of collagen fibers in the proposed model to reproduce the creep behavior.

One assumption made in formulating the model was that the collagen fibers and the proteoglycan-rich matrix were both strained when the entire tissue was strained due to their arrangement in parallel (see Figure 2.1). This was different from what was assumed in a recent model

proposed to describe only relaxation by Gupta et al. [33]. In their model, the cross-linked fibrils, the inter-fiber and inter-fibrillar matrices were arranged in series and, thus, deformed with the entire tissue but independently. The assumption made here appeared to be more plausible: when the crimped and straight collagen fibers were strained, the proteoglycan-rich matrix that surrounded them was also strained. Moreover, according to the model the sliding between the fibers, which was represented by the Maxwell-type viscoelastic element, was mainly responsible for the mechanical response of the tissue when the collagen fibers were crimped.

It is worth noticing that, while the model presented here was for parallel-fibered collagenous tissues, it could be extended to describe the viscoelasticity of other connective tissues having specific material symmetry or random networks of collagen fibers, as already done by one of the authors [15]. The orientation of collagen fibers was shown not to affect the time-dependent properties of connective tissues [53]. Therefore, experimental methods such as those pioneered by Sacks[59] to incorporate information about the orientation of collagen fibers into structural models for nonlinear elastic properties of thick soft tissues could be also extended to viscoelastic models.

Chapter 3

Mathematical Models for the Elastic and Viscoelastic Properties of a Collagen Fiber

3.1 Introduction

The mechanical behavior of collagenous tissues such as ligaments and tendons is determined by their constituent collagen fibers. The collagen fibers are indeed considered to be the main load bearing components of these tissues. Each collagen fiber is composed of numerous collagen fibrils that are usually aligned along one direction. The collagen fibrils are, in turn, made up of microfibrils that are composed of five strands of collagen molecules, which are

staggered along the axial microfibril direction [62]. The microfibrils in a collagen fibril are stabilized by covalent crosslinks and are embedded in a proteoglycan-rich matrix. Crosslinks are deemed responsible for stabilizing and reinforcing a single collagen fiber [58, 13]. The density of crosslinks increases with age and mature crosslinks are stronger than immature crosslinks [9]. The types and locations of mature crosslinks in ligaments and tendons remain elusive [57]. The increase in crosslinks influences the mechanical properties of collagen fibers, ligaments and tendons by producing, for example, an increase in their stiffness [54, 34].

Puxkandl et al. [54] studied the effect of crosslinks by performing tensile tests and synchrotron X-ray scattering on normal and crosslink deficient rat tail tendons. In their study, the ultimate load and stiffness were much higher in normal rat tail tendons than in crosslink deficient rat tail tendons, but the ultimate deformation for these two groups of tendons was not significantly different. The tendons were also modeled as a series of two different Kelvin-Voigt elements: the first one represented the contribution of collagen fibrils and their crosslinks and the second one represented the contribution of the proteoglycan-rich matrix. In the first Kelvin-Voigt element, the elastic modulus of the spring was assumed to depend on the density of the crosslinks in the fibrils while the viscosity of the dashpot was assumed to be due to the friction between the collagen molecules in fibrils. Although the model was not compared to the experimental data at the fibril level, it was shown to fit well tensile data of normal and crosslink-deficient rat tail tendons.

Hansen et al. [34] performed tensile tests on fibrils by using atomic force microscopy and on fascicles by employing a custom-built tensile testing device. The fibers and fascicles

were excised from normal and chemically treated rat tail tendons. The chemical treatment was used to induce crosslinks in the tendons. The authors found that the elastic modulus was considerably higher for fibrils but only slightly higher for fascicles when extracted from chemically treated rat tail tendons. Thus, they concluded that the strength of the whole tissue depends mainly on the crosslinks that are present at the collagen fibril level.

Recently, Gupta et al. [33] employed high time resolution synchrotron X-ray diffraction and confocal microscopy to investigate stress-relaxation both at the fibril and fiber levels in rat tail tendons. In order to interpret the results of the experiments, the authors proposed a viscoelastic model which consists of an arrangement in series of a Kelvin-Voigt element and two different Maxwell elements. The Kelvin-Voigt element represented the collagen fibrils with their crosslinks, one Maxwell element represented the inter-fibril proteoglycan-rich matrix while the other Maxwell element represented the inter-fiber ground substance. The model fitted well stress relaxation data at both fibril and fiber levels. These results indicated that the mechanisms governing stress relaxation at the fibril and fiber length scales are different.

In this study, a viscoelastic model for individual collagen fibers is formulated by considering their composition and structure including the microfibrils, crosslinks and surrounding matrix. As indicated in previous studies [54, 34, 33], the fibrils, cross-links and matrix are responsible for the elasticity and viscoelasticity of collagenous fibers and tissues. In the model, each fiber is assumed to consist of an arrangement in series of a linear elastic spring, which represents the mechanical contribution of the microfibrils, with an arrangement in parallel

of elastic springs and viscous dashpots, which represent the mechanical contributions of the crosslinks and matrix among fibrils (Figure 3.1). The crosslinks are assumed to gradually break under strain and, consequently, the matrix is assumed to change its viscous properties. Incremental stress relaxation tests are conducted on dry collagen fibers reconstituted from rat tail tendons to determine their elastic and viscoelastic properties. The elastic and total stress-strain curves and the stress relaxation at different levels of strain are then used to estimate the parameters of the model and evaluate its predictive capability.

3.2 Model Formulation

3.2.1 Preliminaries

In formulating the model, an individual collagen fiber is assumed to consist of a linear elastic spring with elastic constant E_m and a series of linear elastic springs with elastic constants E_l and viscous dashpots with viscous constants η_m, which are arranged in series as shown in Figure 3.1. The linear elastic spring with elastic constant E_m represents the total contribution of the microfibrils while the linear elastic springs with elastic constants E_l represent the contributions of the crosslinks existing among microfibrils, which gradually break under strain. The viscous dashpots with viscous constants η_m represent the contribution of the matrix. Because the crosslinks among microfibrils break under strain, the interaction between the microfibrils and the matrix is assumed to be altered under strain. Specifically, the

viscous constant of the matrix, η_m, is equal to η_{m_u} for the crosslinks which are unbroken and is equal to η_{m_b} for the crosslinks that are broken. A schematic of the model is presented in Figure 3.1.

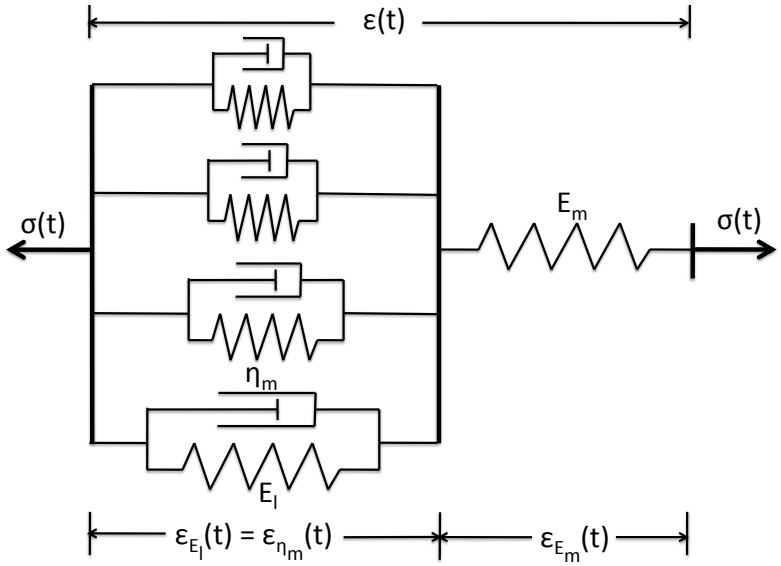

Figure 3.1: Schematic of the viscoelastic model.

3.2.2 General Framework

As shown in Figure 3.1, the total stress of a collagen fiber, $\sigma(t)$, is given by

$$\sigma(t) = \sigma_{E_m}(t) = \sigma_{E_l}(t) + \sigma_{\eta_m}(t)\,, \tag{3.1}$$

where $\sigma_{E_m}(t)$, $\sigma_{E_l}(t)$ and $\sigma_{\eta_m}(t)$ are the stresses of the microfibrils, crosslinks and matrix, respectively. Thus, according to Eq. 3.1 the contributions of the crosslinks and matrix to the total stress of a collagen fiber are different.

The total strain of a collagen fiber, $\varepsilon(t)$, is

$$\varepsilon(t) = \varepsilon_{E_m}(t) + \varepsilon_{E_l}(t) = \varepsilon_{E_m}(t) + \varepsilon_{\eta_m}(t)\,, \tag{3.2}$$

where $\varepsilon_{E_m}(t)$, $\varepsilon_{E_l}(t)$ and $\varepsilon_{\eta_m}(t)$ are the strains of the microfibrils, crosslinks and matrix, respectively. It follows from Eq. 3.2 that $\varepsilon_{E_l}(t) = \varepsilon_{\eta_m}(t)$ that is the crosslinks and the matrix are subjected to the same strain.

The stress of the microfibrils is defined as

$$\sigma_{E_m}(t) = E_m \varepsilon_{E_m}(t)\,, \tag{3.3}$$

where E_m denotes the elastic constant of the microfibrils. It must be emphasized that $\sigma_{E_m}(t)$, $\varepsilon_{E_m}(t)$ and E_m represent the stress, strain and elastic modulus, respectively, of all the microfibrils forming the collagen fiber.

The stress determined by the crosslinks in the collagen fiber is defined by using an approach similar to the one presented by Raischel et al. [56] and De Tommasi et al. [14] for different materials. The crosslinks are assumed to break when their strains ε_{E_l} reach some values $\varepsilon_b \geq 0$ that are defined by an exponential probability density function. Specifically, the stress of the crosslinks is given by

$$\sigma_{E_l}(t) = E_l \varepsilon_{E_l}(t)(1 - P(\varepsilon_{E_l}(t))) + E_l \int_0^{\varepsilon_{E_l}(t)} \varepsilon_b p(\varepsilon_b) d\varepsilon_b\,, \tag{3.4}$$

where E_l is the elastic constant of the crosslinks. In Eq. 3.4, $p(\varepsilon_b)$ is the probability density function of an exponential distribution defined, for $\varepsilon_b \geq 0$, as

$$p(\varepsilon_b) = \alpha e^{-\alpha \varepsilon_b}\,, \tag{3.5}$$

where $\alpha > 0$ denotes the so-called rate parameter and, for $\varepsilon_b \geq 0$, $P(\varepsilon_{E_l})$ denotes the exponential cumulative distribution function defined as

$$P(\varepsilon_{E_l}) = 1 - e^{-\alpha\varepsilon_{E_l}} \,. \tag{3.6}$$

The first term on the right-hand side of Eq. 3.4 is the stress of all the unbroken crosslinks while the second term is the stress of all the broken crosslinks. The stress of the broken crosslinks is not transferred to the unbroken crosslinks.

The stress of the matrix, $\sigma_{\eta_m}(t)$, is defined by taking into account the differences in the viscous constants determined by the breakage of crosslinks. Thus, the stress of the matrix is defined as

$$\sigma_{\eta_m}(t) = \eta_{m_u}\varepsilon'_{\eta_m}(t)\left(1 - \int_0^{\varepsilon_{\eta_m}(t)} p(\varepsilon_b)d\varepsilon_b\right) + \eta_{m_b}\varepsilon'_{\eta_m}(t)\int_0^{\varepsilon_{\eta_m}(t)} p(\varepsilon_b)d\varepsilon_b \,, \tag{3.7}$$

where η_{m_u} and η_{m_b} denote the viscous constants of the matrix associated with the unbroken or broken crosslinks, respectively, and the prime denotes the differentiation with respect to t. In Eq. 3.7, the first term on the right hand side represents the contribution of the matrix with unbroken crosslinks while the second term represents the contribution of the matrix with broken crosslinks. It is assumed that the portion of the matrix with unbroken crosslinks and the remaining portion of the matrix with broken crosslinks are subjected to the same strain, $\varepsilon_{\eta_m}(t)$.

From Eqs. 3.3, 3.4, 3.7 it follows that Eq. 3.1 can be rewritten as

$$E_m\varepsilon_{E_m}(t) = E_l\varepsilon_{E_l}(t)(1 - P(\varepsilon_{E_l}(t))) + E_l \int_0^{\varepsilon_{E_l}(t)} \varepsilon_b p(\varepsilon_b) d\varepsilon_b + \eta_{m_u}\varepsilon'_{\eta_m}(t) \left(1 - \int_0^{\varepsilon_{\eta_m}(t)} p(\varepsilon_b) d\varepsilon_b\right) + \eta_{m_b}\varepsilon'_{\eta_m}(t) \int_0^{\varepsilon_{\eta_m}(t)} p(\varepsilon_b) d\varepsilon_b \,. \quad (3.8)$$

Moreover, since $\varepsilon_{E_l}(t) = \varepsilon_{\eta_m}(t) = \varepsilon(t) - \varepsilon_{E_m}(t)$ from Eq. 3.2 and, hence, $\varepsilon'_{E_l}(t) = \varepsilon'_{\eta_m}(t) = \varepsilon'(t) - \varepsilon'_{E_m}(t)$, Eq. 3.8 can be rewritten as

$$\varepsilon'_{E_m}(t) = \varepsilon'(t) + \frac{\frac{E}{\alpha}\left(e^{-\alpha(\varepsilon(t)-\varepsilon_{E_m}(t))} - 1\right) - \varepsilon_{E_m}(t)}{A(\tau_{m_u}, \tau_{m_b}, \varepsilon_{E_m}(t), \varepsilon(t), \alpha)} \,, \quad (3.9)$$

where $E = \frac{E_l}{E_m}$ and, for ease of writing, $A = A(\tau_{m_u}, \tau_{m_b}, \varepsilon_{E_m}(t), \varepsilon(t), \alpha)$ is set to be

$$A(\tau_{m_u}, \tau_{m_b}, \varepsilon_{E_m}(t), \varepsilon(t), \alpha) = \tau_{m_b} + (\tau_{m_u} - \tau_{m_b})e^{-\alpha(\varepsilon(t)-\varepsilon_{E_m}(t))} \quad (3.10)$$

where $\tau_{m_u} = \frac{\eta_{m_u}}{E_m}$ and $\tau_{m_b} = \frac{\eta_{m_b}}{E_m}$ are relaxation times.

By recalling Eqs. 3.1 and 3.3, the total stress of a collagen fiber can be written as

$$\sigma(t) = E_m\varepsilon_{E_m}(t) \,. \quad (3.11)$$

After differentiating both sides of Eq. 3.11 with respect to t, one obtains that

$$\sigma'(t) = E_m\varepsilon'_{E_m}(t) \,. \quad (3.12)$$

Eqs. 3.9 and 3.12 form a system of ordinary differential equations that, with appropriate initial conditions, can be solved to describe the mechanical behavior of a collagen fiber.

3.2.3 Total Stress of a Collagen Fiber

In order to describe the total (elastic and viscous) stress-strain curve of a collagen fiber as computed from incremental stress relaxation tests, the system of ordinary differential equations given by Eqs. 3.9 and 3.12 can be solved by assuming that that the strain of the collagen fiber, $\varepsilon(t)$, has the form

$$\varepsilon(t) = at \tag{3.13}$$

where $t > 0$ and a is a constant representing the strain rate. It must be noted that during incremental stress relaxation tests the strain rate used to strain the collagen fiber to different increasing levels of strain does not change and is constant.

3.2.4 Elastic Stress of a Collagen Fiber

The elastic stress-strain curve of a collagen fiber is assumed to be determined only by its constituent microfibrils and their crosslinks. The contribution of the matrix represented by the viscous dashpots in Figure 3.1 is neglected. Thus, the collagen fiber is modeled as shown schematically in Figure 3.2.

The elastic stress of a collagen fiber, $\sigma_e(t)$, is then given by

$$\sigma_e(t) = \sigma_{E_m}(t) = \sigma_{E_l}(t)\,, \tag{3.14}$$

while the elastic strain of the collagen fiber, $\varepsilon_e(t)$, is given by

$$\varepsilon_e(t) = \varepsilon_{E_m}(t) + \varepsilon_{E_l}(t)\,. \tag{3.15}$$

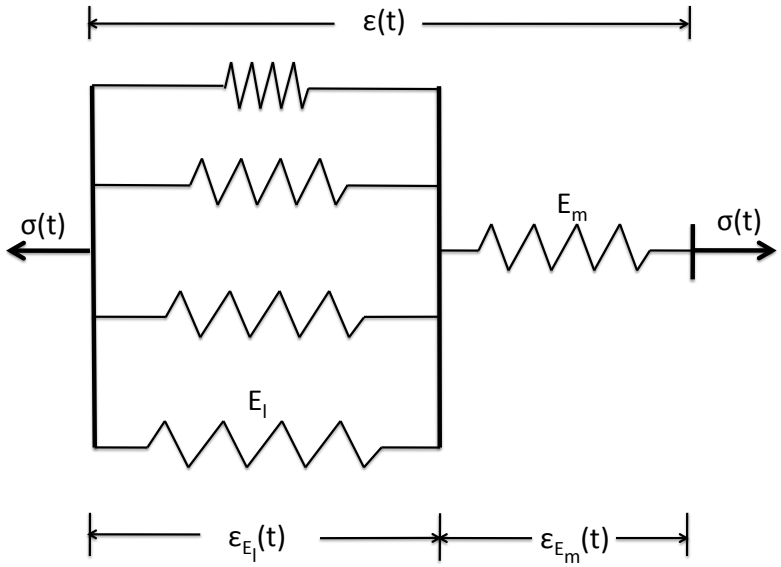

Figure 3.2: Schematic of the elastic model.

From Eqs. 3.3 and 3.4, one observes that Eq. 3.14 can be rewritten as

$$E_m \varepsilon_{E_m}(t) = E_l \varepsilon_{E_l}(t)(1 - P(\varepsilon_{E_l}(t))) + E_l \int_0^{\varepsilon_{E_l}(t)} \varepsilon_b p(\varepsilon_b) d\varepsilon_b \,. \tag{3.16}$$

By differentiating both sides of Eq. 3.16 with respect to ε_e and suppressing the time dependency, one has that

$$\frac{d\varepsilon_{E_m}}{d\varepsilon_e} = \frac{E_l}{E_m} e^{-\alpha \varepsilon_{E_l}} \frac{d\varepsilon_{E_l}}{d\varepsilon_e} \,. \tag{3.17}$$

By recalling that $\varepsilon_{E_l} = \varepsilon_e - \varepsilon_{E_m}$ from Eq. 3.15, Eq. 3.17 can be written as

$$\frac{d\varepsilon_{E_m}}{d\varepsilon_e} = \frac{E}{e^{\alpha(\varepsilon_e - \varepsilon_{E_m})} + E} \,. \tag{3.18}$$

where, as before, $E = \frac{E_l}{E_m}$. From Eqs. 3.3 and 3.14, it follows that the elastic stress of a

crosslinked collagen fiber is

$$\sigma_e = E_m \varepsilon_{E_m} \,. \tag{3.19}$$

By differentiating Eq. 3.19 with respect to ε_e, one obtains that

$$\frac{d\sigma_e}{d\varepsilon_e} = E_m \frac{d\varepsilon_{E_m}}{d\varepsilon_e} \,. \tag{3.20}$$

The system of ordinary differential equations formed by Eq. 3.18 and Eq. 3.20 with appropriate initial conditions can be used to compute the elastic stress-strain relationship for a collagen fiber.

3.2.5 Stress Relaxation of a Collagen Fiber

The stress relaxation of the collagen fiber can be determined by solving the system of ordinary differential equations formed by Eqs. 3.9 and 3.12. The strain history of the collagen fiber, $\varepsilon(t)$, is assumed to have the form

$$\varepsilon(t) = \begin{cases} at & \text{for } 0 \leq t < t_0 \,, \\ \varepsilon_0 & \text{for } t \geq t_0 \,, \end{cases} \tag{3.21}$$

where a and t_0 are constants. Specifically, the constant a represents the strain rate used to increase the strain from zero to a constant value, ε_0, which is mantained during stress relaxation starting at a time t_0.

For $0 \leq t < t_0$, $\varepsilon'(t) = a$. By imposing the initial condition $\sigma(0) = 0$ and noting that $\varepsilon_{E_m}(0) = 0$, the system of ordinary differential equations, Eqs. 3.9 and 3.12, can be solved

to determine $\sigma(t_0)$ and $\varepsilon_{E_m}(t_0)$, which are then used as initial conditions when solving the system of differential equations for $t > t_0$. For $t > t_0$, $\varepsilon(t) = \varepsilon_0$ and $\varepsilon'(t) = 0$ and by imposing the previously determined initial conditions on $\sigma(t_0)$ and $\varepsilon_{E_m}(t_0)$ the system of ordinary differential equation can be solved to compute the stress $\sigma(t)$ which defines the stress relaxation of the collagen fiber.

3.3 Results

3.3.1 Parameter Estimation

There were 4 parameters, $\{E, \alpha, \tau_{m_u}, \tau_{m_b}\}$, in the proposed modeling framework that needed to be estimated by using experimental data to describe the mechanical behavior of a collagen fiber. In this study, the model was validated with the incremental stress relaxation data collected from 14 reconstituted collagen fibers of rat tail tendons. The incremental stress relaxation test is the experiment that performed by ramping up a specimen at a constant strain rate to an incremental strain level and then the specimen is held at that strain level to perform the relaxation test. After the stress decreases to an equilibrium stress during relaxation, the specimen is then ramped up at the same strain rate to a higher incremental strain level and is held at that strain level to perform another relaxation test. These incremental strain and stress relaxation tests are cyclically repeated until the specimen fails [63]. For the experimental data used in this work, the incremental stress relaxation tests were performed

at strain levels of 2.4%, 4.8%, 7.3%, 9.7% and 12.1%. The peak stresses at different strain levels during each relaxation test were used to generate the so-called total stress-strain data while the equilibrium stresses were used to create the so-called elastic strain-strain data. The average values of the elastic stress-strain, total strain-strain and stress relaxation data at different strain levels were computed and plotted with their standard deviation in Figure 3.3-Figure 3.9.

The elastic constant of the microfibrils, E_m, was set to be equal to 12 GPa as suggested by preliminary molecular dynamics studies carried out by the authors. The values of the parameters were determined uniquely by using the experimental data and implementing the nonlinear least squares method in Matlab (the MathWorks, Inc.). The first set of parameters, E and α, which determine the elastic response of the collagen fiber, were found by curve fitting the system of ordinary differential equations, Eqs. 3.18 and 3.20, to the average elastic strain-strain data. The results of the fitting and the experimental data are shown in Figure 3.3. It was found that $E = 0.14$ and $\alpha = 9.4$ provided the best fit with $R^2 = 0.99$.

During incremental stress-relaxation tests, each collagen fiber was strained to different strain levels at the same strain rate of $\varepsilon' = 0.16\%$ sec^{-1}. Therefore, in order to fit the average of the total strain-stress curves by using the system of ordinary differential equations formed by Eqs. 3.9 and 3.12, it was assumed that $a = 0.16\%$ sec^{-1} in Eq. 3.13. After setting $E = 0.14$ and $\alpha = 9.4$, the parameters τ_{m_u} and τ_{m_b} were determined to be 1.2 s and 3.0 s, respectively. The results of the fitting are presented in Figure 3.4 where $R^2 = 0.99$.

The average of stress relaxation data recorded by subjecting the collagen fibers to a constant

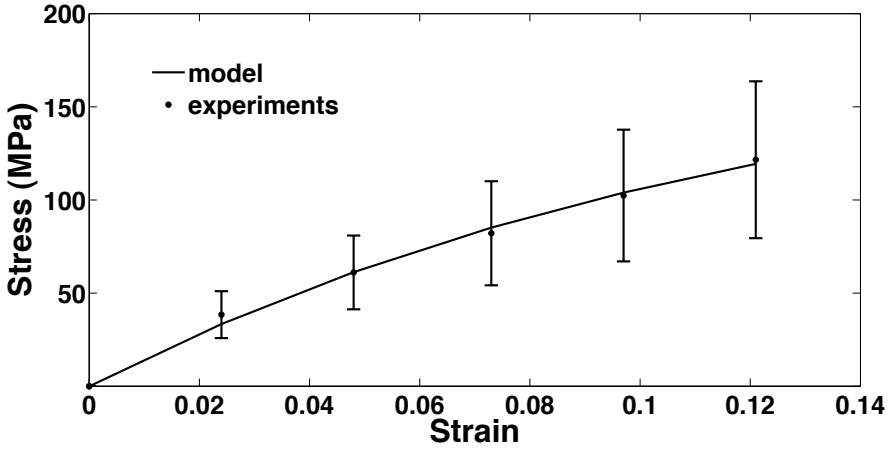

Figure 3.3: Experimental data and model fit with $E = 0.14$ and $\alpha = 9.4$ illustrating the elastic stress-strain curve of reconstituted collagen fibers of rat tail tendons.

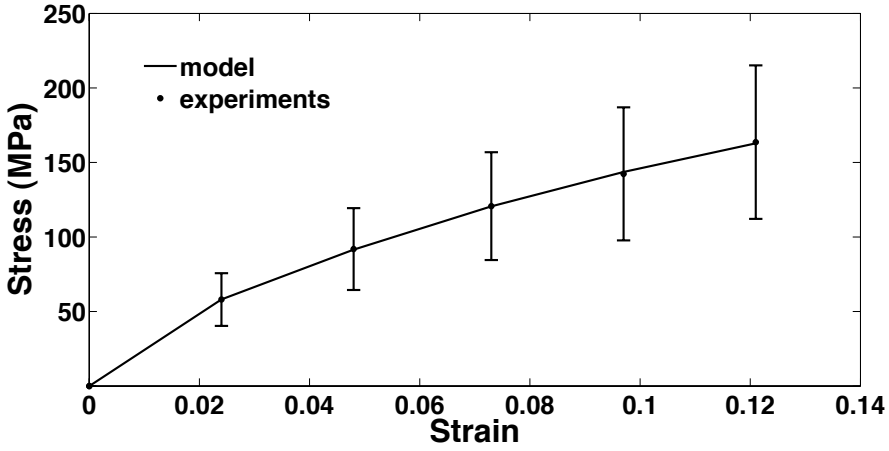

Figure 3.4: Experimental total stress-strain curve and model fit.

strain of 7.3% was used to compute the value of τ_{m_b} in the model represented by Eqs. 3.9 and 3.12 while the other parameters were fixed to the values computed by fitting the elastic and total stress-strain data. The parameter τ_{m_b} was assumed to have different values in stress

relaxation experiments and total stress-strain curves because of the influence of different strain rates. The value of the constant a was set to be 0.0016 sec^{-1} in Eq. 3.21, which is used to determine the initial conditions for the system of differential equations given by Eqs. 3.9 and 3.12. The value of τ_{m_b} that provided the best fit was found to be 851 s. The results of the fitting are shown in Figure 3.5 ($R^2 = 0.8467$).

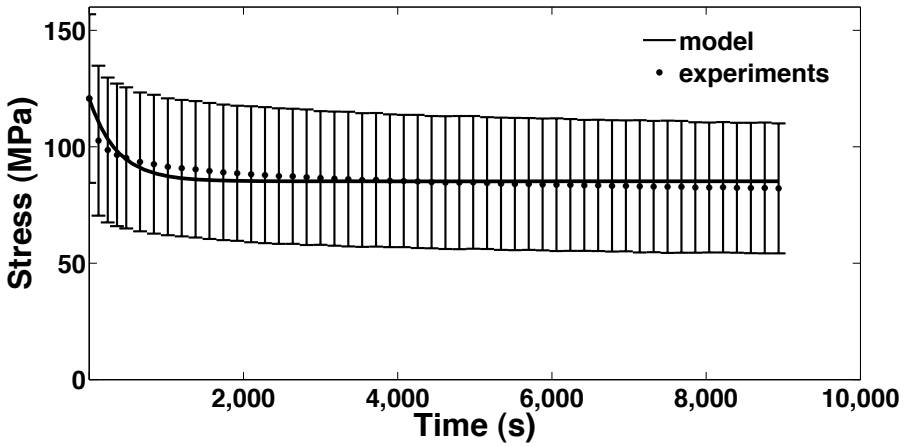

Figure 3.5: Stress relaxation at strain of 0.073: experimental data and model fit.

The values of the parameters, $\{E, \alpha, \tau_{m_u}\}$, which were found from fitting the total and elastic stress-strain data and the value of the parameter τ_{m_b}, which was determined from fitting the stress relaxation data collected at 7.3% strain, were then employed to predict stress relaxation of the collagen fibers at different strains: 2.4%, 4.8%, 9.7% and 12.1%. The initial conditions for the system of ordinary differential equations for stress relaxation were computed by using the solution of the system of ordinary differential equations obtained with the total strain stiffening data. The comparison between the model predictions for stress relaxation and the experimental data are shown in Figure 3.6-Figure 3.9.

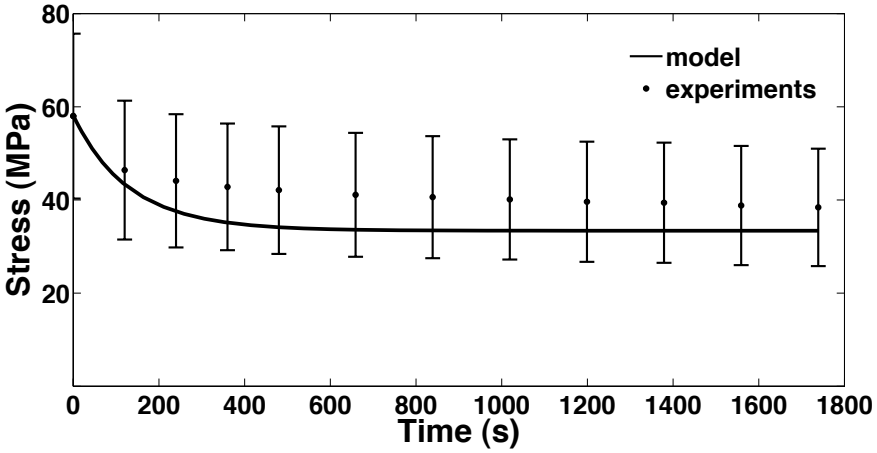

Figure 3.6: Stress relaxation at strain of 0.024: experimental data and model prediction.

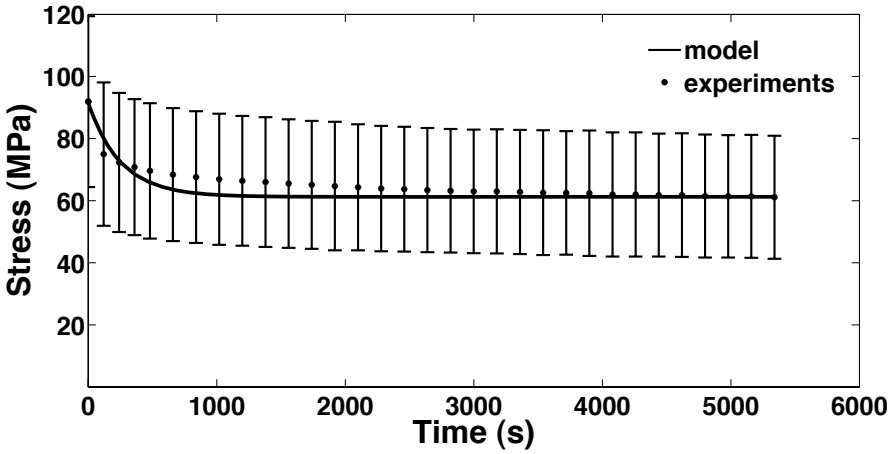

Figure 3.7: Stress relaxation at strain of 0.048: experimental data and model prediction.

3.3.2 Influence of Parameters on Model Predictions

The role of each model parameter in describing the total and elastic stress-strain relationships and stress relaxation of collagen fibers was investigated. The predictions of the proposed models were plotted for various values the parameters. The parameters, which were not

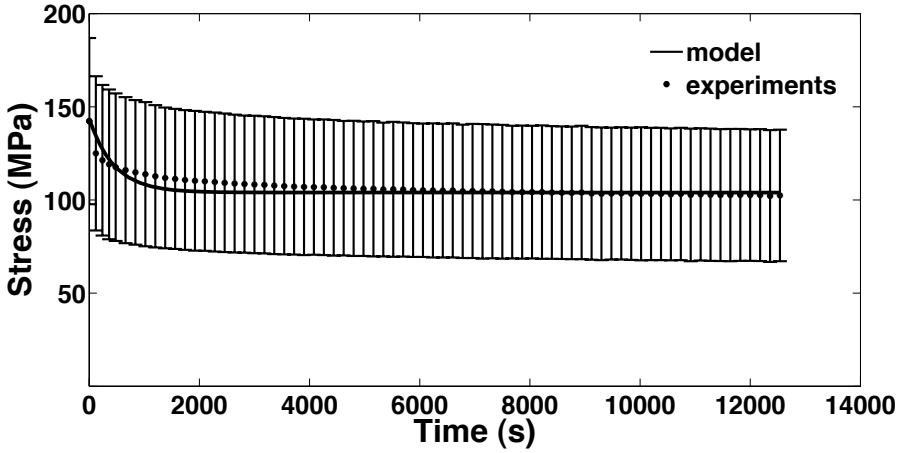

Figure 3.8: Stress relaxation at strain of 0.097: experimental data and model prediction.

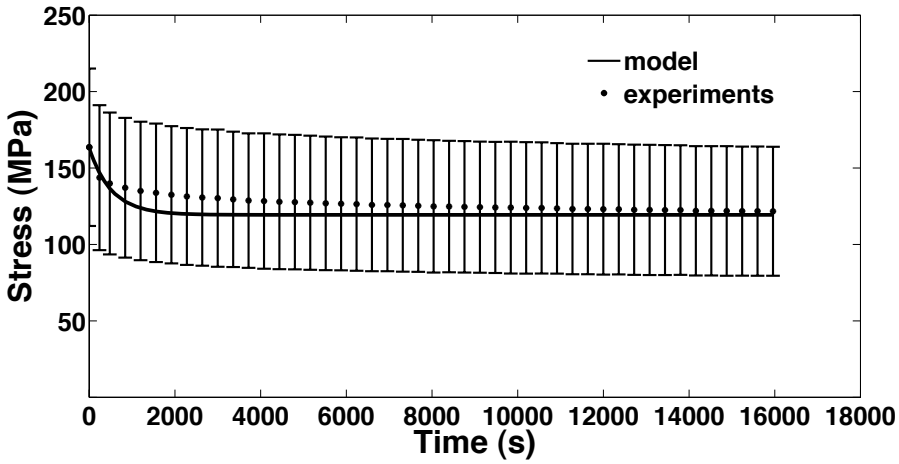

Figure 3.9: Stress relaxation at strain of 0.121: experimental data and model prediction.

varied, were fixed to the values obtained from curve fitting the total and elastic strain-strain and stress relaxation experimental data, namely $E = 0.14$, $\alpha = 9.4$, $\tau_{m_u} = 1.2$ s and $\tau_{m_b} = 851$ s. It was observed that as the constant E increased, the stiffness of the collagen fiber significantly increased with strain (Figure 3.10). For stress relaxation, one could observe

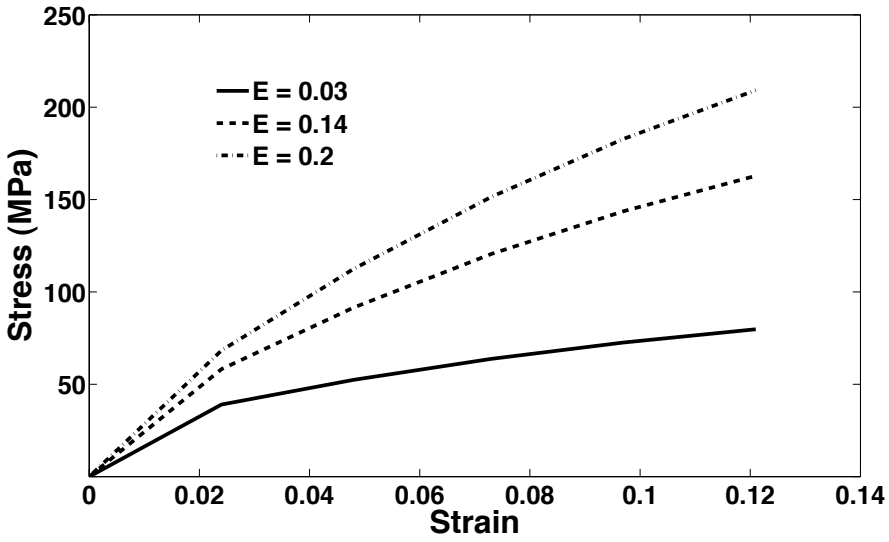

Figure 3.10: Influence of the model parameter E on total strain-stiffening behavior.

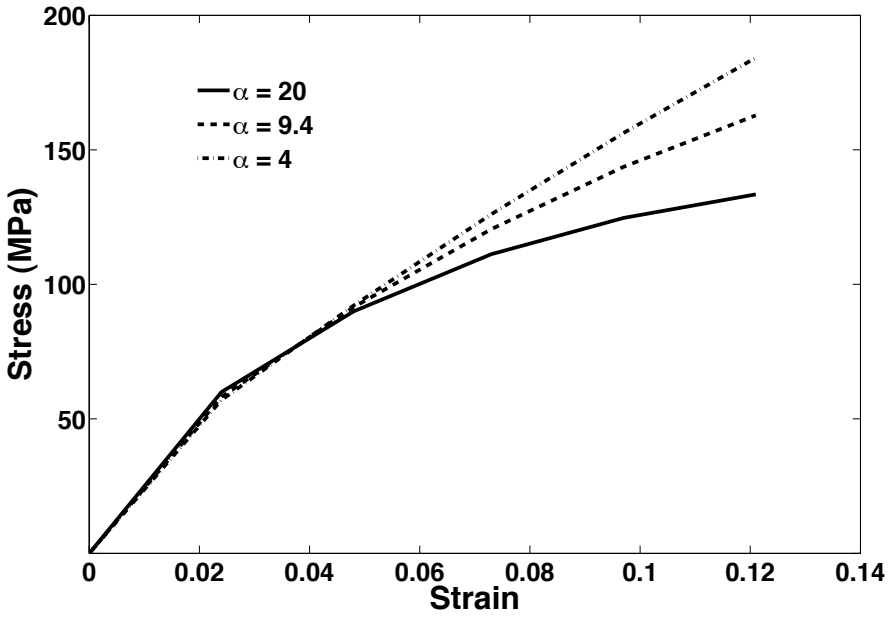

Figure 3.11: Influence of the rate parameter, α, on total strain-stiffening behavior.

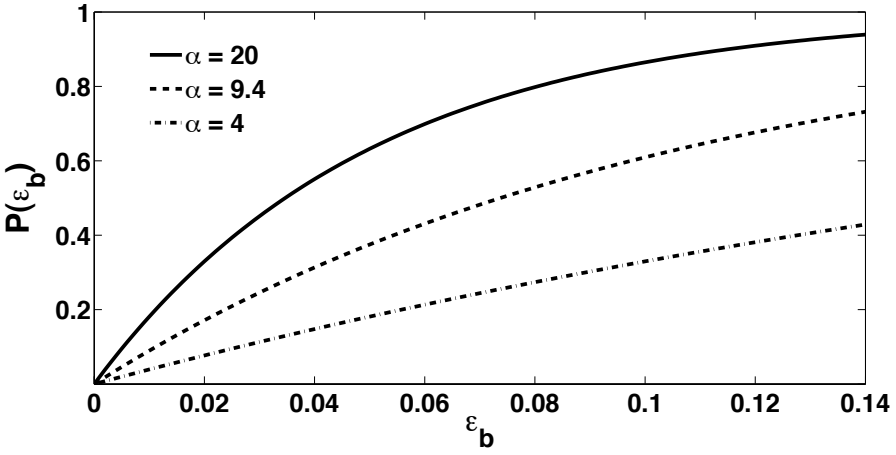

Figure 3.12: Influence of the rate parameter, α, on the exponential cumulative distribution function.

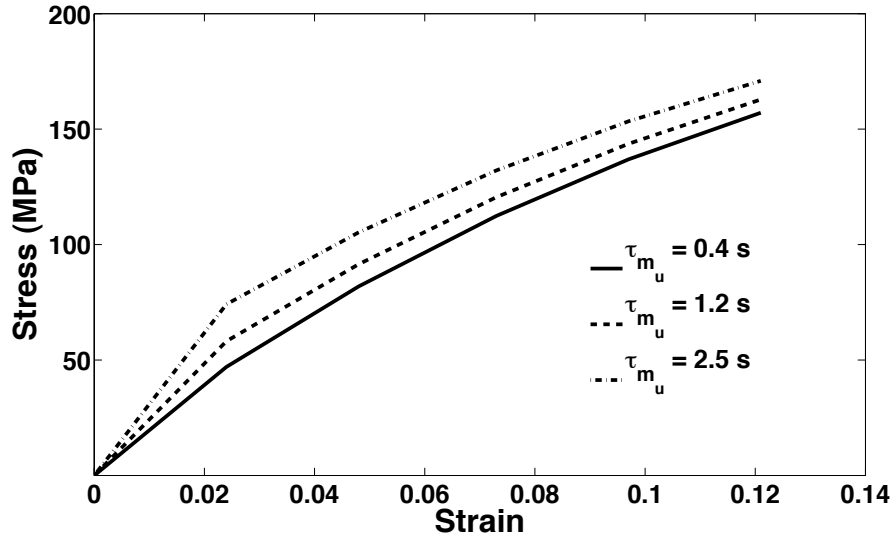

Figure 3.13: Influence of the model parameter τ_{m_u} on the total strain-stiffening behavior.

that when E increased, the stress reached a higher equilibrium value and in a shorter time (Figure 3.15).

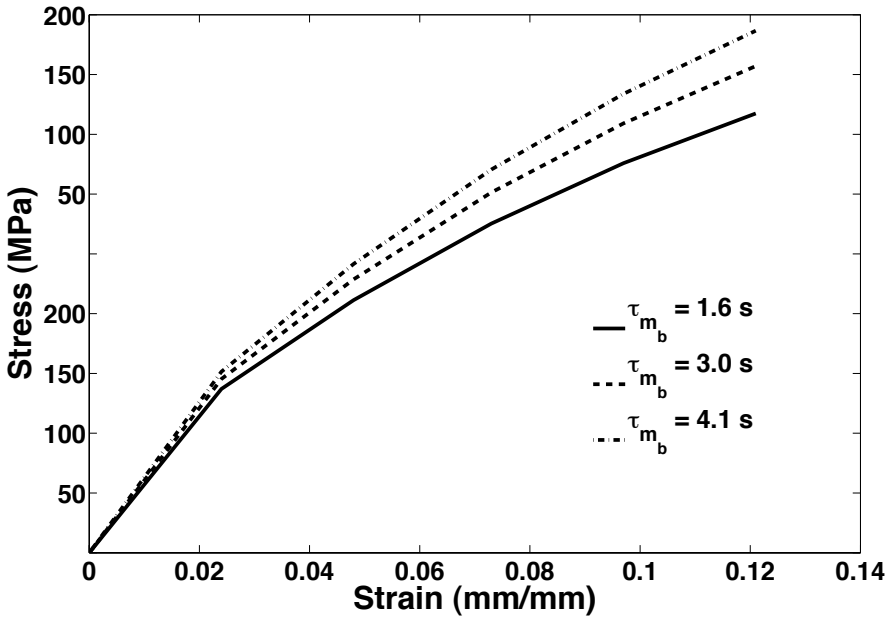

Figure 3.14: Influence of the model parameter τ_{m_b} on the total strain-stiffening behavior.

The effect of the rate parameter, α, of the exponential probability density function on the total stress-strain behavior is shown in Figure 3.11 while the corresponding probability density function is presented in Figure 3.12. As α increased, the probability that the crosslinks break became higher for lower values of the strain (Figure 3.12) and, consequently, the stress in the total stress-strain curve became lower (Figure 3.11). Stress relaxation was also influenced by the value of α: as α increased the value of the equilibrium stress decreased and the time needed to reach such equilibrium stress also increased (Figure 3.16).

The relaxation times τ_{m_u} and τ_{m_b} determined the total stress-strain behavior of collagen fibers. As shown in Figure 3.13 and Figure 3.14, the stress increased with increasing strain as τ_{m_u} and τ_{m_b} increased, respectively. It was also observed that, for large value of the

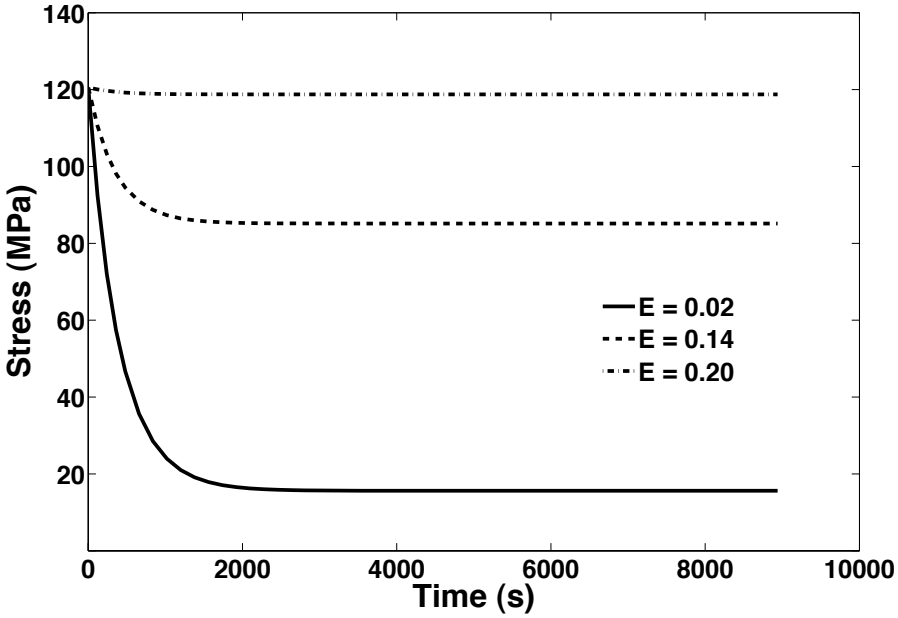

Figure 3.15: Influence of the model parameter E on stress relaxation.

strain, the stiffness decreased as τ_{m_u} increased while it increased as τ_{m_b} increased. Finally, the influence of the relaxation times, τ_{m_u} and τ_{m_b}, on the stress relaxation are shown in Figure 3.17 and Figure 3.18, respectively. As τ_{m_u} and τ_{m_b} increased, the stress increased over time and reached the equilibrium state value in a longer interval of time.

3.4 Discussion and Conclusions

In this work, a novel viscoelastic model was presented to illustrate the results of incremental stress relaxation tests conducted on dry collagen fibers reconstituted from rat tail tendons. The model, for which the schematic is presented in Figure 3.1, was formulated

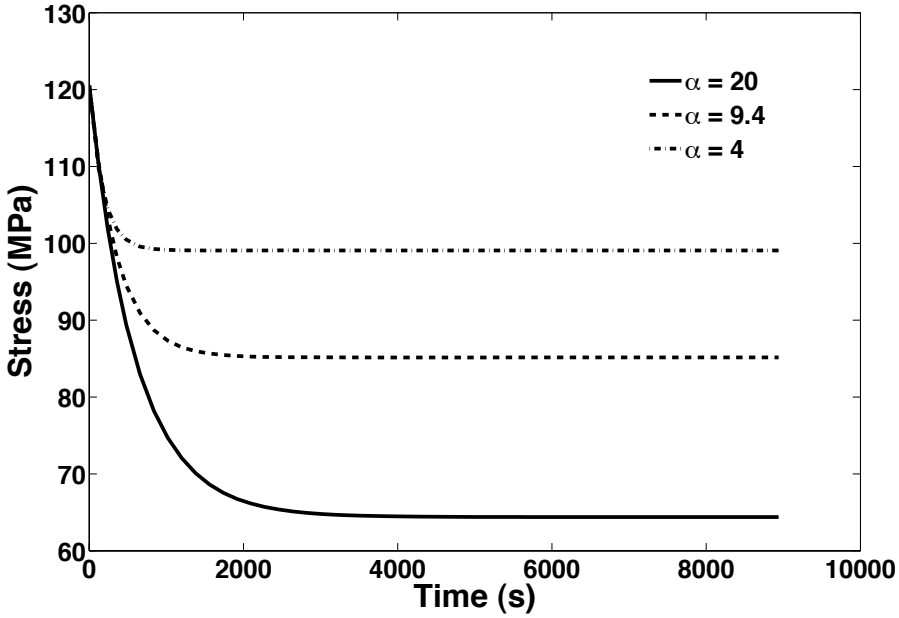

Figure 3.16: Influence of the rate parameter α on stress relaxation.

by accounting for the mechanical contributions of the microfibrils, the crosslinks among microfibrils and the surrounding matrix in a collagen fiber. The continuous and progressive failure of crosslinks was assumed to be responsible for the nonlinearity that characterize the total and elastic stress-strain curves computed from incremental stress relaxation tests at different levels of strain. The viscous properties of the matrix were assumed to change as the crosslinks progressively fail thus inducing nonlinearities in stress relaxation and total stress-strain responses.

The parameters in the proposed model were directly related to the structure and composition of a collagen fiber. They were estimated by fitting total stress-strain, elastic stress-strain and stress-relaxation data as shown in Figure 3.3, Figure 3.4 and Figure 3.5, respectively.

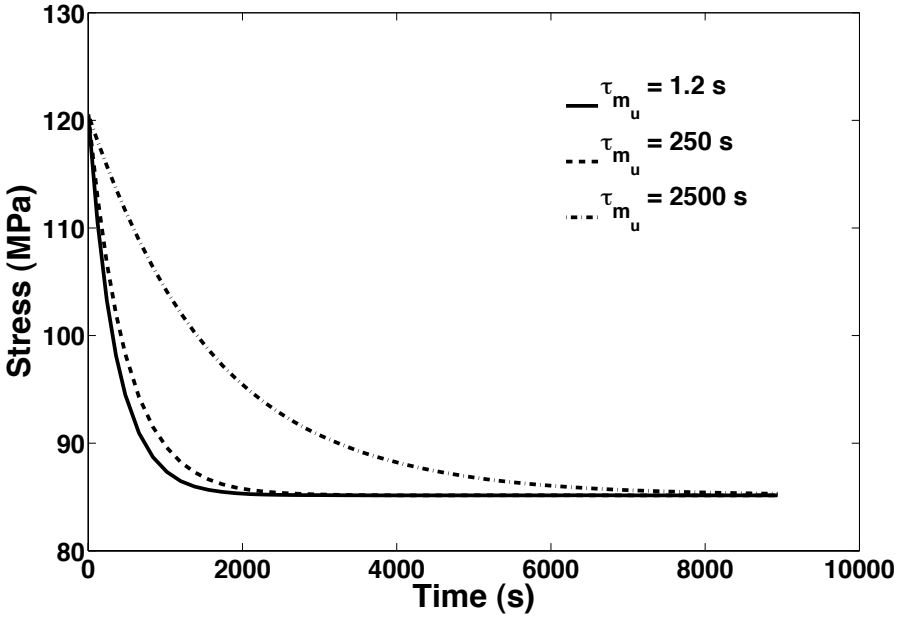

Figure 3.17: Influence of the model parameter τ_{m_u} on stress relaxation.

The elastic modulus of the microfibrils, E_m, comprising the collagen fiber was fixed to be 12 GPa. This value was estimated from molecular dynamics simulations and fell within the range of values reported in the literature [28]. The parameters, which were determined from the elastic stress-strain data, were $E = 0.14$ and $\alpha = 9.4$. The value for the parameter E indicated that the microfibrils were stiffer than the crosslinks in the collagen fiber. The parameter α defined the probability density function that governed the continuos breakage of the crosslinks. Figure 3.12 indicated that at 12% strain more than 70% of the crosslinks failed. The total stress-strain data obtained from the incremental stress relaxation tests were used to estimate the parameters τ_{m_u} and τ_{m_b}, which denoted the relaxation times of the matrix with unbroken and broken crosslinks. The values found for these parameters,

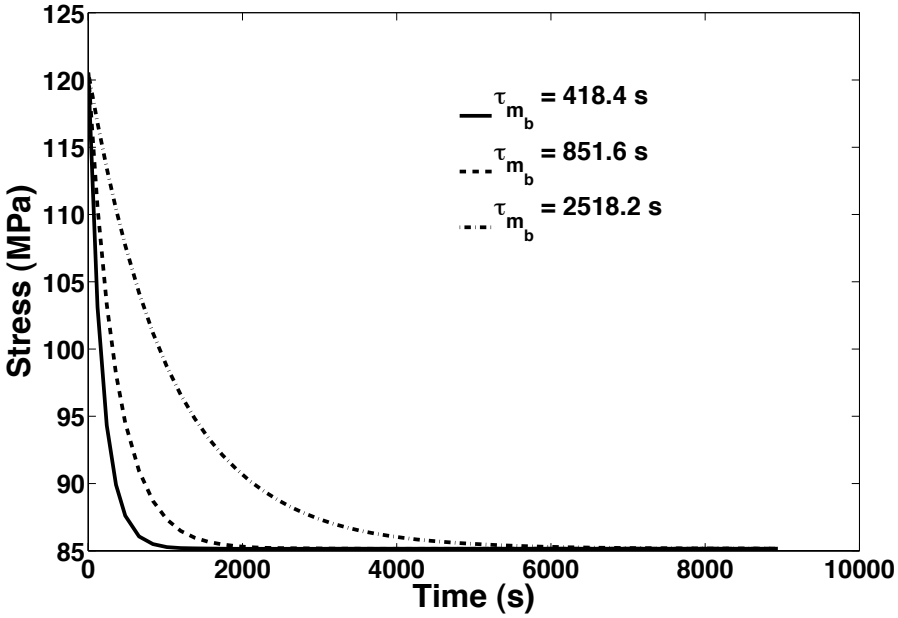

Figure 3.18: Influence of the model parameter τ_{m_b} on stress relaxation.

$\tau_{m_u} = 1.2$ s and $\tau_{m_b} = 3.0$ s, suggested that the time for relaxation is longer for the matrix having broken crosslinks.

The predictions of the stress relaxation response at different strain levels, 2.4%, 4.8%, 9.7% and 12.1%, were presented in Figure 3.6-Figure 3.9. These predictions were conducted by using the values of the parameters estimated by fitting the elastic and total stress-strain data and the stress relaxation data collected at 7.3% strain. The stress values predicted by the system of ordinary differential equations fell within the range of values recorded from the experiments. However, there was a common trend in the predictions that appeared to be in contrast with the experimental observations: the stress reached equilibrium values earlier in time during relaxation. By changing the relaxation times, τ_{m_u} and τ_{m_b}, of the matrix with

unbroken and broken cross-links, the experimental data could have been fitted by the model. Indeed, as demonstrated in Figure 3.17 and Figure 3.18, these two parameters defined the interval of time required for the stress to reach equilibrium during stress relaxation.

The influence of each parameter on the predictions of total and elastic stress-strain relations and stress relaxation were presented in Figure 3.10-Figure 3.18. In Figure 3.10 the total stress-strain response was shown for different numerical values of E. The parameter E, which represented the elastic modulus of the crosslinks relative to the elastic modulus of the microfibrils, played a significant role on increasing the stiffness of the collagen fibers. These findings are in agreements with previous studies in which an increase in crosslinks produced an increase in the stiffness of collagenous tissues [54, 34]. The parameters, E, also determined the values of the equilibrium stress during relaxation (Figure 3.15). Indeed, as E increased, the values of the equilibrium stress increased while the values of the relaxation time decreased. These results indicated that the collagen fiber reached equilibrium during relaxation in a shorter interval of time when it had more crosslinks as indicated by published experimental studies [72].

In Figure 3.11 the total stress-strain curve of the collagen fiber was presented for different values of the rate parameter, α, of the exponential probability density function that defined the continuos failure of crosslinks while in Figure 3.12 the corresponding cumulative density functions were presented. As α increased, the percentage of crosslinks that failed also increased, especially at large strains, (Figure 3.12) and, hence, the total stress of the collagen fiber decreased at these strains (Figure 3.11). This continuos mechanism of progressive fail-

ure of the crosslinks in the collagen fiber is similar to the one proposed by other investigators for modeling the breakage of fibers in bundles of elastic fibers [56]. In this study, the parameter α also contributed to define the stress relaxation in collagen fibers as illustrated in Figure 3.16. The stress relaxation was more pronounced for collagen fibers having a higher percentage of broken crosslinks for which α had greater values (Figure 3.12).

The total stress-strain curve of each collagen fiber computed from incremental stress relaxation tests was found to be bilinear. This bilinear behavior was also reported by other researchers who investigated the mechanical properties of dry collagen fibers [40]. In the proposed model, the bilinearity in the total stress-strain response was determined by the different relaxation times of the matrix with unbroken and broken crosslinks introduced via τ_{m_u} and τ_{m_b}, respectively. One could observe from Figure 3.13 that in a collagen fiber the stress over strain increased with τ_{m_u}, while the stiffness increased for small values of the strain and, although only slightly, decreased for large values of the strain. Unlike τ_{m_u}, the stress over small values of the strain remained almost unchanged while it increased for large values of the strain when τ_{m_b} increased. Consequently, the stiffness of the collagen fiber for small values of the strain remained unchanged while it increased for large values of the strain. These parametric studies indicated that the viscous properties of the matrix with unbroken crosslinks had a significant role on the total stress of the collagen fiber at small strain while the viscous property of the matrix with broken crosslinks had a significant role on the total stress at large strain.

The relaxation times τ_{m_u} and τ_{m_b} also influenced the stress relaxation as illustrated in Fig-

ure 3.17 and Figure 3.18, respectively. It was clearly shown when the relaxation times had greater values, the stress of the collagen fiber reached equlibrium after a longer interval of time while the value of the stress at equlibrium was unaffected. Two different relaxation times, a fast relaxation time and a slow relaxation time, were also observed in other experimental studies on rat tail tendon collagen fibers [72, 33].

In conclusion, a new modeling framework was presented for describing the mechanical response of collagen fibers exhibited during incremental stress relaxation tests. The microfibrils and the crosslinks among them were assumed to be responsible for their elasticity while the matrix was responsible for their viscosity. The modeling approach adopted here could be extended to describe other viscoelastic phenomena in collagen fibers such as, for example, creep and could be also applied to describe the viscoelasticity of other collagenous tissues. More importantly, it could be employed to illustrate the role of crosslink density on the mechanical behavior of the collagenous fibers and tissues.

Chapter 4

Mathematical Models for Preconditioning in Ligaments and Tendons

4.1 Introduction

The mechanical properties of ligaments and tendons depend on their stress or strain history [26]. The influence of stress or strain history is taken into consideration when designing and conducting mechanical experiments. Indeed, it has been experimentally observed that even when ligament and tendon specimens have similar characteristics, such as size, age, weight, temperature and storage conditions, they often exhibit different mechanical properties due

to different stress or strain history determined, for example, by specimen handling and preparation [31, 60, 64, 27, 75, 20, 29, 3, 67, 68]. In order to obtain consistent results, experimentalists in biomechanics usually subject ligaments and tendons to a process called preconditioning.

Preconditioning is an experimental procedure in which cyclic loading (or stretching) is applied to soft biological specimens before recording the results of mechanical experiments until the recorded stress-strain curves from successive cycles remain unchanged. Preconditioning can be performed by controlling the load or the displacement. In load controlled experiments, the maximum load of each cycle is kept constant while, in displacement controlled experiments, the maximum displacement of each cycle is maintained constant. This procedure provides the same stress (or strain) history to all the specimens before testing. The hysteresis, which is observed in successive cycles, decreases during preconditioning due to changes occurring in the internal structure of the tissues [26].

As many other biological tissues, ligaments and tendons are usually preconditioned before performing tensile, relaxation, creep and hysteresis tests. This process significantly influences their mechanical properties [31, 60, 64, 27, 75, 20, 29, 3, 67, 68]. For example, Schatzmann et al. performed tensile tests of human quadriceps tendons and patellar ligaments before and after preconditioning. They found that the ultimate failure load and stiffness of these tissues were higher after preconditioning [60]. Graf et al. performed relaxation experiments of primate patellar tendons before and after preconditioning and showed that the relaxation times were lower after preconditioning [31].

The stress softening during preconditioning appears to be similar to the well known stress softening phenomenon of rubberlike materials, the so-called Mullins effect. There are, however, several important differences between the softening phenomenon in rubber-like materials and soft biological tissues. In rubber-like materials, the softening appears during cyclic loading (or stretching) up to strain values that are lower or equal to the maximum strain value applied during previous cycles. When the strain is greater than the maximum strain applied in the previous cycle, the stress-strain curve follows the same stress-strain path of the previous cycle. It has been speculated that stress softening in rubber-like materials is determined by the breakage of the bonding between filler particles, the slippage of the filler molecules on the polymer chains and the disentanglement of the chains. However, none of the mentioned mechanisms has been proved to explain all the features of Mullins effect, such as stress softening, residual strain and recovery [19].

Little is known about the micro-structural changes occurring during preconditioning. In order to understand the mechanism of preconditioning, Yahia and Drouin compared the energy absorption (area in a hysteresis cycle) of the first and the last hysteresis cycle during preconditioning of normal canine anterior cruciate ligaments (ACLs) and treated canine ACLs in which the hyaluronic acid was enzymatically digested. They found that the energy absorption of the first hysteresis cycle of treated ACLs was much smaller than the energy absorption of the first hysteresis cycle of normal ACLs. The energy absorption was not significantly different for the last hysteresis cycle for both groups. Therefore, Yahia and Drouin suggested that the interfibrillar matrix containing water and other material such as

proteoglycans and hyaluronic acid might be responsible for the observed hysteresis during preconditioning [80].

Several models have been developed to explain the stress softening and energy dissipation during preconditioning [2, 66, 49, 6, 46, 45]. Carew et al. tried to establish a protocol for preconditioning of porcine aortic valve cusps by using quasilinear viscoelastic (QLV) theory [2]. Their simulation did not predict well the maximum stress of each cyclic loading due to the fact that the authors did not incorporate any structural mechanism into the model. Later, Nava et al. introduced a phenomenological softening mechanism into a QLV model to describe preconditioning of bovine liver [49]. Softening was assumed to be a function of the deformation history and a softening variable that changed over time. The model showed good prediction although the values of the model parameters were not presented by the authors.

Sverdlik and Lanir proposed a structural model to describe the tensile and relaxation properties of tendons including preconditioning effects [66]. In their work, the fiber's straightening strain was assumed to change over time during preconditioning due to increasing fiber elongation. The results obtained from the model for stress relaxation before and after preconditioning had a good agreement with some but not all the experimental data. The fitting of the model to tensile data before preconditioning was partially good. However, no comparison of the model with tensile data after preconditioning was presented. Later, Lokshin and Lanir applied the same assumption of increasing fiber elongation in order to describe preconditioning of rat skin and rabbit skin [46, 45]. Ciarletta et al. modeled the stress softening

and energy dissipation associated with preconditioning by accounting for the breakage of the collagen fibers. Their model was shown to have a good fit with tensile loading and unloading experimental data from tendons but the prediction of the model with independent set of data was not presented [6]. Both Sverdlik and Lanir's work and Ciarletta et al.'s work did not report the stress-strain curves during preconditioning which would help to characterize and justify the softening mechanism of ligaments and tendons.

Currently, there is still no standard protocol used for preconditioning by experimental biomechanicians [8]. Therefore, developing mechanical models, which can elucidate the role of the structural components of biological tissue during preconditioning could help in defining important standard parameters that can guide the design of the experiments. In this study, a viscoelastic model for parallel-fibered collageneous tissues, such as ligaments and tendons, which describes their viscoelastic behavior exhibited during preconditioning is presented. The tissues are assumed to be composed of variously undulated, linear elastic collagen fibers. The collagen fibers are parallel to the loading direction and are embedded in a viscoelastic matrix. The elastic modulus of the collagen fibers and the elastic modulus of the matrix were assumed to gradually decrease for each successive cycle to characterize the softening during preconditioning. The model parameters and the predictive capability are validated by using data collected from rat medial collateral ligaments (MCLs). Stress-strain curves of successive cycles during preconditioning are predicted by the model in order to determine a protocol of preconditioning.

4.2 Model Formulation

The creep-relaxation model presented in Chapter 2 has been modified to incorporate softening that is associated with preconditioning. A schematic and basic assumptions of the proposed model are described in detail hereafter.

4.2.1 Preliminaries and Basic Assumptions

As mentioned earlier, ligaments and tendons are composed mainly of collagen fibers arranged parallel to the physiological direction of loading. The collagen fibers are embedded in a proteoglycan-rich matrix. The collagen fibers are assumed to have different waviness and exhibit linear elastic behavior after becoming straight under tension. The elastic modulus of each straight fiber is defined as E_f. The matrix surrounding the fibers is assumed to behave as a viscoelastic material. It is modeled as a Maxwell element, which is composed of a spring and a dashpot connected in series. The spring of the matrix is assumed to have an elastic modulus E_m and the dashpot of the matrix is assumed to have a coefficient of viscosity η_m. Thus, the tissues (ligaments or tendons) are modeled as an arrangement in parallel of different linear springs and a series of a linear spring and a linear dashpot. The schematic of the proposed model described is shown in Figure 4.1.

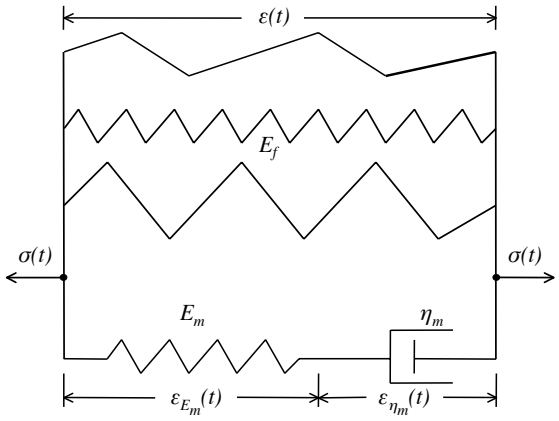

Figure 4.1: Schematic of viscoelastic model.

4.2.2 Modeling Framework

The total stress of the tissue, $\sigma(t)$, where t denotes the time, is given by

$$\sigma(t) = \sigma_f(t) + \sigma_m(t)\,, \tag{4.1}$$

where $\sigma_f(t)$ is the stress of the collagen fibers and $\sigma_m(t)$ is the stress of the matrix. Moreover, the total strain of the tissue, $\varepsilon(t)$, is

$$\varepsilon(t) = \varepsilon_f(t) = \varepsilon_m(t)\,, \tag{4.2}$$

where $\varepsilon_f(t)$ is the strain of the fibers and $\varepsilon_m(t)$ is the strain of the matrix.

Due to the arrangement in series of the elastic spring and viscous dashpot of the matrix, one has that

$$\sigma_m(t) = \sigma_{E_m}(t) = \sigma_{\eta_m}(t)\,, \tag{4.3}$$

where $\sigma_{E_m}(t)$ and $\sigma_{\eta_m}(t)$ are the elastic and viscous stresses of the matrix, respectively. Furthermore, the strain of the matrix, $\varepsilon_m(t)$, is

$$\varepsilon_m(t) = \varepsilon_{E_m}(t) + \varepsilon_{\eta_m}(t)\,, \tag{4.4}$$

where $\varepsilon_{E_m}(t)$ and $\varepsilon_{\eta_m}(t)$ are the strain of the spring and the strain of the viscous dashpot for the matrix, respectively.

The elastic stress of the matrix is defined as

$$\sigma_{E_m}(t) = E_m \varepsilon_{E_m}(t) \tag{4.5}$$

where E_m denotes the elastic modulus of the matrix. The viscous stress of the matrix is defined as

$$\sigma_{\eta_m}(t) = \eta_m \varepsilon'_{\eta_m}(t)\,, \tag{4.6}$$

where η_m denotes the viscous modulus of the matrix and a prime denotes the differentiation with respect to t.

After noting that $\sigma_m(t) = \sigma_{E_m}(t)$ from Eq. 4.3 and that $\sigma_m(t) = \sigma(t) - \sigma_f(t)$ from Eq. 4.1, Eq. 4.5 can be rewritten as

$$\varepsilon_{E_m}(t) = \frac{\sigma(t) - \sigma_f(t)}{E_m}\,. \tag{4.7}$$

Moreover, since $\varepsilon_{\eta_m}(t) = \varepsilon_m(t) - \varepsilon_{E_m}(t)$ from Eq. 4.4 and $\varepsilon(t) = \varepsilon_m(t)$ from Eq. 4.2, Eq. 4.6 becomes

$$\sigma_{\eta_m}(t) = \eta_m \varepsilon'(t) - \eta_m \varepsilon'_{E_m}(t)\,. \tag{4.8}$$

By recalling that $\sigma_m(t) = \sigma_{\eta_m}(t)$ from Eq. 4.3 and using Eq. 4.8, Eq. 4.1 takes the form

$$\sigma(t) = \sigma_f(t) + \eta_m \varepsilon'(t) - \eta_m \varepsilon'_{E_m}(t)\,. \tag{4.9}$$

Finally, after computing $\varepsilon'_{E_m}(t)$ from Eq. 4.7 and substituting the resulting expression into Eq. 4.9 one obtains the governing equation for the system described in Fig. 4.1

$$\sigma'(t) + \frac{E_m}{\eta_m}\sigma(t) = \sigma'_f(t) + \frac{E_m}{\eta_m}\sigma_f(t) + E_m \varepsilon'(t)\,. \tag{4.10}$$

The ratio $\frac{\eta_m}{E_m}$ is a characteristic time, τ, usually called the *relaxation time*. The above governing equation can be then rewritten as

$$\sigma'(t) + \frac{\sigma(t)}{\tau} = \sigma'_f(t) + \frac{\sigma_f(t)}{\tau} + E_m \varepsilon'(t)\,. \tag{4.11}$$

Once the stress of collagen fibers, $\sigma_f(t)$, is defined, the governing Eq. 4.11 with appropriate initial conditions can be used to describe hysteresis phenomenon under cyclic loading.

4.2.3 Stress of Collagen Fibers

The stress of the fibrous component of the tissues, $\sigma_f(t)$, is defined by using a structural approach as previously done by other investigators [43, 15, 16]. The collagen fibers are assumed to become straight at different strains, $\varepsilon_s \geq 0$, defined by the following Weibull probability density function

$$p(\varepsilon_s) = \frac{\alpha}{\beta}\left(\frac{\varepsilon_s}{\beta}\right)^{\alpha-1} e^{-\left(\frac{\varepsilon_s}{\beta}\right)^{\alpha}} \quad \text{with} \quad \int_0^{\infty} p(\varepsilon_s)d\varepsilon_s = 1\,, \tag{4.12}$$

where $\alpha > 0$ is the so-called *shape parameter* and $\beta > 0$ is the so-called *scale parameter*. The stress of collagen fibers is given for $\varepsilon \geq \varepsilon_s$ by

$$\sigma_f(t) = \int_0^{\varepsilon(t)} E_f(\varepsilon(t) - \varepsilon_s) p(\varepsilon_s) d\varepsilon_s \,, \tag{4.13}$$

where E_f denotes the elastic modulus of each straight collagen fiber. The above equation can also be written as (see Appendix A)

$$\sigma_f(t) = E_f \left[\varepsilon(t) - \frac{\beta}{\alpha} \gamma \left(\frac{1}{\alpha}, \left(\frac{\varepsilon(t)}{\beta} \right)^{\alpha} \right) \right] , \tag{4.14}$$

where

$$\gamma(x, y) = \int_0^y \xi^{x-1} e^{-\xi} d\xi \tag{4.15}$$

is the so-called *lower incomplete gamma function.*

4.2.4 Stress Relaxation

Relaxation is a continuous decrease in stress that is observed in collagenous tissues when they are subjected to a constant strain. First, one must note that for any strain history, $\varepsilon(t)$, the solution to the governing Eq. 4.11 is

$$\sigma(t) = \sigma_f(t) + \frac{\int_0^t E_m \varepsilon'(t) e^{t/\tau} dt + C}{e^{t/\tau}} \,, \tag{4.16}$$

where C is a constant that is determined by the initial condition. In order to describe relaxation by using Eq. 4.16, the strain history of the tissue, $\varepsilon(t)$, is assumed to have the

form

$$\varepsilon(t) = \begin{cases} at & \text{for } 0 \leq t < t_0\,, \\ \varepsilon_0 & \text{for } t \geq t_0\,, \end{cases} \tag{4.17}$$

where a, ε_0 and t_0 are constants and $at_0 = \varepsilon_0$. For $0 \leq t < t_0$, $\varepsilon'(t) = a$ and, hence, Eq. 4.16 takes the form

$$\sigma(t) = \sigma_f(t) + E_m a\tau[1 - e^{-\frac{t}{\tau}}] + Ce^{\frac{-t}{\tau}}\,. \tag{4.18}$$

By imposing the initial condition $\sigma(0) = 0$ and noting that $\varepsilon(0) = 0$, one obtains that $C = 0$ in Eq. 4.18. Therefore, in the interval $0 \leq t < t_0$, the stress of the tissue is

$$\sigma(t) = \sigma_f(t) + E_m a\tau[1 - e^{-\frac{t}{\tau}}]\,. \tag{4.19}$$

For $t > t_0$, $\varepsilon(t) = \varepsilon_0$ and $\varepsilon'(t) = 0$ so that Eq. 4.16 becomes

$$\sigma(t) = \sigma_f(t) + Ce^{\frac{-t}{\tau}}\,. \tag{4.20}$$

By using the initial condition computed from Eq. 4.19 at $t = t_0$ and using Eg. 4.20, one obtains that

$$C = E_m a\tau(e^{\frac{t_0}{\tau}} - 1)\,. \tag{4.21}$$

For $t > t_0$, the stress of the tissue can be written as

$$\sigma(t) = \sigma_f(t) + E_m a\tau\left(e^{\frac{t_0 - t}{\tau}} - e^{-\frac{t}{\tau}}\right)\,. \tag{4.22}$$

The above equation describes the relaxation that is exhibited by the tissue when a constant strain ε_0 is applied. In this case, the stress of the collagen fibers, $\sigma_f(t)$, defined by Eq. 4.14

is constant and has the form

$$\sigma_f(t) = E_f \left[\varepsilon_0 - \frac{\beta}{\alpha} \gamma \left(\frac{1}{\alpha}, \left(\frac{\varepsilon_0}{\beta} \right)^{\alpha} \right) \right] . \tag{4.23}$$

4.2.5 Strain Controlled Hysteresis Phenomenon

A hysteresis phenomenon is observed in collagenous tissues when they are subjected to cyclic stretching. Recall that for any strain history, $\varepsilon(t)$, the solution to the governing Eq. 4.11 is

$$\sigma(t) = \sigma_f(t) + \frac{\int_0^t E_m \varepsilon'(t) e^{t/\tau} dt + C}{e^{t/\tau}} , \tag{4.24}$$

where C is a constant that is determined by the initial condition. In order to describe hysteresis of each cyclic loading by using Eq. 4.24, the cyclic strain history of the tissue, $\varepsilon(t)$, is assumed to have the form

$$\varepsilon(t) = \begin{cases} bt - (2i-2)bt_0 & \text{for } (2i-2)t_0 \leq t < (2i-1)t_0 \text{ , (loading)} \\ -bt + (2i)bt_0 & \text{for } (2i-1)t_0 \leq t < (2i)t_0 \text{ , (unloading)} \end{cases} \tag{4.25}$$

where b and t_0 are constants, i is a positive integer that denotes the number of hysteresis cycles and the maximum strain of the hysteresis cycle is $\varepsilon_M = bt_0$.

For $0 \leq t < t_0$, $\varepsilon'(t) = b$ and, hence, Eq. 4.24 takes the form

$$\sigma(t) = \sigma_f(t) + E_m b \tau_l [1 - e^{-\frac{t}{\tau_l}}] + C e^{\frac{-t}{\tau_l}} . \tag{4.26}$$

where τ in Eq. 4.24 was replaced by τ_l to represent the relaxation time for the loading path of every cycle.

By imposing the initial condition $\sigma(0) = 0$ and noting that $\varepsilon(0) = 0$, one obtains that $C = 0$ in Eq. 4.26. Therefore, in the interval $0 \leq t < t_0$, the stress of the tissue is

$$\sigma(t) = \sigma_f(t) + E_m b\tau_l[1 - e^{-\frac{t}{\tau_l}}]\,. \tag{4.27}$$

For $t_0 \leq t < 2t_0$, $\varepsilon'(t) = -b$ so that Eq. 4.24 becomes

$$\sigma(t) = \sigma_f(t) - E_m b\tau_u[1 - e^{\frac{(t_0-t)}{\tau_u}}] + Ce^{\frac{-t}{\tau_u}}\,. \tag{4.28}$$

where τ in Eq. 4.24 was replaced by τ_u to represent the relaxation time for the unloading path of every cycle.

By using the initial condition $\sigma(t_0) = \sigma_f(t_0) + E_m b\tau_l[1 - e^{-\frac{t_0}{\tau_l}}]$ computed by using Eqs. 4.27-4.28, one obtains that

$$C = E_m b\tau_l(1 - e^{\frac{t_0}{\tau_l}})e^{\frac{t_0}{\tau_u}}\,. \tag{4.29}$$

For $t_0 \leq t < 2t_0$, the stress of the tissue can be written as

$$\sigma(t) = \sigma_f(t) - E_m b\tau_u[1 - e^{-\frac{(t_0-t)}{\tau_u}}] + \left[E_m b\tau_l(1 - e^{\frac{t_0}{\tau_l}})e^{\frac{t_0}{\tau_u}}\right] e^{\frac{-t}{\tau_u}}\,. \tag{4.30}$$

Equations 4.27 and 4.30 above describe the hysteresis that is exhibited by the tissue when a loading strain $\varepsilon = bt$ and an unloading strain $\varepsilon = -bt + 2bt_0$ are applied, respectively. In these case, the stress of the collagen fibers, $\sigma_f(t)$, defined by Eq. 4.14 can be rewritten as

$$\sigma_f(t) = E_f\left[bt - \frac{\beta}{\alpha}\gamma\left(\frac{1}{\alpha}, \left(\frac{bt}{\beta}\right)^{\alpha}\right)\right] \text{ (loading)} \tag{4.31}$$

$$\sigma_f(t) = E_f \left[(-bt + 2t_0) - \frac{\beta}{\alpha} \gamma \left(\frac{1}{\alpha}, \left(\frac{(-bt + 2t_0)}{\beta} \right)^{\alpha} \right) \right] \text{ (unloading) .} \tag{4.32}$$

The stress-strain relationships for all the cycles that follow the 1^{st} cycle can be similarly computed by extending the above formulation.

4.2.6 Stress Softening and Energy Dissipation during Preconditioning

Stress softening and energy dissipation during preconditioning occur due to changes of the internal structure of the tissues. It has been experimentally observed that the maximum stresses and hysteresis (energy dissipation) of successive stress-strain cycles gradually decrease during preconditioning. The stress-strain cycles finally remain unchanged when the tissues are completely preconditioned.

To model the stress softening and energy dissipation during cyclic stretching, the maximum stress during each cycle is assumed to be determined only by the collagen fibers and, thus, the elastic modulus of the straight collagen fibers can be computed by the following relationship

$$E_f^{(i)} = \frac{\sigma^{(i)}(\varepsilon_{Max})}{f(\varepsilon_{Max})} . \tag{4.33}$$

where ε_{Max} is the maximum strain of the tissue, i denotes the number of cycles and $f = f(\varepsilon_{Max})$ is a constant. It must be noted that for every cycle $f = f(\varepsilon_{Max})$ has the same constant value since it depends only on the maximum strain which is constant for cyclic

loading experiments performed by controlling the strain.

The value of the elastic modulus of the matrix $E_m^{(i)}$ is also assumed to change during each cycle and can be computed by curve fitting the experimental data of the loading stress-strain curves of each cycle. The parameters α, β and τ_l are assumed to have the same values for all cycles. The changing of E_f and E_m of each cycle characterized the stress softening and the decreasing of the hysteresis of each cycle during preconditioning, respectively.

4.3 Results

4.3.1 Parameter Estimation

There were 6 parameters E_f, α, β, E_m, τ_l, τ_u that needed to be estimated to describe the viscoelastic properties of ligaments and tendons during preconditioning by using the proposed model. In order to estimate the model parameters, three sets of experimental data on stress relaxation that were collected by subjecting three rat medial collateral ligaments to three different constant strain levels, $\varepsilon_0 = 1.11\%, 1.53\%$ and 1.85%, along their physiological loading direction were used to estimate the model parameters. The ramp up tensile tests that preceded the relaxation tests at three strain levels, $\varepsilon_0 = 1.11\%, 1.53\%$ and 1.85%, were conducted at constant strain rates of $\varepsilon'(t) = a = 0.15\%/s, 0.30\%/\text{s}$ and $0.25\%/\text{s}$, respectively. Experimental data on preconditioning that were collected by subjecting one medial collateral ligament to 30 loading cycles along the physiological loading direction were also used. The

maximum strain for each loading cycle was set to be $\varepsilon_{Max} = 3.4\%$ and the strain rate was set to $\varepsilon'(t) = b = 23\%/\text{s}$ for the loading path and $\varepsilon'(t) = -b = -23\%/\text{s}$ for the unloading path.

The two parameters E_m and τ, which characterized the mechanical response of the proteoglycan-rich matrix, and the constant stress of the collagen fibers, σ_f, were evaluated by curve fitting Eq. 4.22 to the three sets of stress relaxation data collected at $\varepsilon_0 = 1.11\%$, $\varepsilon_0 = 1.53\%$ and $\varepsilon_0 = 1.85\%$. It must be noted that for each stress relaxation test, $\varepsilon_0 = 1.11\%, 1.53\%$ and 1.85% and, therefore, $t_0 = 7.52$ s, 5.09 s and 7.32 s, since the experiments were conducted at constant strain rates, $\varepsilon'(t) = a = 0.15\%/s, 0.30\%/\text{s}$ and $0.25\%/\text{s}$, respectively. The curve fitting was performed by employing the Levenberg-Marquardt nonlinear least squares algorithm implemented in Matlab (The MathWorks, Inc.). The results of the curve fitting are shown in Figure 4.2-Figure 4.4. Finally, the three values of the parameters E_m and τ, which were obtained by curve fitting, and the value of the parameter σ_f were averaged to be $E_m = 62 \mp 18$ MPa, $\tau = \tau_l = 13 \mp 4$ s and $\sigma_f = 1.07 \mp 0.4$. These values of E_m and τ were then used to represent the mechanical response of the proteoglycan-rich matrix.

The three parameters, E_f, α, and β, which defined the response of the collagen fibers, were computed by curve fitting Eqs. 4.19 and 4.14 to the nonlinear tensile stress-strain data of the first loading cycle of the preconditioning data. The strain history was set to be $\varepsilon(t) = bt$ with $b = 23\%/\text{s}$ while $E_m = 62$ MPa and $\tau_l = 13$ s. The parameters were uniquely estimated to be $E_f = 467$ MPa, $\alpha = 2.01$ and $\beta = 0.017$ by using the Levenberg-Marquardt nonlinear least squares algorithm by imposing that the parameters were non-negative ($R^2 = 0.99$). In

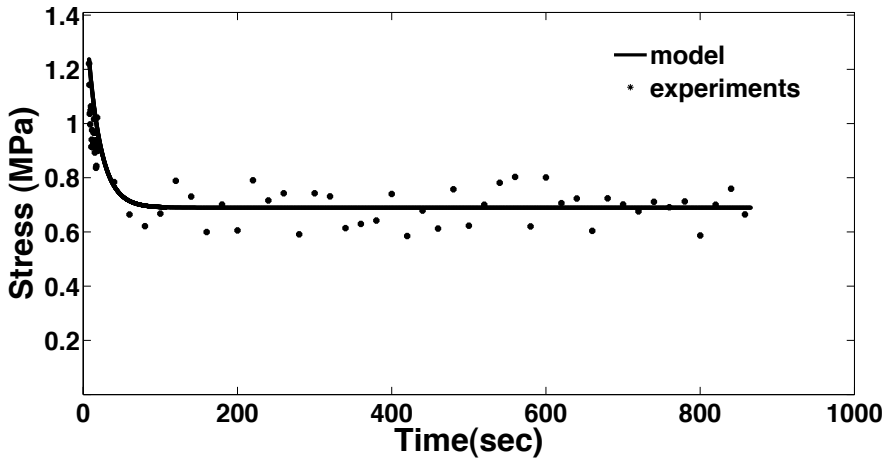

Figure 4.2: Stress relaxation data at $\varepsilon_0 = 1.11\%$ and model fit with $E_m = 43.62$ MPa, $\tau = 16.9$ s and $\sigma_f = 0.6896$ MPa ($R^2 = 0.83$).

Figure 4.5, the stress-strain data and the model fit are reported.

For the unloading stress-strain curve of the first cycle, the relaxation time of the proteoglycan-rich matrix, τ_u, was assumed to be different from the relaxation time of the loading stress-strain curve, τ_l. Therefore, the viscoelastic response of the proteoglycan-rich matrix exhibited during unloading was computed by curve fitting Eq. 4.30 with Eq. 4.14 to the unloading stress-strain data of the first cycle of the preconditioning. The strain history was set to be $\varepsilon(t) = -bt + 2bt_0$ with $b = 23\%/\text{s}$ and $E_f = 467$ MPa, $\alpha = 2.01$, $\beta = 0.01703$ and $E_m = 62$ MPa. The parameter was uniquely estimated to be $\tau_u = 0.010$ by using the Levenberg-Marquardt nonlinear least squares algorithm ($R^2 = 0.99$). In Figure 4.6, the stress-strain data and the model fit are reported.

The parameters, which were estimated by curve fitting the experimental data as described

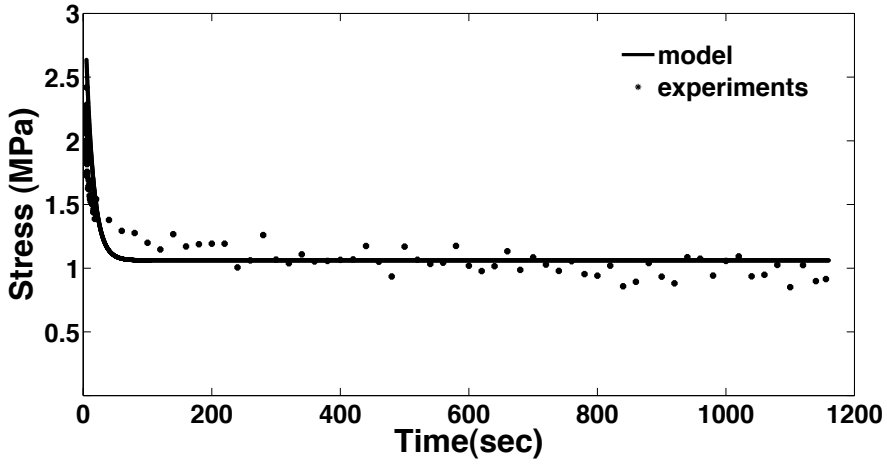

Figure 4.3: Stress relaxation data at $\varepsilon_0 = 1.53\%$ and model fit with $E_m = 80.06$ MPa, $\tau = 11.65$ s and $\sigma_f = 1.061$ MPa ($R^2 = 0.91$).

above, described only the first cycle during preconditioning. As mentioned earlier, the parameters that described the stress softening were $E_f^{(i)}$ and $E_m^{(i)}$ during each i cycle. The values of the parameter $E_f^{(i)}$ for $i > 1$ were estimated by using Eq. 4.33 where the maximum stress of each cycle during preconditioning was provided by the experiments. The constant value of $f = f(\varepsilon_{Max})$ was found to be 0.024 by using Eq. 4.33, $\sigma_{Max}^1 = 11.3$ MPa given by the experiments and $E_f^{(1)} = 467$ MPa computed by curve fitting loading stress-strain data of the first cycle. After determining the constant $f = f(\varepsilon_{Max})$, Eq. 4.33 could be used to estimate the parameter, $E_f^{(i)}$, for $i > 1$ that is associated with different cycles during preconditioning. The values of $E_f^{(i)}$ versus the number i of cycles are presented in Figure 4.7.

The parameter E_m also determined the stress softening behavior of the tissues during preconditioning. Its value for each cycle, $E_m^{(i)}$, was computed by curve fitting Eq. 4.27 with Eq. 4.14

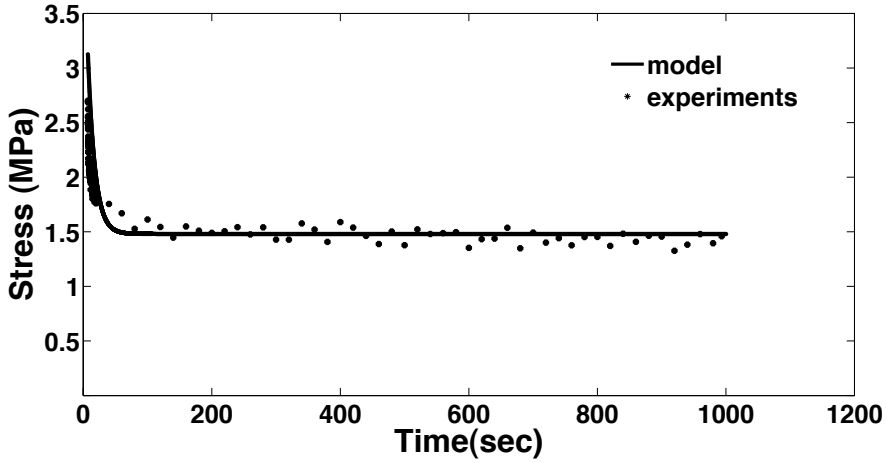

Figure 4.4: Stress relaxation data at $\varepsilon_0 = 1.85\%$ and model fit with $E_m = 64.28$ MPa, $\tau = 10.98$ s and $\sigma_f = 1.48$ MPa ($R^2 = 0.90$).

to the loading stress-strain data of each cycle of preconditioning. The strain history was set to be $\varepsilon(t) = bt$ with $b = 23\%/\text{s}$. The parameters α, β, and τ_l were assumed to have the same values for each cycle and, thus, were computed by fitting the first loading stress-strain curve of preconditioning as described above. The value of $E_f^{(i)}$ for each cycle was estimated by knowing $\sigma_{(i)}$ from the experiments and using $f = f(\varepsilon_{Max}) = 0.024$. The parameter $E_m^{(i)}$ of each cycle was found uniquely by using the Levenberg-Marquardt nonlinear least squares algorithm. In Figure 4.7, the values of the $E_m^{(i)}$ are plotted versus the numbers of cycles.

After all the parameters were computed for each cycle, the loading and unloading stress-strain curves for the 1^{st}, 3^{rd}, 5^{th}, 10^{th}, 15^{th}, 20^{th}, 25^{th} and 30^{th} cycles were predicted by the model and the results were compared with the experimetal data in Figure 4.8-Figure 4.15. Moreover, the successive stress-strain curves of the 1^{st}, 3^{rd}, 5^{th}, 10^{th}, 15^{th}, 20^{th}, 25^{th} and

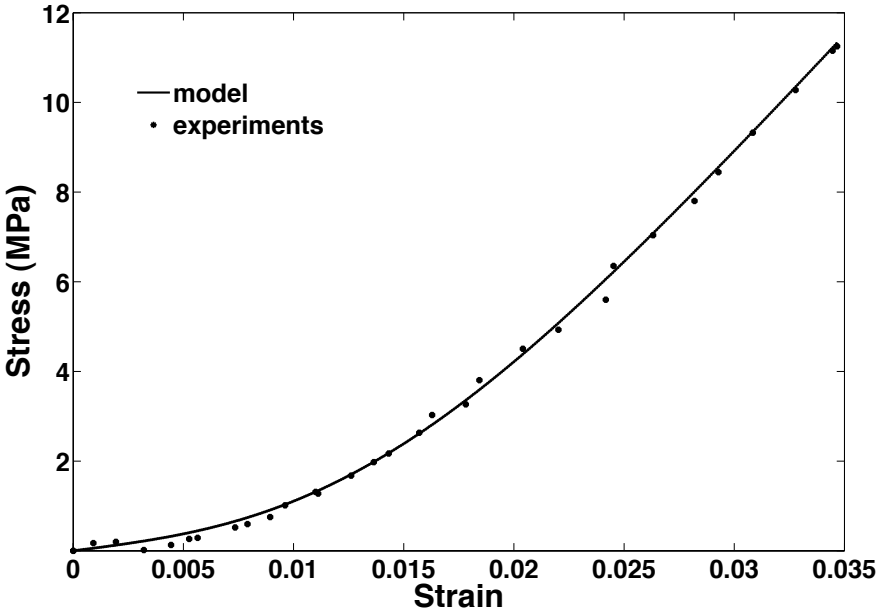

Figure 4.5: Loading stress-strain data for the 1^{st} cycle and model fit with $E_f = 467$ MPa, $\alpha = 2.01$ and $\beta = 0.017$ ($R^2 = 0.99$).

30^{th} cycles which were collected from preconditioning experiments and computed from the model are shown in Figure 4.16 and Figure 4.17, respectively.

4.3.2 Influence of model parameters on preconditioning

The influence of the model parameters E_f and E_m on preconditioning was studied by varying their numerical values. The parameters obtained from curve fitting the relaxation, loading and unloading stress-strain data during preconditioning were used as baseline for each parametric study. In Figure 4.18 the influence of E_f on the preconditioning response is illustrated. One could observed that as E_f decreased, the maximum stress of each cycle and the stress

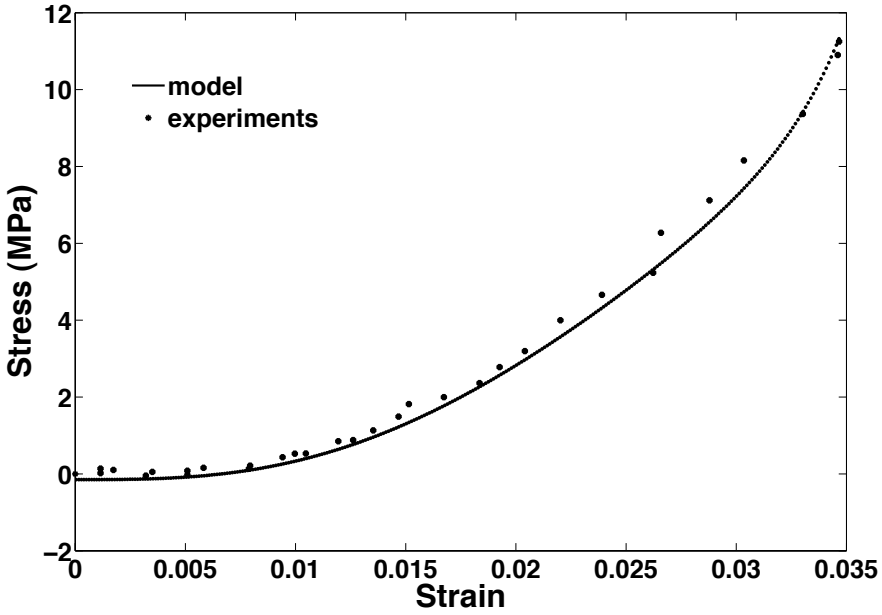

Figure 4.6: Unloading stress-strain data for the 1^{st} cycle and model fit with $\tau_u = 0.010$ ($R^2 = 0.99$).

over strain for the loading and unloading paths significantly decreased, while the amount of hysteresis of each cycle remained almost unchanged. The effect of E_m on preconditioning is presented in Figure 4.19. It could be noted that as E_m decreased, the amount of hysteresis of each cycle significantly decreased, while the maximum stress of each cycle slightly decreased. Moreover, the stress over strain for the loading path also decreased, while the stress over strain for the unloading path remained unchanged for every cycle.

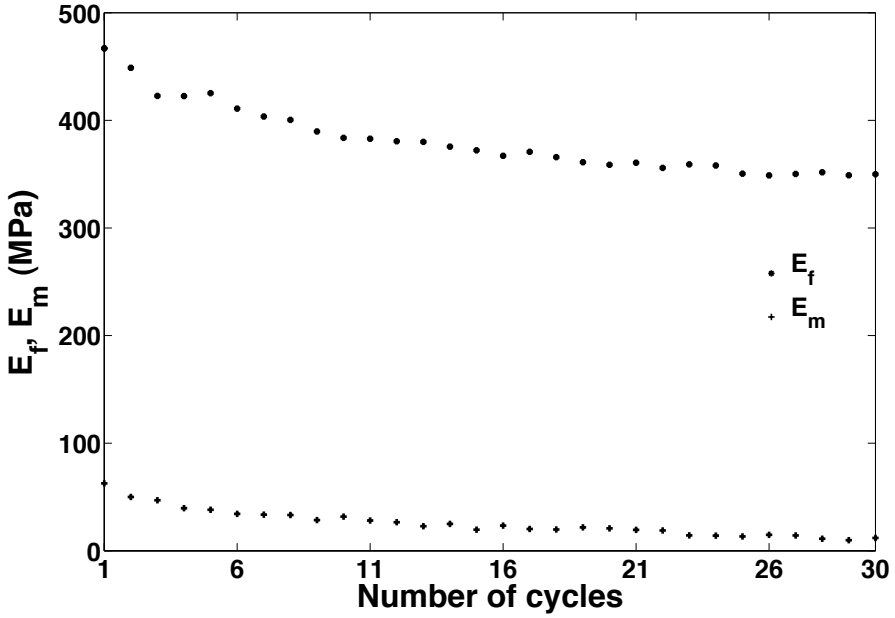

Figure 4.7: Values of $E_f^{(i)}$ and $E_m^{(i)}$ versus the number i of loading cycles during preconditioning.

4.4 Discussion and Conclusions

The structural changes that occur into biological tissues during preconditioning are still unknown. Few structurally-based models have been proposed to describe the preconditioning process of ligaments and tendons [66, 6]. However, more theoretical studies are needed to elucidate the mechanisms that govern the preconditioning process in order to develop predictive tools that can be used to establish standard preconditioning protocols.

A simple viscoelastic model was presented to describe the preconditioning process in parallel-fibered collagenous tissues such as ligaments and tendons. The model, schematically pre-

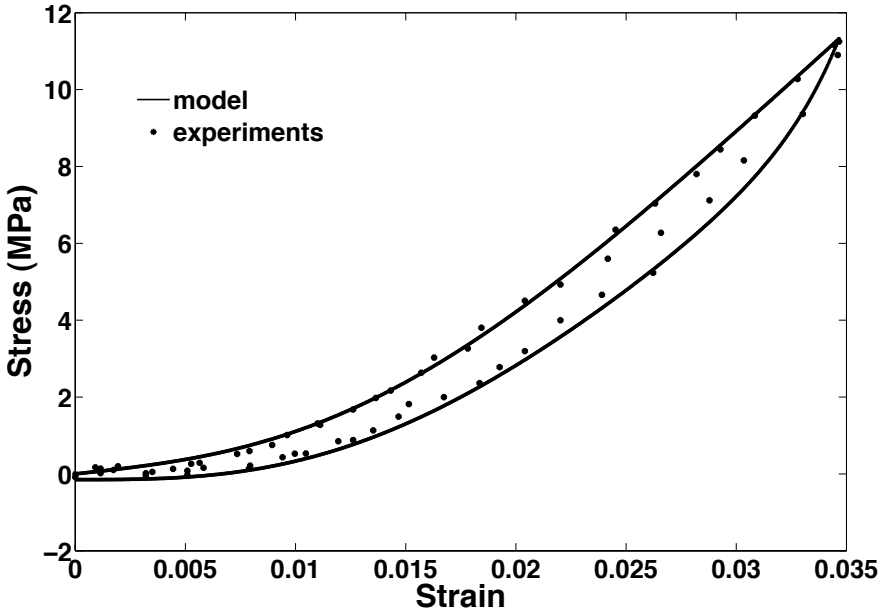

Figure 4.8: Stress-strain data for the 1^{st} cycle of preconditioning and model fit.

sented in Figure 4.1, was formulated by accounting for the mechanical contributions of the collagen fibers and the surrounding proteoglycan-rich matrix. The model formulation presented here took into account the gradual straightening of collagen fibers during the loading path and the gradual crimping during the unloading path of each cyclic loading of preconditioning. The straightening and crimping of the collagen fibers were responsible for the nonlinearities observed in the stress-strain curves. The proteoglycan-rich matrix was assumed to be responsible for the hysteresis in each loading cycle. The decreasing of elastic moduli of the straight collagen fibers and matrix, namely E_f, and E_m, determined the decreasing of the maximum stresses and hysteresis of successive stress-strain cycles during preconditioning. Due to the lack of published experimental data, the model parameters were

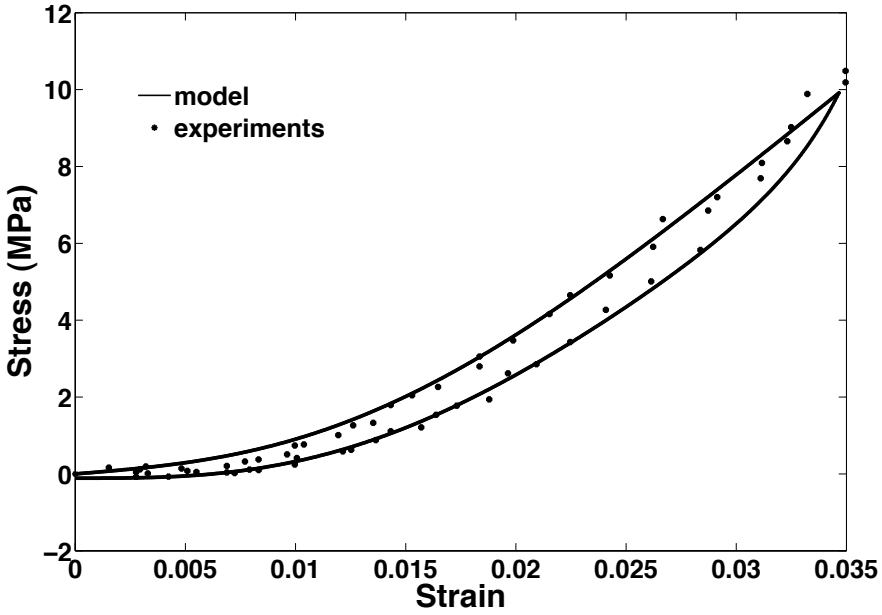

Figure 4.9: Stress-strain data for the 3^{rd} cycle of preconditioning and model prediction.

estimated by using preliminary experimental data that were collected on rat medial collateral ligaments in our laboratory. Although the model seemed promising, more experimental data are needed for fully validating it.

The results of curve fitting the model to stress relaxation and loading and unloading stress-strain data of the 1^{st} preconditioning cycle were presented in Figures 4.2, 4.3, 4.4, 4.5 and 4.6. The elastic modulus of the proteoglycan-rich matrix E_m was estimated to have an average value of 62 MPa from three sets of stress relaxation data. The viscous modulus of the matrix for the loading path was estimated to be $\eta_{m_l} = \tau_l E_m = 825$ MPa s while the viscous modulus of the matrix for the unloading path was found to be $\eta_{m_u} = \tau_u E_m = 0.638$ MPa s. The elastic modulus of the individual collagen fiber E_f was estimated to be 467

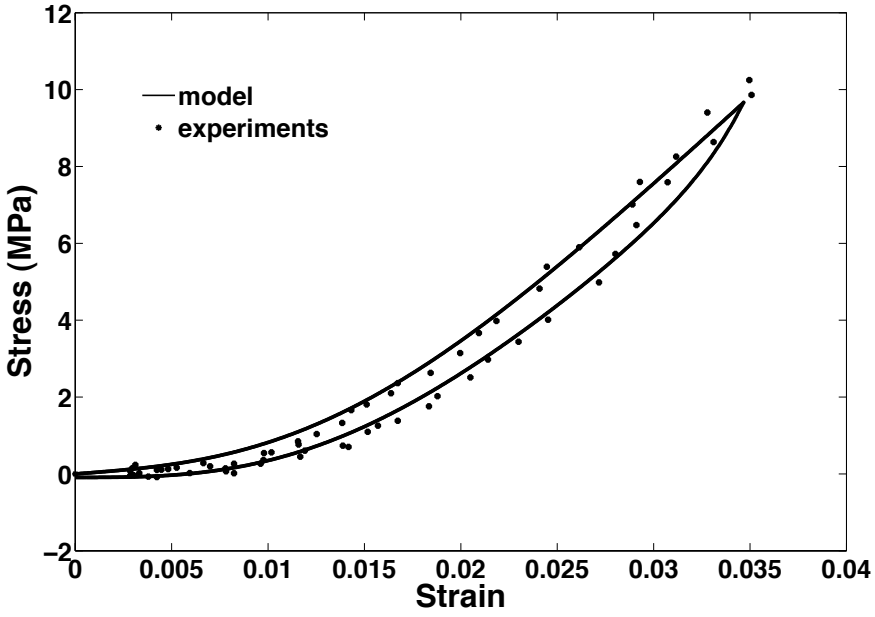

Figure 4.10: Stress-strain data for the 5^{th} cycle of preconditioning and model prediction.

MPa. The shape parameter α and scale parameter β of the Weibull probability function defined the strain-based recruitment and crimping processes of collagen fibers during loading and unloading stress-strain paths. In order to describe successive cycles of preconditioning, the parameters E_f and E_m were assumed to have different values in each cycle while all the other parameters in the model were assumed have the values computed during the 1^{st} preconditioning cycle.

The values of parameter $E_f^{(i)}$ of each cycle were estimated by knowing the maximum stress of each cycle. After determining the value of $E_f^{(i)}$ of each cycle, the values of the parameter $E_m^{(i)}$ of each cycle were estimated by curve fitting the model to the loading stress-strain path of each cycle while fixing the other model parameters. The values of $E_f^{(i)}$ and $E_m^{(i)}$ for each

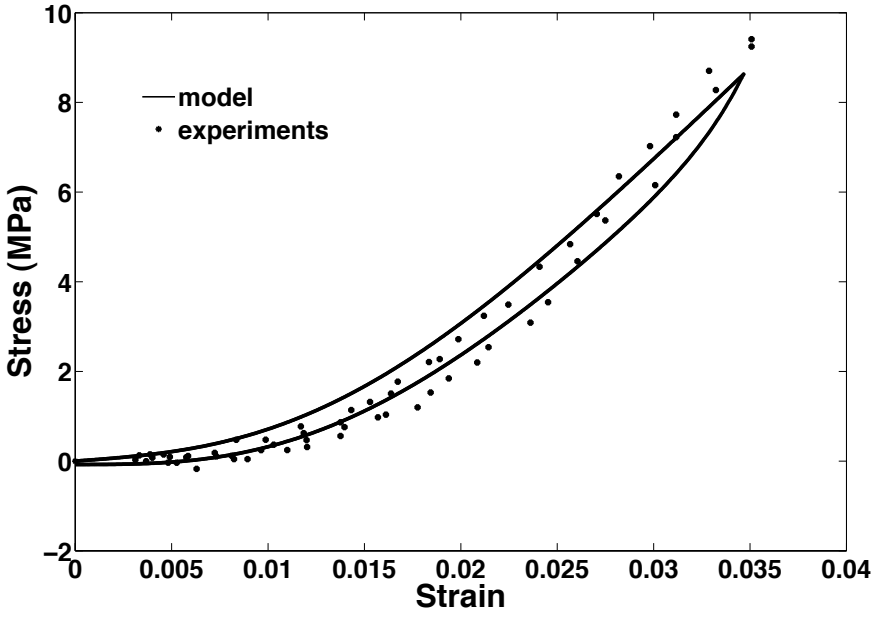

Figure 4.11: Stress-strain data for the 10^{th} cycle of preconditioning and model prediction.

cycle were presented in Figure 4.7 where it could be seen that they exponentially decreased for successive cycles during preconditioning and they became constant at the 25^{th}-30^{th} cycle. The decreasing of $E_f^{(i)}$ and $E_m^{(i)}$ can be attributed to the breaking of the bonding of the collagen fibers and the matrix. According to experimental observations [80], the breakage of bonds between the fibers and the matrix such as hydrogen bonds [65] play a significant role on the stress softening and energy dissipation observed during preconditioning. In the proposed model, the bonding between the fibers and the matrix was not explicitly modeled. However, the mechanical contribution of such bonding was inherently included in the elastic moduli of the fibers and the matrix. Thus, at the first cyclic loading of the preconditioning process, the parameter E_f could be assumed to represent the elastic modulus of the straight

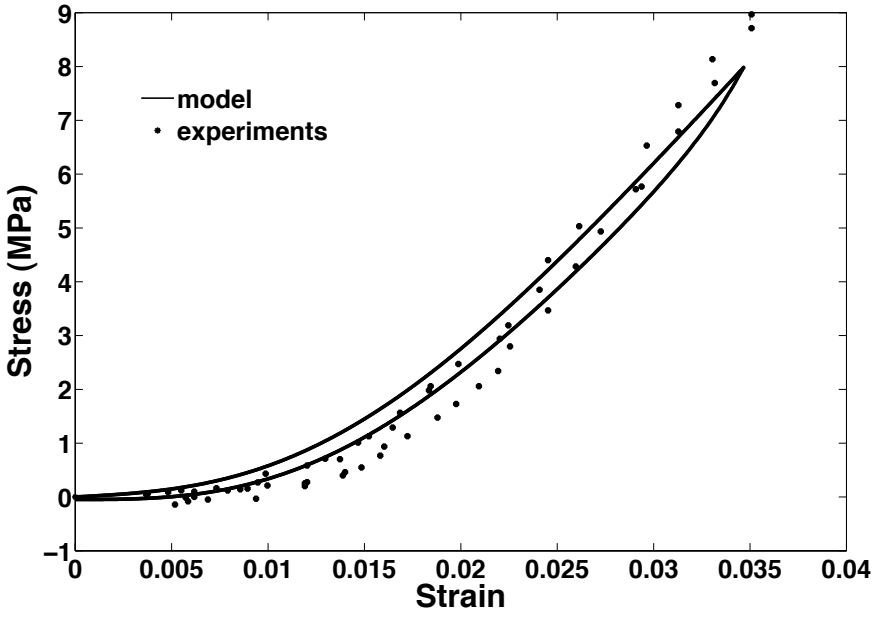

Figure 4.12: Stress-strain data for the 15^{th} cycle of preconditioning and model prediction.

fibers and the inherent coupling with the matrix. Similarly, the parameter E_m could be assumed to represent the elastic modulus of the matrix and the inherent coupling with the collagen fibers. After the first loading cycle of preconditioning, the bonding between collagen fibers and matrix was assumed to gradually decrease and, therefore, caused the decreasing in the parameters $E_f^{(i)}$ and $E_m^{(i)}$. There was no bonding between the collagen fibers and the matrix when $E_f^{(i)}$ and $E_m^{(i)}$ remained unchanged as the number i of cycles increased. Therefore, the constant values of $E_f^{(i)}$ and $E_m^{(i)}$ for $i = 25 \ldots 30$ represented the true value of the elastic modulus of an individual straight fiber and the true value of the elastic modulus of the proteoglycan-rich matrix, respectively. The constant value of $E_f^{(i)}$ was found to be 350 MPa, which is within the range of the values of the modulus of an individual fiber found in

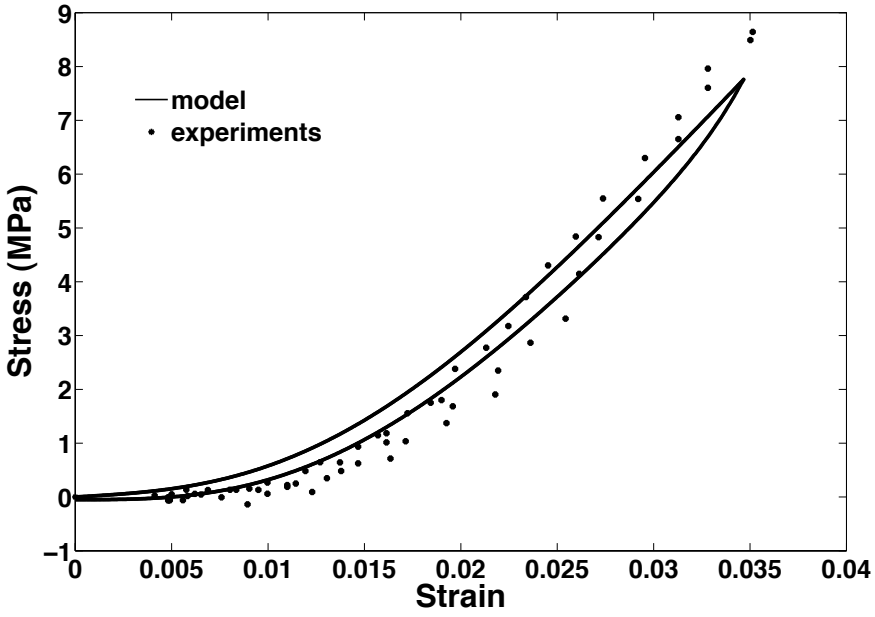

Figure 4.13: Stress-strain data for the 20^{th} cycle of preconditioning and model prediction.

literature [30] and the constant value of $E_m^{(i)}$ was found to be 12 MPa.

The stress-strain of the loading and unloading paths of the 1^{st}, 3^{rd}, 5^{th}, 10^{th}, 15^{th}, 20^{th}, 25^{th} and 30^{th} cycle, which were predicted from the model were compared to the experimental data in Figure 4.8-Figure 4.15, respectively. According to these comparisons, the model simulations and the experimental data agreed well for the 1^{st} to 10^{th} cycles while they showed small errors for the 15^{th} to 30^{th} cycles. These errors might come from the shape parameter, α, and the scale parameter, β, which describe the recruitment of the fibers. In this work, α and β were not allowed to change in each cycle while the elastic modulus of the straight fiber, $E_f^{(i)}$, changed in every cycle. If the breakage of the bonding between the fibers and the matrix affects the recruitment process of the fibers, the errors could be minimized

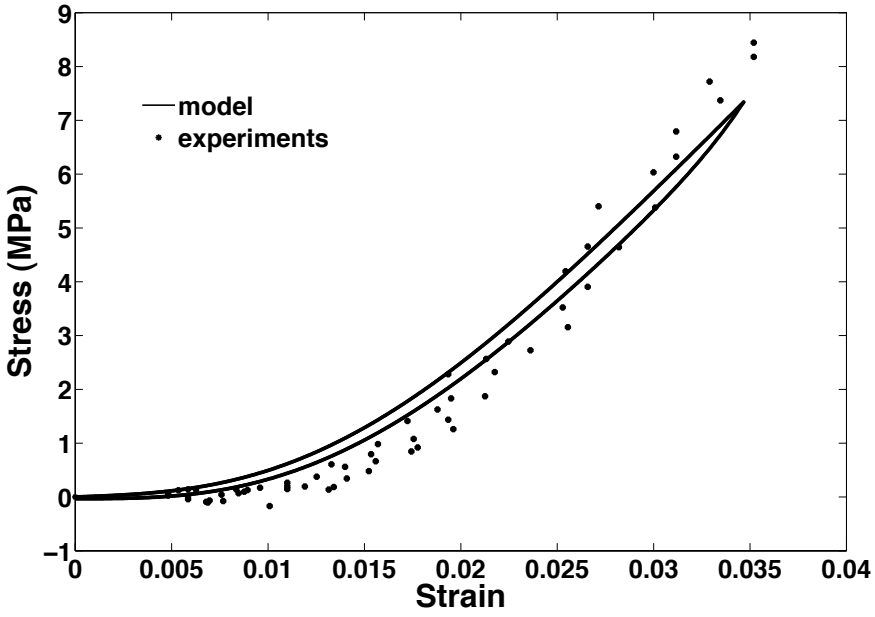

Figure 4.14: Stress-strain data for the 25^{th} cycle of preconditioning and model prediction.

by allowing α and β to change values for every cycle. However, the model predictions and the experimental data showed the same trend of decreasing maximum stress and hysteresis in successive cycles during preconditioning. Both the experimental data and the model predictions showed that the stress-strain curves of the cyclic loading remained unchanged at the 25^{th}-30^{th} cycle as presented in Figure 4.16 and Figure 4.17, respectively.

The influence of the parameters E_f and E_m to preconditioning process were presented in Figure 4.18 and Figure 4.19, respectively. In Figure 4.18, the maximum stress and the stress over strain of the loading and unloading paths of each cycle decreased as E_f decreased. It was found that, unlike E_m, E_f played a significant role on decreasing the maximum stresses of successive stress-strain cycles. In Figure 4.19, the stress over strain of the loading path

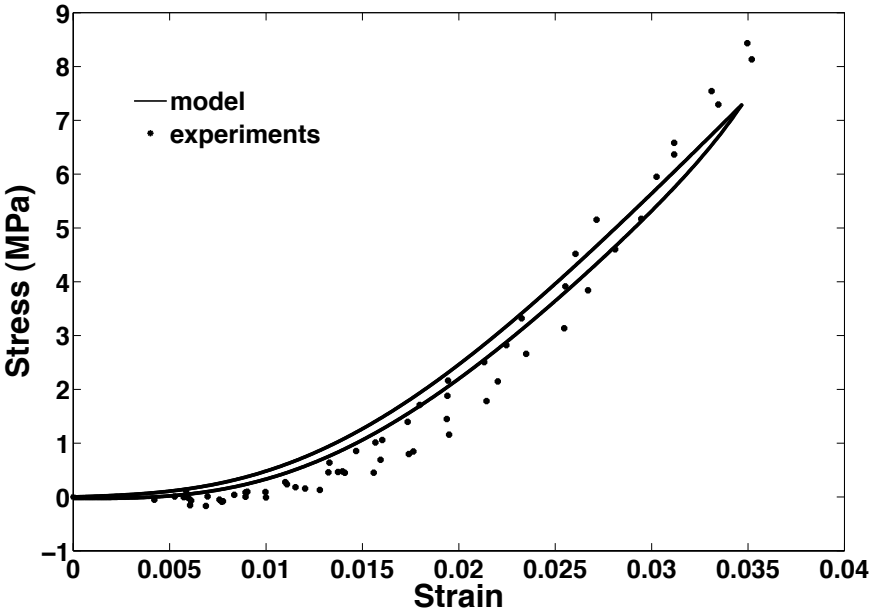

Figure 4.15: Stress-strain data for the 30^{th} cycle of preconditioning and model prediction.

and the amount of hysteresis of each cycle decreased as E_m decreased. Thus, E_m was crucial in decreasing the hysteresis of successive stress-strain cycles but E_f did not influence such decrease in hysteresis.

Preconditioning is usually performed at very small strains to avoid structural damage to the tissues, specifically damage to the collagen fibers. It has been suggested by Provenzano et al. that for rat medial collateral ligaments the collagen fibers are not damaged when strained below 5.14% strain [51]. Therefore, the experimental data collected in our lab did not produce damage to the fibers. In previous studies [66, 6] the stress softening in preconditioning was assumed to be due damage in the collagen fibers, which may have unlikely occurred in our experiments due to the small strains used. Furthermore, in these studies, the stress-

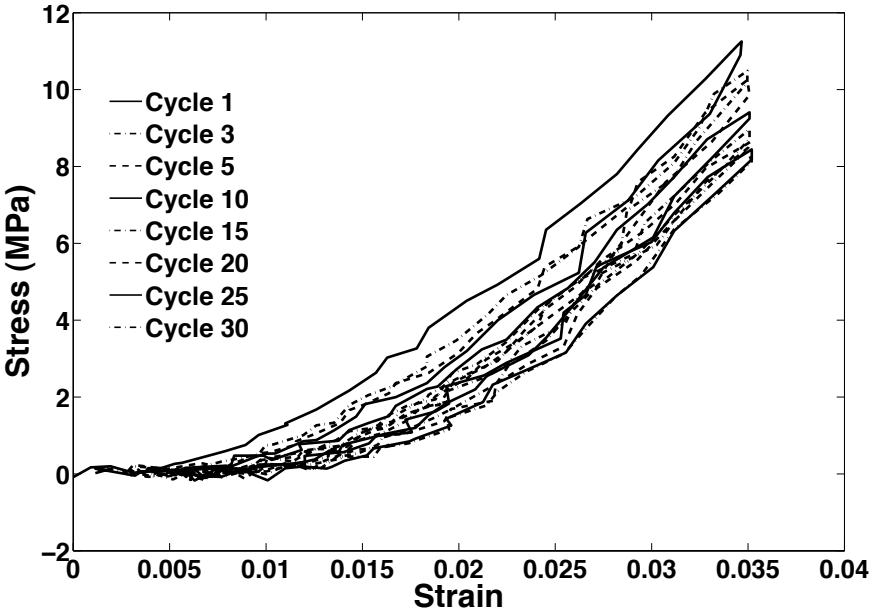

Figure 4.16: Experimental stress-strain data of preconditioning.

strain curves during preconditioning were not predicted and this prediction could help in understanding the origin of the stress softening mechanism in ligaments and tendons.

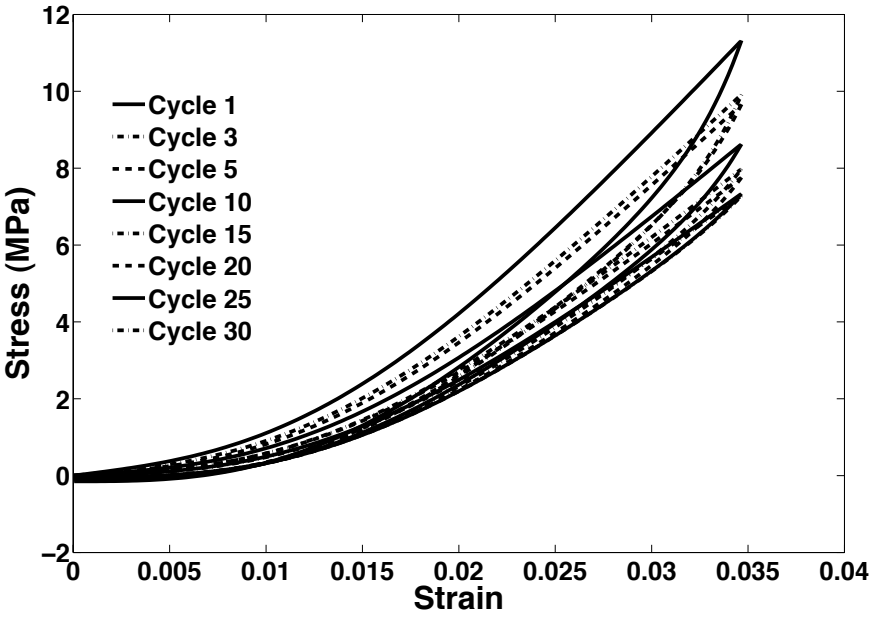

Figure 4.17: Stress-strain data during preconditioning predicted from the model.

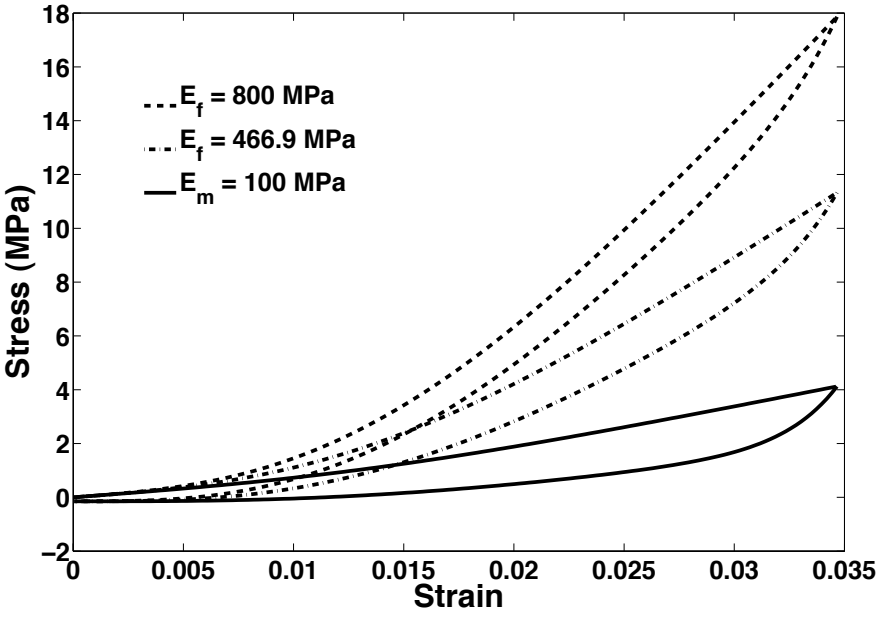

Figure 4.18: Influence of E_f on preconditioning.

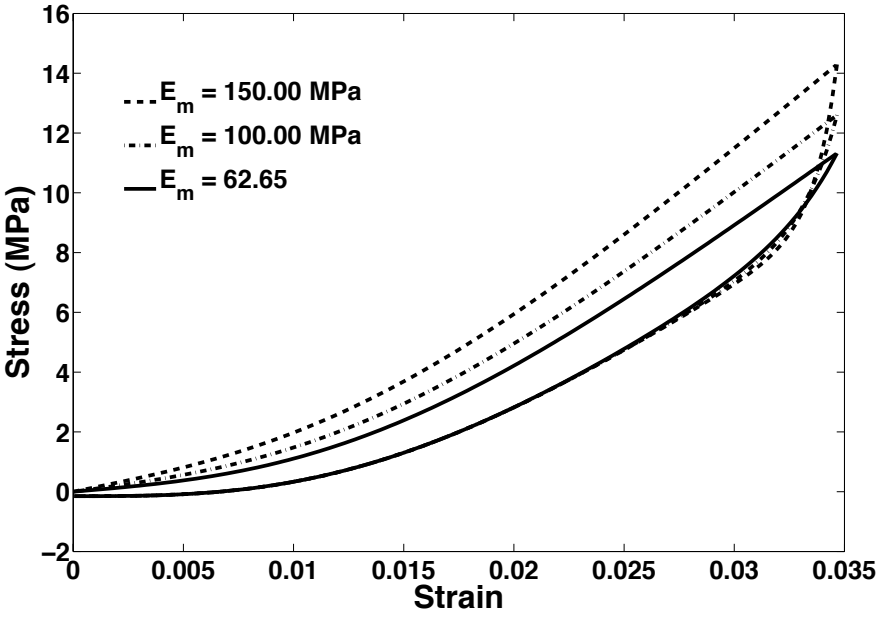

Figure 4.19: Influence of E_m on preconditioning.

Chapter 5

Conclusions

In this dissertation, nonlinear viscoelastic models were presented to illustrate tensile, creep and stress relaxation behaviors of ligaments and tendons (Chapter 2). In these models, the fibers' recruitment process in the tissues was assumed to determine the nonlinearity of the elastic stress-strain response. The viscoelastic properties of the tissues were assumed to be due to the proteoglycan-rich matrix surrounding fibers. Both the fibers and matrix were assumed to be perfectly bonded to each other by molecular interactions and, hence, they were assumed to be subjected to the same strain. The exact mechanisms of interaction between the collagen fibers and the surrounding matrix are, however, still unknown. It is possible that the strain of the fibers and the strain of the matrix are very different.

Because ligaments and tendons can be idealized as two-phase composite materials made of a hard phase, the fibers, and a soft phase, the matrix, the interaction between these two

components could be modeled by using the shear lag theory [11, 82]. Shear lag models take into account the difference in strains of the matrix and fibers, which causes shear stress at the surface of the fibers and a shear stress distribution in the matrix. These models have not been applied to soft biological tissues due perhaps to their complex morphology which makes them very different from conventional composite materials. Future studies will be carried out to investigate the capabilities of shear lag models in describing the shear stress between the fibers and the matrix in collagenous tissues.

The models presented in Chapter 2 showed very good agreement with the experimental data by Hingorani et al. [35]. The model parameters were physically meaningful and were related to the main components of ligaments and tendons. Although the theoretical findings are promising, more experimental data are required in order to validate and improve the proposed modeling framework. For example, quasi-static stress-strain data collected from rat medial collateral ligaments or stress-strain data collected from a single collagen fiber under the same experimental conditions used by Hingorani et al. would have been useful to determine the values of elastic parameters of the fibers independently from the values of the viscoelastic parameters of the matrix.

The models in Chapter 2 can be improved by incorporating additional structural information. In formulating the models, only the mechanical contributions of the fiber and the proteoglycan-rich matrix surrounding the fibers were considered. This leads to one relaxation time for describing the viscoelastic properties of the tissue. The models could be extended to capture a second relaxation time of the tissue by including the mechanical contribution

of the proteoglycan-rich matrix surrounding the fibrils as done by Gupta et al. [33] for a model for stress relaxation. Finally, it must be noted that the proposed model can also be extended to describe the viscoelasticity of other connective tissues having specific material symmetry or random networks of collagen fibers, as already done by other authors [15].

In Chapter 4, the models presented in Chapter 2 were extended to describe the preconditioning process in ligaments and tendons. The models and the experimental data showed very good qualitative agreement under the assumption that softening during preconditioning was the result of a decrease in the elastic moduli of the fibers and matrix. The values of the model parameters were physically meaningful with numerical values close to the values of similar parameters reported in the literature. It was speculated that the decrease in elastic moduli was due to the breaking of bonds between the fibers and matrix when the tissue undergoes cyclic loading. However, the interaction between the fibers and matrix was not explicitly incorporated into the model and future experimental and theoretical studies need to be carried out to elucidate and model such interaction.

In order to model the softening process in preconditioning by considering the structure of the tissue, more experimental data are required. Two sets of preconditioning experiments conducted by controlling strain and stress and collected from the same types of ligaments and tendons should be performed. Moreover, the orientation and waviness of the fibers before and after the tissue is subjected to cyclic tensile tests during preconditioning should be quantified by using imaging techniques such as, for example, optical coherence tomography. The fibers' recruitment of each cycle during preconditioning could be different due to the breaking of

the bonding between the fibers and the matrix or the entanglement of the crimped fibers. Therefore, also the fibers' recruitment needs to experimentally measured.

In chapter 3, a new modeling framework is presented for describing the mechanical response of a single type I collagen fiber exhibited during incremental stress relaxation tests. The microfibrils and the crosslinks among them were assumed to be responsible for the elasticity of the collagen fiber while the matrix was responsible for its viscosity. The models showed good agreement with the experimental data and their predictive capabilities was good given the large variation observed in the experimental data. These models could be extended to describe other viscoelastic phenomena in collagen fibers such as creep or the viscoelasticity of other types of collagen fibers. More importantly, the models could be improved to illustrate the role of crosslink density on the mechanical behavior of collagenous fibers and tissues.

In conclusion, the proposed viscoelastic models for a single collagen fiber, ligaments and tendons can help in clarifying the role of each of their main structural components in defining their overall mechanical response. Once fully validated with experimental and structural data, the models can be used as predictive tools for designing replacement grafts for ligaments and tendons.

Bibliography

[1] A. J. Bailey, R. G. Paul, and L. Knott. Review mechanisms of maturation and ageing of collagen. *Mechanisms of Ageing and Development*, 106:1–56, 1998.

[2] E. O. Carew, J. E. Barber, and I. Vesely. Role of preconditioning and recovery time in repeated testing of aortic valve tissues: Validation through quasilinear viscoelastic theory. *Annals of Biomedical Engineering*, 28:1093–1100, 2000.

[3] T. Cheng and R. Z. Gan. Mechanical properties of anterior malleolar ligament from experimental measurement and material modeling analysis. *Biomechanics and Modeling in Mechanobiology*, 7:387–394, 2008.

[4] D. Chimich, N. Shrive, C. Frank, L. Marchuk, and R. Bray. Water content alters viscoelastic behaviour of the normal adolescent rabbit medial collateral ligament. *Journal of Biomechanics*, 25:831–7, 1992.

[5] P. Ciarletta and B. Amar. A finite dissipative theory of temporary interfibrillar bridges in the extracellular matrix of ligaments and tendons. *Journal of The Royal Society Interface*, 6:909–24, 2009.

[6] P. Ciarletta, P. Dario, and S. Micera. Pseudo - hyperelastic model of tendon hysteresis from adaptive recruitment of collagen type i fibrils. *Biomaterials*, 29:764–770, 2008.

[7] P. Ciarletta, S. Micera, D. Accoto, and P. Dario. A novel microstructural approach in tendon viscoelastic modeling at the fibrillar level. *Journal of Biomechanics*, 39:2034–2042, 2006.

[8] N. Conza. Engineering issues in experimental biomedicine series. part 3: Tissue preconditioning. *Experimental Techniques*, 29:43–46, 2005.

[9] C. Couppe, P. Hansen, M. Kongsgaard, V. Kovanen, C. Suetta, and P. Aagaard. Mechanical properties and collagen cross-linking of the patellar tendon in old and young men. *Journal of Applied Physiology*, 107:880–886, 2009.

[10] S. C. Cowin. How is a tissue built? *Journal of Biomechanical Engineering*, 122:553–569, 2000.

[11] H. L. Cox. The elasticity and strength of paper and other fibrous materials. *British Journal of Applied Physics*, 3:72–79, 1952.

[12] D. M. Daniel, W. H. Akeson, and J. J. O' Connor. *Knee Ligaments: Structure, Function, Injury and Repair*. Raven, New York, 1 edition, 1990.

[13] P. F. Davison and M. Brennan. The organization of crosslinking in collagen fibrils. *Connective Tissue Research*, 11:135–151, 1983.

[14] D. De Tommasi, G. Puglisi, and G. Saccomandi. A micromechanics-based model for the mullins effect. *Journal of Rheology*, 50:495, 2006.

[15] R. De Vita and W. S. Slaughter. A structural constitutive model for the strain rate-dependent behavior of anterior cruciate ligaments. *International Journal of Solids and Structures*, 43:1561–1570, 2006.

[16] R. De Vita and W. S. Slaughter. A constitutive equation for the failure behavior of medial collateral ligaments. *Biomechanics and Modeling in Mechanobiology*, 6:189–197, 2007.

[17] W. F. Decraemer, M. A. Maes, and V. J. Vanhuyse. An elastic stress - strain relation for soft biological tissues based on a structural model. *Journal of Biomechanics*, 13:463–468, 1979.

[18] W. F. Decraemer, M. A. Maes, V. J. Vanhuyse, and P. Vanpeperstraete. A non-linear viscoelastic constitutive equation for soft biological tissues based upon a structural model. *Journal of Biomechanics*, 13:559–564, 1980.

[19] J. Diani, B. Fayolle, and P. Gilormini. A review on the mullins effect. *European Polymer Journal*, 45:601–612, 2009.

[20] C. Dorow, N. Krstin, and F. G. Sander. Experiments to determine the material properties of the periodontal ligaments. *Journal of Orofacial Orthopedics*, 63:94–104, 2002.

[21] R. Einat and Y. Lanir. Recruitment Viscoelasticity of the Tendon. *Journal of Biomechanical Engineering*, 131:111008, 2009.

[22] D. M. Elliott, P. S. Robinson, J. A. Gimbel, J. J. Sarver, J. A. Abboud, R. V. Lozzo, and L. J. Soslowsky. Effect of altered matrix protiens on quasilinear viscoelastic properties on transgenic mouse tail tendons. *Annals of Biomedical Engineering*, 31:599–605, 2003.

[23] P. Flaud and D. Quemada. A structural viscoelastic model of soft tissues. *Biorheology*, 25:95–105, 1988.

[24] M. Franchi, M. Fini, M. Quaranta, V. De Pasquale, M. Raspanti, G. Giavaresi, V. Ottani, and A. Ruggeri. Crimp morphology in relaxed and stretched rat achilles tendon. *Journal of Anatomy*, 210:1–7, 2007.

[25] P. Fratzl. *Collagen: Structure and mechanics*. Springer, Germany, 1 edition, 2008.

[26] Y. C. Fung. *Biomechanics: Mechanical properties of living tissues*. Springer-Verlag, New York, 2 edition, 1993.

[27] J. R. Funk, G. W. Hall, J. R. Crandall, and W. D. Pilkey. Linear and quasi-linear viscoelastic characterization of ankle ligaments. *Journal of Biomechanical Engineering*, 122:15–21, 2000.

[28] A. Gautieri, S. Vesentini, A. Redaelli, and M.J. Buehler. Hierarchical nanomechanics of collagen microfibrils. *Nature Proceedings*, 2010.

[29] F. Genna, L. Annovazzi, C. Bonesi, P. Fogazzi, and C. Paganelli. On the experimental determination of some mechanical properties of porcine periodontal ligament. *Meccanica*, 43:55–73, 2008.

[30] E. Gentleman, A. N. Lay, D. A. Dickerson, E. A. Nauman, G. A. Livesay, and K. C. Dee. Mechanical characterization of collagen fibers and scaffolds for tissue engineering. *Biomaterials*, 24:3805–3813, 2003.

[31] K. Graf, B., JR. Vanderby, R., J. Ulm, M., P. Rogalski, R., and J. Thielke, R. Effect of preconditioning on the viscoelastic response of primate patellar tendon. *The Journal of Arthroscopic and Related Surgery*, 10:90–96, 1994.

[32] L.Y. Griffin, J. Agel, M.J. Albohm, E.A. Arendt, R.W. Dick, W.E. Garrett, J.G. Garrick, T.E. Hewett, L. Huston, M.L. Ireland, et al. Noncontact anterior cruciate ligament injuries: risk factors and prevention strategies. *Journal of the American Academy of Orthopaedic Surgeons*, 8(3):141, 2000.

[33] H. S. Gupta, J. Seto, S. Krauss, P. Boesecke, and H. R. C. Screen. In situ multilevel analysis of viscoelastic deformation mechanisms in tendon collagen. *Journal of Structural Biology*, 169:183–191, 2010.

[34] P. Hansen, T. Hassenkam, R. B. Svensson, P. Aagaard, T. Trappe, B. T. Haraldsson, M. Kjaer, and P. Magnusson. Glutaraldehyde cross-linking of tendon: Mechanical effects at level of the tendon fascicle and fibril. *Connective Tissue Research*, 50:211–222, 2009.

[35] V. Hingorani, R., P. Provenzano, P., S. Lakes, R., A. Escarcega, and R. Vanderby, JR. Nonlinear viscoelasticity in rabbit medial collateral ligament. *Annals of Biomedical Engineering*, 32:306–312, 2004.

[36] M. Israelowitz, S. W. H. Rizvi, J. Kramer, and H. P. V. Schroeder. Computational modeling of type i collagen fibers to determine the extracellular matrix structure of connective tissues. *Protein Engineering, Design, and Selection*, 18:329–335, 2005.

[37] G. A. Johnson, G. A. Livesay, S. L. Y. Woo, and K. R. Rajagopal. A single integral finite strain viscoelastic model of ligamnets and tendons. *Journal of Biomechanical Engineering*, 118:221–226, 1996.

[38] K. E. Kadler. Extracellular matrix 1: Fibril-forming collagens. *Protein Profile*, 2:491–619, 1995.

[39] J. Kastelic, A. Galeski, and E. Baer. The multicomposite structure of tendon. *Connective Tissue Research*, 6:11–13, 1978.

[40] Y. P. Kato, D. L. Christiansen, R. A. Hahn, S-J Shieh, J. D. Goldstein, and F. H. Silver. Mechanical properties of collagen fibres: a comparison of reconstituted and rat tail tendon fibres. *Biomaterials*, 10:38–42, 1989.

[41] K. Komatsu. Mechanical strength and viscoelastic response of the periodontal ligament in relation to structure. *Journal of Dental Biomechanics*, 2010:1–18, 2009.

[42] R. S. Lakes and R. Vanderby Jr. Interrelation of creep and relaxation: A modeling approach for ligaments. *Journal of Biomechanic Engineering*, 121:612–615, 1999.

[43] Y. Lanir. A structural theory for the homogeneous biaxial stress-strain relationship in flat collageneous tissues. *Journal of Biomechanics*, 12:423–436, 1979.

[44] Y. Lanir. A microstructural model for the rheology of mammalian tendon. *Journal of Biomechanical Engineering*, 102:332–339, 1980.

[45] O. Lokshin and Y. Lanir. Micro and macro rheology of planar tissues. *Biomaterials*, 30:3118–3127, 2009.

[46] O. Lokshin and Y. Lanir. Viscoelasticity and preconditioning of rat skin under uniaxial stretch: Microstructural constitutive characterization. *Transaction of the American Society of Mechanical Engineers: Journal of Biomechanical Engineering*, 131:1–10, 2009.

[47] R. J. Minns and D. S. Jackson. The role of the fibrous components and ground substance in the mechanical properties of biological tissues: A preliminary investigation. *Journal of Biomechanics*, 6:153–165, 1973.

[48] H. Miyazaki and K. Hayashi. Tensile tests of collagen fibers obtained from the rabbit patellar tendon. *Biomedical Microdevices*, 2:151–157, 1999.

[49] A. Nava, E. Mazza, O. Haefner, and M. Bajka. Experimental observation and modeling of preconditioning in soft biological tissues. *Lecture Notes in Computer Science*, 3078:1–8, 2004.

[50] P. Provenzano, R. Lakes, T. Keenan, and R. Vanderby Jr. Nonlinear ligament viscoelasticity. *Annals of Biomedical Engineering*, 29:908–914, 2001.

[51] P. P. Provenzano, D. Heisey, K. Hayashi, R. Lakes, and R. Vanderby Jr. Subfailure damage in ligament: A structural and cellular evaluation. *Journal of Applied Physiology*, 92:362–371, 2002.

[52] P. P. Provenzano, R. S. Lakes, D. T. Corr, and R. Vanderby Jr. Application of nonlinear viscoelastic models to describe ligament behavior. *Biomechanics and Modeling in Mechanobiology*, 1:45–57, 2002.

[53] P. P. Purslow, T. J. Wess, and D. W. Hukins. Collagen orientation and molecular spacing during creep and stress-relaxation in soft connective tissues. *Journal of Experimental Biology*, 201:135–142, 1998.

[54] R. Puxkandl, I. Zizak, O. Paris, J. Keckes, W. Tesch, S. Bernstorff, P. Purslow, and P. Fratzl. Viscoelastic properties of collagen: Synchrotron radiation investigations and structural model. *Philosophical Transactions of the Royal Society*, 357:191–197, 2002.

[55] K. M. Quapp and J. A. Weiss. Material characterization of human medial collateral ligament. *Transaction of the American Society of Mechanical Engineers: Journal of Biomechanical Engineering*, 120:757–763, 1998.

[56] F. Raischel, F. Kun, and H.J. Herrmann. Failure process of a bundle of plastic fibers. *Physical Review E*, 73:66101, 2006.

[57] K. Reiser, J. Mccormick, R., and B. Rucker, R. Enzymatic and nonenzymatic cross-linking of collagen and elastin. *The Federation of American Societies for Experimental Biology Journal*, 6:2439–2449, 1992.

[58] S. P. Robins. Analysis of the crosslinking components in collagen and elastin. *Methods of Biochemical Analysis*, 28:330–379, 1982.

[59] S. M. Sacks. Incorporation of SALS-derived fiber orientation data into a structural constitutive model for planar collagenous tissues. *Journal of Biomechanical Engineering*, 25:280–287, 2003.

[60] L. Schatzmann, P. Brunner, and H. U. Staubli. Effect of cyclic preconditioning on the tensile properties of human quadriceps tendons and patellar ligaments. *Knee Surgery Sports Traumatology Arthroscopy*, 6:56–61, 1998.

[61] R. C. Screen, H., C. Shelton, J., H. Chhaya, V., V. Kayser, M., L. Bader, D., and A. Lee, D. The influence of noncollagenous matrix components on the micromechanical environment of tendon fascicles. *Annals of Biomedical Engineering*, 33:1090–1099, 2005.

[62] F. H. Silver, J. W. Freeman, and G. P. Seehra. Collagen self assembly and the development of tendon mechanical properties. *Journal of Biomechanics*, 36:1529–1553, 2003.

[63] F.H. Silver, D.L. Christiansen, P.B. Snowhill, and Y. Chen. Role of storage on changes in the mechanical properties of tendon and self-assembled collagen fibers. *Connective Tissue Research*, 41:155–164, 2000.

[64] U. Staubli, H., L. Schatzmann, P. Brunner, L. Rincon, and L. P. Nolte. Mechnical tensile properties of the quadriceps tendon and patellar ligament in young adults. *The American Journal of Sports Medicine*, 27:27–34, 1999.

[65] E. Suzuki, R. D. B. Fraser, and T. P. MacRae. Role of hydroxyproline in the stabilization of the collagen molecule via water molecules. *International Journal of Biological Macromolecules*, 2:54–56, 1980.

[66] A. Sverdlik and Y. Lanir. Time-dependent mechanical behavior of sheep digital tendons, including the effects of preconditioning. *Transaction of the American Society of Mechanical Engineers: Journal of Biomechanical Engineering*, 124:78–84, 2002.

[67] A. Teramoto and Z. P. Luo. Temporary tendon strengthening by preconditioning. *Clinical Biomechanics*, 23:619–622, 2008.

[68] A. Teramoto, W. R. Su, and Z. P. Luo. Effect of cyclic preconditioning on the failure load, strength and stiffness of multiple rat tendons and ligaments. *Journal of Musculoskeletal Research*, 11:89–95, 2008.

[69] G. M. Thornton, C. B. Frank, and N. G. Shrive. Ligament creep can be predicted from stress relaxation by incorporating fiber recruitment. *Journal of Rheology*, 45:493–507, 2001.

[70] G. M. Thornton, A. Oliynyk, C. B. Frank, and N. G. Shrive. Ligament creep cannot be predicted from stress relaxation at low stress: A biomechanical study of the rabbit medial collateral ligament. *Journal of Orthopaedic Research*, 15:652–656, 1997.

[71] G. M. Thornton, N. G. Shrive, and C. B. Frank. Ligament creep recruits fibres at low stresses and can lead to modulus-reducing fibre damage at higher creep stresses: A study in rabbit medial collateral ligament model. *Journal of Orthopaedic Research*, 20:967–974, 2002.

[72] R. Usha, V. Subramanian, and T. Ramasami. Role of secondary structure on the stress relaxation processes on rat tail tendon (rtt) collagen fibre. *Macromolecular Bioscience*, 1:100–107, 2001.

[73] P. Vena, D. Gastaldi, and R. Contro. A constituent-based model for the non linear viscoelastic behaviour of ligaments. *Journal of Biomechanical Engineering*, 128:449–457, 2006.

[74] A. Viidik. A rheological model for uncalcified parallel-fibred collagenous tissue. *Journal of Biomechanics*, 1:3–11, 1967.

[75] J. A. Weiss and J. C. Gardiner. Computational modeling of ligament mechanics. *Critical Reviews in Biomedical Engineering*, 29:1–70, 2001.

[76] L. Y. Woo, S., P. O. Newton, D. A. Mackenna, and R. M. Lyon. A comparative evaluation of the mechanical properties of the rabbit medial collateral and anterior cruciate ligaments. *Journal of Biomechanics*, 25:377–386, 1986.

[77] L. Y. Woo, S., K. J. Ohiand, and J. A. Weiss. Aging and sex-related changes in the biomechanical properties of the rabbit medial collateral ligament. *Mechanisms of Aging and Development*, 56:129–142, 1990.

[78] S. L. Y. Woo. Mechanical properties of tendons and ligaments I. quasi-static and non-linear viscoelastic properties. *Biorheology*, 19:385–396, 1982.

[79] L. H. Yahia and G. Drouin. Microscopical investigation of canine anterior cruciate ligament and patellar tendon: Collagen fascicle morphology and architecture. *Journal of Orthopaedic Research*, 7:243–251, 1989.

[80] L. H. Yahia and G. Drouin. Study of the hysteresis phenomenon on canine anterior cruciate ligaments. *Journal of Biomedical Engineering*, 12:57–61, 1990.

[81] E. Yamamoto, K. Hayashi, and N. Yamamoto. Mechanical properties of collagen fascicles from the rabbit patellar tendon. *Transaction of the American Society of Mechanical Engineers: Journal of Biomechanical Engineering*, 121:124–131, 1999.

[82] P. Zhao and S. Ji. Refinements of shear-lag model and its applications. *Tectonophysics*, 279:37–53, 1997.

Appendix A

Stress of Collagen Fibers

From Eq. 2.13, which represents the stress of the collagen fibers, it easily follows that

$$\frac{\sigma_f(t)}{E_f} = \varepsilon(t)\int_0^{\varepsilon(t)} p(\varepsilon_s)d\varepsilon_s - \int_0^{\varepsilon(t)} \varepsilon_s p(\varepsilon_s)d\varepsilon_s\,, \tag{A.1}$$

where $p(\varepsilon_s)$ is the Weibull probability density function already defined in Eq. 2.12. Moreover, it must be noted that

$$\int_0^{\varepsilon(t)} p(\varepsilon_s)d\varepsilon_s = 1 - e^{-\left(\frac{\varepsilon(t)}{\beta}\right)^{\alpha}}\,, \tag{A.2}$$

which is the so-called *Weibull cumulative distribution function.*

Let $\xi = \left(\frac{\varepsilon_s}{\beta}\right)^{\alpha}$. Then, $d\xi = \frac{\alpha}{\beta}\left(\frac{\varepsilon_s}{\beta}\right)^{\alpha-1} d\varepsilon_s$ so that

$$\int_0^{\varepsilon(t)} \varepsilon_s p(\varepsilon_s)d\varepsilon_s = \int_0^{\varepsilon(t)} \varepsilon_s \frac{\alpha}{\beta}\left(\frac{\varepsilon_s}{\beta}\right)^{\alpha-1} e^{-\left(\frac{\varepsilon_s}{\beta}\right)^{\alpha}} d\varepsilon_s \;= \beta\int_0^{\left(\frac{\varepsilon(t)}{\beta}\right)^{\alpha}} \xi^{\frac{1}{\alpha}} e^{-\xi}\, d\xi\,. \tag{A.3}$$

By recalling that the *lower incomplete gamma function* is defined as

$$\gamma(x,y) = \int_0^{y} \xi^{x-1} e^{-\xi} d\xi\,, \tag{A.4}$$

one obtains that

$$\int_0^{\left(\frac{\varepsilon(t)}{\beta}\right)^\alpha} \xi^{\frac{1}{\alpha}} e^{-\xi}\, d\xi = \gamma\left(\frac{1}{\alpha}+1, \left(\frac{\varepsilon(t)}{\beta}\right)^\alpha\right). \tag{A.5}$$

Moreover, by applying the following formula

$$\gamma(x,y) = (x-1)\gamma(x-1,y) - y^{x-1}e^{-y}, \tag{A.6}$$

one has that

$$\gamma\left(\frac{1}{\alpha}+1, \left(\frac{\varepsilon(t)}{\beta}\right)^\alpha\right) = \frac{1}{\alpha}\gamma\left(\frac{1}{\alpha}, \left(\frac{\varepsilon(t)}{\beta}\right)^\alpha\right) - \frac{\varepsilon(t)}{\beta}e^{-\left(\frac{\varepsilon(t)}{\beta}\right)^\alpha}. \tag{A.7}$$

Finally, Eq. A.1 can be rewritten as

$$\sigma_f(t) = E_f\left[\varepsilon(t) - \frac{\beta}{\alpha}\gamma\left(\frac{1}{\alpha}, \left(\frac{\varepsilon(t)}{\beta}\right)^\alpha\right)\right]. \tag{A.8}$$